Development of Anthropomorphic Prosthetic Hand and its Control Scheme for Transhumeral Amputees

by

Sarmad Shams

A Dissertation Submitted to the
Graduate School of Sciences and Engineering
in Partial Fulfillment of the Requirements for
the Degree of

Doctor of Philosophy

in

Bio-Medical Science and Engineering

August 2017

Development of Anthropomorphic Prosthetic Hand and its Control Scheme for Transhumeral Amputees

Koç University

Graduate School of Sciences and Engineering

This is to certify that I have examined this copy of a doctoral dissertation by

Sarmad Shams

and have found that it is complete and satisfactory in all respects,
and that any and all revisions required by the final
examining committee have been made.

Committee Members:

Prof. Dr. Ismail Lazoğlu (Advisor)

Prof. Dr. Kemal Türker (Co-Advisor)

Prof. Dr. Halil Kavaklı

Assoc. Prof. Dr. Kaan Güven

Assist. Prof. Dr. Ali Fethi Okyar

Assist. Prof. Dr. Seyed Ehsan Layegh Khavidaki

Date: 17th August. 2017

To my wonderful wife Anam Iqbal &
lovely girls Munazzah Haq & Ayesha Haq

ABSTRACT

An artificial hand or prosthesis is a device used by the amputee to replace his/her missing limb or limb portion. The prosthesis improves the life of the amputee by allowing them to perform activities of daily life without anyone's assistance. This dissertation describes the designing, mechanism analysis, FEA simulations, experimental analysis, the control scheme and development of a linear actuator based anthropomorphic prosthetic hand (MARCAPH) for transhumeral or near-elbow amputees. The MARCAPH comprises of 4 underactuated fingers with four bar mechanism, driven by the linear actuator through slider crank mechanism and a thumb driven by the linear actuator using slider crank mechanism. Each finger is derived individually by a linear actuator to perform the flexion-extension motion. On the other hand, the thumb is controlled by 2 actuators, one for circumduction and one for flexion-extension. The MARCAPH mechanism is analyzed using MATLAB and then design in a CAD software. The designed CAD model of the finger and thumb is then simulated using FEA software. The final design passes through a number of modifications and redesigning before achieving desired ruggedness, clearance, and interference, in order to produce the grips that are essential for activities of daily living (ADL). The prosthetic hand is then 3D printed, assembled and experimented under predefined conditions to ensure that the 3D printed hand is capable of performing the simulated grips. Each grip of the prosthetic hand is achieved by using position control algorithm underneath the finite state machine, that is, controlled by 2 channel differential EMG electrodes placed on the biceps and triceps muscles of the amputee's arm. This dissertation also covers the design process, kinematics, and control scheme developed for the MARCAPH. Moreover, in the last chapter, a brief comparison is provided between the MARCAPH and available state of the art prosthetic hands data.

ÖZETÇE

Suni bir el ya da protez, ampüte tarafından kaybedilen uzuv ya da uzuv parçasının yerine geçmesi için geliştirilen bir cihazdır. Protez, kişilerin başkalarından yardım almadan günlük yaşantılarını gerçekleştirmelerine izin vererek ampüte kalan kişilerin yaşamlarını iyileştirir. Bu tez, transhumeral ya da dirsek altı ampüteleri için doğrusal aktüatör tabanlı bir antropomorfik protez el (MARCAPH) tasarımı ve protezin mekanizma analizi, FEA simülasyonları, deneysel analizi ve kontrol şeması üzerinedir. MARCAPH, doğrusal aktüatör tarafından sürgü krank mekanizması ile düşük seviyede sürülen, dört çubuğa sahip 4 parmak; ve aynı yöntem ile normal seviyede sürülen bir baş parmaktan oluşmaktadır. Her bir parmak, kapanma (flexion) ve açılma (extension) hareketini doğrusal aktüatörler yardımı ile gerçekleştirmektedir. Öte yandan, başparmak, biri sirkümdiksiyon (circumduction) biri de açılma ve kapanma hareketleri için 2 farklı aktüatör tarafından kontrol edilir. MARCAPH'nin çalışma mekanizması MATLAB kullanılarak, dizaynı ise bir CAD yazılımı kullanılarak analiz edilmiştir. Parmaklar ve başparmağının tasarlanmış CAD modeli daha sonra FEA yazılımı kullanılarak simüle edilirmiştir. Nihai tasarım, günlük yaşam aktiviteleri (ADL) için gerekli el kavrama hareketlerini elde etmek için gereken dayanıklılık, fiziksel boyut aralıkları ve yüzey pürüzlük parametrelerine ulaşmak için birçok modifikasyondan geçmiştir. 3D basım teknolojisi ile üretilmiş ve monte edilmiş protez elin simüle edilmiş kavrama hareketlerini gerçekleştirebildiğinden emin olmak için, MARCAPH önceden belirlenmiş koşullar altında test edilmiştir. Protez elin her kavraması, sonlu durum makinesinin altında konum kontrol algoritması kullanılarak, yani, ampüte kolunun biseps ve triseps kaslarına yerleştirilen 2 kanallı diferansiyel EMG elektrotlar tarafından kontrol edilmektedir. Bu tez, MARCAPH'nin tasarım sürecini ve kinematik ve kontrol şemasını da kapsamaktadır. Üstelik, son bölümde, MARCAPH ile mevcut protez el performansı arasında kısa bir karşılaştırma yapılmaktadır.

ACKNOWLEDGMENTS

First of all, I thank to Almighty Allah, for His blessings, including this opportunity to obtain a graduate degree in highly research environment of Manufacturing & Automation Research Center (MARC), Graduate School of Science and Engineering, Koç University, Istanbul, Turkey.

I would like to thank my advisor Dr. Ismail Lazoğlu for his valuable guidance and extraordinary support. I greatly appreciate his patience and encouragement throughout the graduate program. I also like to extend my deepest gratitude to my co-advisor Dr. Kemal Turker for his guidance throughout the research program. The time I spent in MARC aided in the fruition of my thesis.

I would like to thank Dr. Halil Kavaklı, Dr. Kaan Güven, Dr. Ali Fethi Okyar and Dr. Seyed Ehsan Layegh Khavidaki for their guidence, time, and efforts for the evaluation of my thesis.

I would like to thank my family, especially my parents, uncles, aunts, sisters and brothers for their support over the years, which has given me strength, courage and helped me to overcome various challenges. My sincere appreciation goes to all my lab mates in MARC, especially Muhammad Akmal for his valuable guidance and kind support. In addition, I also like to thank Çağlar Öztürk, Ibrahim Başar Aka, Ísmail Enes Yiğit, Talha Irfan Khan, Haris Sheh Zad, Uğur Birbilen and Muzaffer Bütün for their help and assistance. Moreover, the time I spent with MARC members Adnan Hassan, Armin Bijanzad, Abbas Hussein, Abasin Ulasyar, Mostafa Saleh, Erdem Kundakcioglu, & Hosein Khalatbari was very nice and memorable.

Also i want to thank the Pakistani community in Koç University, it is really a pleasurable experience to have them around and taste the Pakistani culture during the cultural events organized time to time.

Finally, I express my profound gratitude to the Higher Education Commission (HEC), Government of Pakistan, for the award of PhD scholarship under the HEC project titled: HRD Initiative-MS Leading to Ph.D. Program of Faculty Development for UESTPS (Batch-II) Phase-I . This opportunity enabled me to pursue my higher education in a technological challenging atmosphere of a reputed university of Turkey. The professional management of our scholarship program was a great source of motivation for us to do research in a stimulating yet conducive environment. The efforts made by HEC helped me in expanding my frontiers of knowledge to the next level.

Sarmad Shams

TABLE OF CONTENTS

LIST OF TABLES

LIST OF FIGURES

NOMENCLATURE

EMG	Electo Myo Gram
EEG	Electro Encephelo Gram
MPL	Modular Prosthetic Limb
DOF	Degree Of Freedom
DOC	Degree Of Control
RP	Revolutionizing Prosthetic
TMR	Targeted Muscle Reinnervation
FSM	Finite State Machine
TBM	Toronto Bloorview Mcmillan
DC	Direct Current
MCP	Meta Carpo Phalange
PP	Proximal Phalange
PIP	Proximal Inter Phalange
DIP	Distal Inter Phalange
MARC	Manufacturing and Automation Research Center
MARCAPH	MARC Anthropomorphic Prosthetic Hand
FEA	Finite Element Analysis
MU	Motor Unit
MUP	MU Potential
RMS	Root Mean Square
ADL	Activities of Daily Life
FSR	Force Sensitive Resistor
CAD	Computer Aided Design
GUI	Graphical User Interface

Chapter 1

INTRODUCTION

A prosthesis is an artificial device used to replace a missing body part or limb through a congenital defect, accident, illness, trauma or injury. The prosthesis should have the appearance or functionality or both similar to the body part it is being used to replace. There are several different kinds of prostheses, but they all can be classified into three main types

1. Cosmetic Prostheses

2. Body Powered Prostheses

3. Electrically Powered Prostheses

1.1 Cosmetic Prostheses

The prosthesis that only contributes towards the appearance of the lost body part and has very little to no functionality is termed as a cosmetic prosthesis. The purpose of the cosmetic prosthesis is to mask the attention of the public during daily life (shown in Fig. 1.1).

1.2 Body Powered Prostheses

Another type of the prosthesis consists of artificial devices that perform a basic operation of opening and closing of the terminal device via cable or tendon. The cable link the body movements to the prosthesis to control it and hence termed as Body

(a)

(b)

Figure 1.1: (a) The normal and amputated finger with the cosmetic prosthesis (b) After wearing the cosmetic prosthesis [Dianceht, 2017]

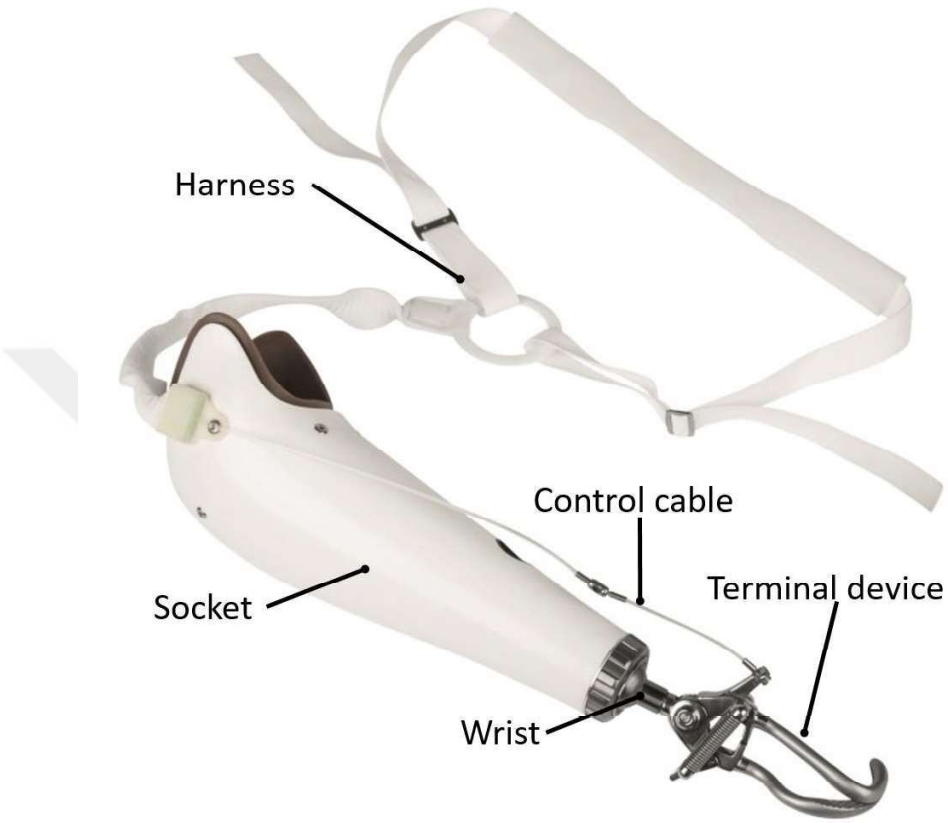

Figure 1.2: A typical prosthesis device [OttoBock, 2017]

Powered Prosthesis. A typical body powered prosthesis is consists of a terminal device or hand tool, harness, control cable, wrist and a socket as shown in Fig. 1.2.

The socket is worn on the amputated limb while the harness is worn on the opposite shoulder as shown in Fig. 1.3. The user can control the opening and closing of the terminal device with the movements of his opposite shoulder. The control cable that attached to harness stretches upon shoulder movement, creates tension in the cable that results in pulling the terminal device and performing the opening function. Similarly, movement of the shoulder in the opposite direction releases the tension in the cable and hence perform the closing of the terminal device. Body-powered prosthesis often has metal hooks as a terminal device instead of fingers. As the hooks serve better in high loading conditions and can pick up smaller things.

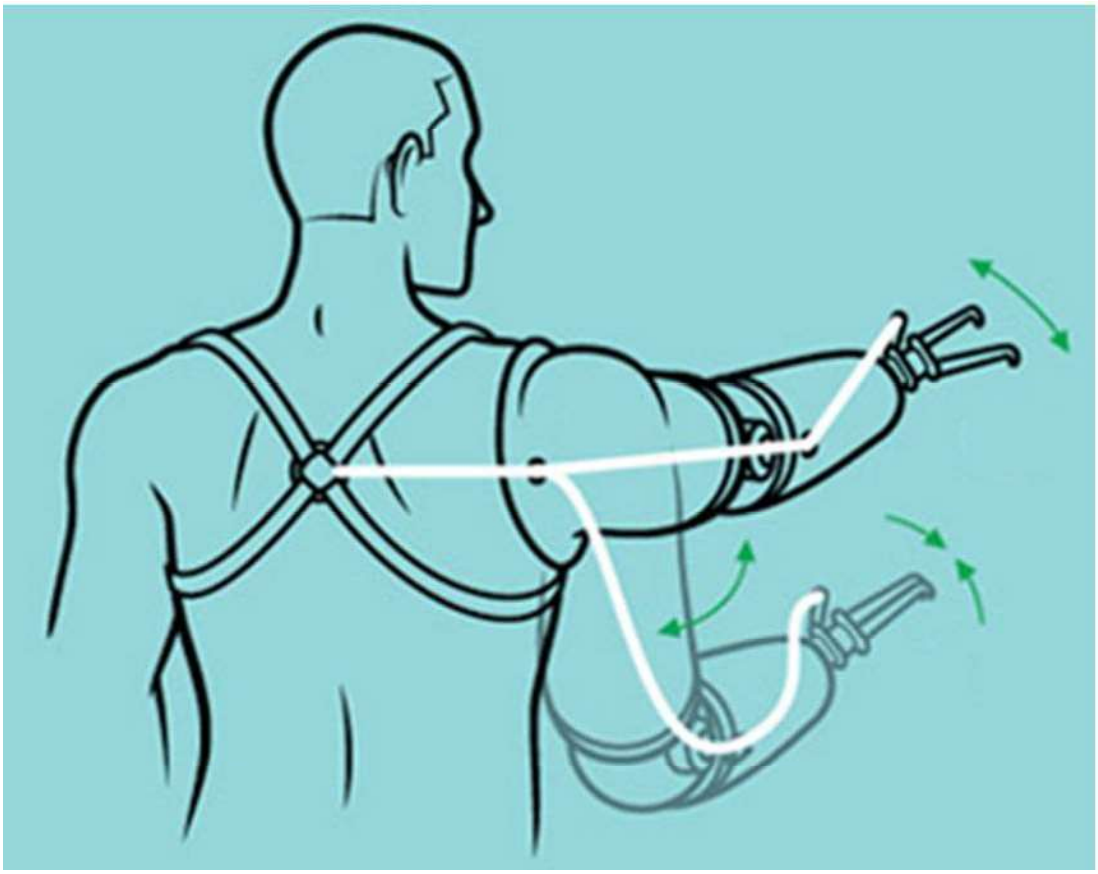

Figure 1.3: Body-powered prosthesis [Chorost, 2012]

1.3 Electrically Powered Prostheses

The prosthesis without an actuator can perform only a basic operation (like body powered prosthesis) or can only be used for the aesthetic look (cosmetic prosthesis), there is a need for a functional and versatile prosthesis that enhance or mimic the functionality of the missing part of the body. This kind of prosthesis usually contains active devices like motors with a complex mechanism to perform the movements and are known as Electrically Powered Prostheses. There are two main types of electrically powered prostheses; Mind-Controlled Prostheses and Myoelectric Prostheses.

1.3.1 Mind Controlled Prostheses

The prostheses usually actuate the motors or actuator to perform the movement. These movements are controlled by the decision performed by the microcontroller based on the signal receives from the sensors. In mind controlled prosthesis the sensors detect the signal of the brain usually called Electro Encephalo Gram (EEG) and send it to the controller after amplification and filtration. The controller then further processes the signals to extract the features presents in the signal and use a pre-train classifier to classify the intentions of the user into the commands understand by the actuators, thus produces the control signal to produce the desired movements.

1.3.2 Myoelectric Prostheses

The myoelectric prostheses use the similar setups as of mind controlled prostheses, but instead of sensing the brain signals, the myoelectric prostheses use to detect the signal at the muscle level called Electro Myo Gram (EMG). The EMG signal detects at the muscle is the intentions of the user to move the missing body part. In the case of hand amputation (see section 1.4 "Level of Amputation") the EMG signals acquired from the forearm region use to predicts the intention of the amputee to move his/her hand. These EMG signals are then processed to perform the desired movements of the finger and hand as intended by the user. The acquisition and control of the myoelectric prostheses are discussed in detail in chapter 6 and 7.

1.4 Level of Amputations

The upper limb amputation can be divided into five different categories according to the level of amputation 1.4. Each level of amputation requires a different type of prosthesis, since each level of amputation left with different sets of muscles, bones, and shape.

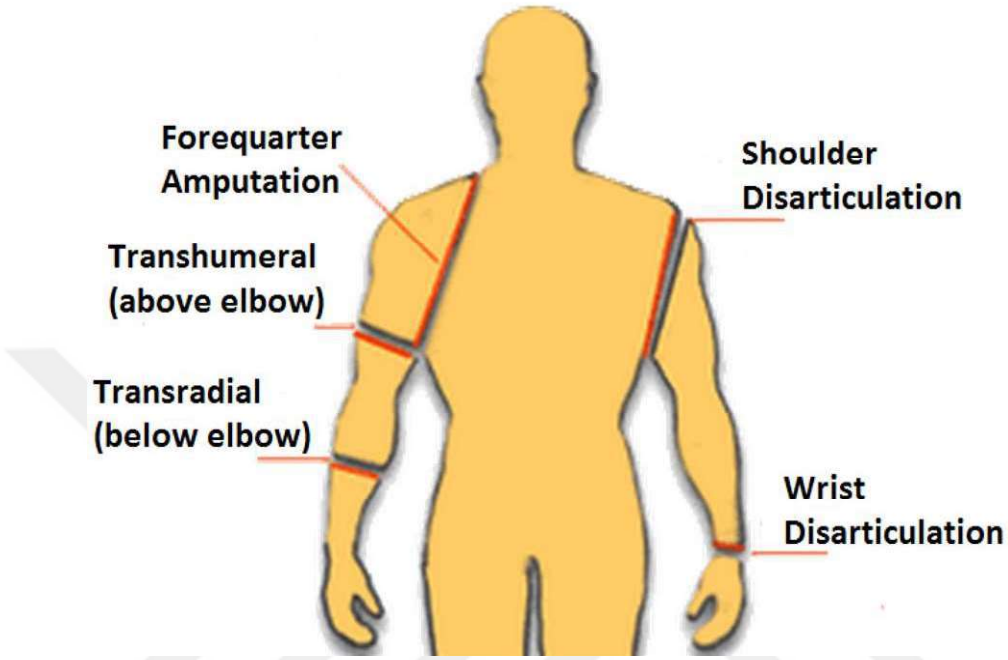

Figure 1.4: Levels of amputations for Upper Limb [Nova Scotia and Wellness, 2017]

1.4.1 Wrist Disarticulation

When the limb is amputated at the level of the wrist, the amputation is known as wrist disarticulation. In wrist disarticulation the muscles and bones of the forearm are intact and the amputee is able to perform the forearm rotation with the use of the forearm muscles. Although the movements at wrist such as wrist flexion-extension and adduction-abduction are lost, but, the muscles responsible to perform the movements are still present at the forearm.

1.4.2 Transradial Amputation

In transradial amputation, the limb is amputated at forearm region. In this type of amputation, the amputee has a significant portion of the bones and muscles of the forearm (as shown in the Fig. 1.4). The amputee still able to perform the rotation of the forearm and a portion of the muscles responsible for the wrist flexion-extension and abduction-adduction are still exist in the amputated limb. This amputation is

also known as below elbow amputation.

1.4.3 Transhumeral Amputation

The transhumeral amputation is also known as above elbow amputation, occurs in the upper arm between shoulder and elbow. In this amputation, the amputee lost his complete arm from elbow to hand. The muscles and bones responsible for the movements of wrist and hand are also lost resulting in the added difficulty for the amputee to control the prosthesis with the residual limb.

1.4.4 Shoulder Disarticulation

In this type of amputation, the limb is amputated at the level of the shoulder, with the shoulder blade remaining. The collarbone may or may not be removed. In this amputation, the amputee lost his complete arm with bones and muscles.

1.4.5 Forequarter Amputation

Forequarter amputation also occurs at the level of the shoulder, but in this type both the shoulder blade and collarbone are removed.

Chapter 2

LITERATURE REVIEW

Since the beginning of the 21st century, the field of prosthesis had captured a lot of attention from the researchers all over the world, which results in a number of indigenous designs, mechanisms and control schemes [Controzzi et al., 2016] [Medynski and Rattray, 2011] [Gibbard, 2013] [Liu et al., 2014] [Bennett et al., 2016]. However, an increase in research and development still in vain, as the fully functional myoelectric control based prosthetic hand is still beyond the access of amputees due to high cost. An amputee can buy a nonfunctional cosmetic hand for USD $3,000 to $5,000. This cosmetic prosthetic hand allows him to get by in public without being noticed. The basic split hooks prosthetic cost around USD $10,000. Furthermore, the cost of commercially available basic myoelectric prosthetic hand model starts from USD $20,000 [Van Der Riet et al., 2013], while a neuroprosthetic arm may cost as much as USD $100,000. The statistics show that there are an estimated 1.9 million amputees in the United States alone, and an average 185,000 amputations performed each year due to peripheral vascular disease and diabetes mainly. Other causes of amputation include injuries in children due to lawn mower with an average of 8,900 amputations. Birth defects also a major cause of amputation of approximately 6,000, amputations and it causes a life long need of the prosthetic device. The Veterans Administration healthcare system is providing services to 40,000 amputees and on average 1,000 soldiers lost their limbs every year. Since the statistical data is limited it has been estimated that in western developed countries the rate of amputation is about 17.1 amputations per 100,000 inhabitants [Strait et al., 2006]. These circumstances have built a huge market for the investors and researchers, the overall prostheses market alone in United States earned revenues of USD $1.45 billions (2006)

Figure 2.1: From left to right: Touch Bionics i-Limb Quantum extra small, small, medium and Large [Bionics, 2017]

and were expecting to reach USD $2 billion in the next seven years.

This chapter reviews the state of the art prosthetic hands available commercially, in research and open source.

2.1 Commercial State of the Arts

There are four main competitors in the market for myoelectric hand prostheses are: Touch bionics, RSL Steeper, Otto Bock and Vincent Systems. The Touch Bionics recently release it state of the art prosthetic hand named: i-Limb Quantum predecessor of i-Limb Ultra. RSL Steeper has released the third version of its myoelectric hand, named, Bebionic3. Otto Bock recently start producing functional wrist for its myoelectric hand Michelangelo and Vincent Systems has the Vincent Evolution 2 as the latest product.

2.1.1 i-Limb by Touch Bionics

The Touch Bionics is one of the leading company in the field of the prostheses, especially in upper extremity [Bionics, 2017]. The current version of the myoelectric

hand, i.e. i-Limb Quantum has four bar mechanism driven by a DC motor via worm gears. The i-Limb Quantum weights between 470 to 630 gm depends on the size of the hand. There are 4 sizes available ultra small, small, medium and large as shown in Fig. 2.1. All sizes are available in Aluminum and recently they have released a Titanium version too which is 30 gm heavier than the Aluminum model. The i-Limb Quantum has four different control modes

1. Trigger muscle control: In this, the users generate send triggers to the prosthesis via his muscles.

2. Quick grips app control: in this mode, the user uses his/her cell phone to communicate with the prosthesis and sends a command to perform a specific grip.

3. i-mo intelligent motion gesture control: In this mode, the user simply moves his/her hand in a specific direction to activate a pre-defined grip.

4. grip chips proximity control: In this mode, the user program a specific grip in the chip and place it in his/her working place. Whenever the hand comes closer or in range to the grip chip, the grip chip communicate and active the specific grip programmed earlier.

2.1.2 Bebionics by Otto Bock

The Otto Bock company recently acquire the Bebionic hand from RSL Steeper and hence add another hand prosthesis to its product line, beside Michelangelo hand [Medynski and Rattray, 2011]. The Bebionic has four bar mechanism driven by a custom made linear actuator. The Bebionic weights between 390 to 600 gm depends on the model, size, and features. The Bebionic is built on an aerospace grade aluminum chassis to keep it light weight. The Bebionic3 is available in three sizes: small, medium, and large as shown in Fig. 2.2. The Bebionic3 uses a Finite State

Figure 2.2: Bebionic V3 all sizes [Medynski and Rattray, 2011]

Machine (FSM) with the 2 EMG signals for opening and closing of the hand grip. The co-contraction or double open signal is used to switch the grip modes.

2.1.3 Vincent Hand by Vincent Systems GmbH

Vincent hand is another state of the art hand prosthesis produces by Vincent Systems [Schulz et al., 2011]. The Vincent hand has four bar mechanism driven by a DC motor via a worm gear. The Vincent hand has two models one is Vincent Evolution 2 for adults (as shown in Fig. 2.3) and second is Vincent Young for children and teenagers. The Vincent hand has an optimized design from a high-strength aluminum alloy. The Vincent Evolution 2 uses a FSM based control scheme with 2 EMG signals. The control scheme has first 5 grips which can be directly accessed from a central position. The associated grips in each first grips group can be reached from there by the trigger signal.

Figure 2.3: Vincent Evolution 2 by Vincent Systems GmbH [Schulz et al., 2011]

2.1.4 Michelangelo by Otto Bock

Michelangelo is a versatile hand prosthesis by Otto Bock Inc. that uses a single DC motor with cam mechanism and links to control all the fingers [OttoBock, 2017]. The thumb uses another small motor to position itself prior to grip. Michelangelo is available in one adult size (as shown in Fig. 2.4) and it weights around 420 gm. The Michelangelo has a unique feature of finger abduction/adduction which is not available in any other commercial prosthetic hand. Besides finger abduction/adduction

Figure 2.4: Michelangelo by Otto bock Inc. [OttoBock, 2017]

Michelangelo hand prosthesis has neutral mode in which hand is completely open, lateral mode when thumb moves sideways to finger and opposition mode in which thumb moves towards a tripod pinch with the index and middle fingers.

2.2 Prosthetic Hand in Research

Researchers in the field of hand prosthesis works to enhance the capabilities of the currently available hand prostheses. In this section, four hand prostheses are discussed among numerous hand prostheses available in the literature due to their different mechanism designs.

Figure 2.5: State of the art Modular Prosthetic Limb by John Hopkins Applied Physics Laboratory, USA [Johannes et al., 2011]

2.2.1 Modular Prosthetic Limb - John Hopkins Applied Physics Lab - USA

The Modular Prosthetic Limb (MPL) (also known as Revolutionizing Prosthetic 2009 (RP2009)) is the most advanced hand prosthesis known to date [Johannes et al., 2011]. The MPL has 26 degrees of freedom (DOF) including wrist, elbow, and shoulder flexion-extension and rotation. Among 26 DOF the MPL contains 17 degrees of control (DOC) which actuated with the help of custom motors and custom onboard motor controllers. MPL uses impedance based feedback control with more than 100

sensors for sensing position, torque, acceleration, force, current, voltage, contact and torque. The mass of the hand with the wrist is around 1.32 kg, while the upper arm weights around 3.5 kg. Carbon fiber and high-strength alloys used during manufacturing play an important role in keeping the weight close to human hand. The Fig. 2.5 shows an adult size MPL with a forearm, elbow, arm, and shoulder joint. The MPL is tested on human subjects who undergoes Targeted Muscle Reinnervation (TMR) surgery [Cheesborough et al., 2015]. In TMR surgery, the residual motor nerves of lost muscles are transferred to the remaining muscles. Hence the lost signal of the lost limb portion can be detected in the remaining muscle. This increase the ability of the amputee to control the hand prosthesis by increasing the EMG signal acquisition sites at the same residual limb with distinguishable signals.

2.2.2 Vanderbilt Hand - Vanderbilt University - USA

Vanderbilt hand is developed by the researchers at the Center for Intelligent Mechatronics Lab in Vanderbilt University, USA. The Vanderbilt hand has 9 DOF with 4 DOC and it weight around 546 gm [Dalley et al., 2009]. The additive direct manufacturing technique is used for the manufacturing of the Vanderbilt hand. The material used for the manufacturing process is Nickel coated thermoplastic. The Vanderbilt hand uses a tendon based mechanism for the flexion-extension of fingers. The Vanderbilt hand has four motors, one for the index finger, one for the middle, ring and little finger and two for the thumb. Three motors are responsible for the opening and closing of the hand while the fourth motor is used for the circumduction of the thumb. The Vanderbilt hand can be controlled via two EMG signals, one for extension and one for flexion, using an FSM is shown in Fig. 2.7. The FSM consists of two basic modes which are thumb opposition and reposition, these modes can be switched by double extension. Then the user can select the next grip by generating a flexion signal. In order to return to the basic grip mode, the user should generate the extension signal.

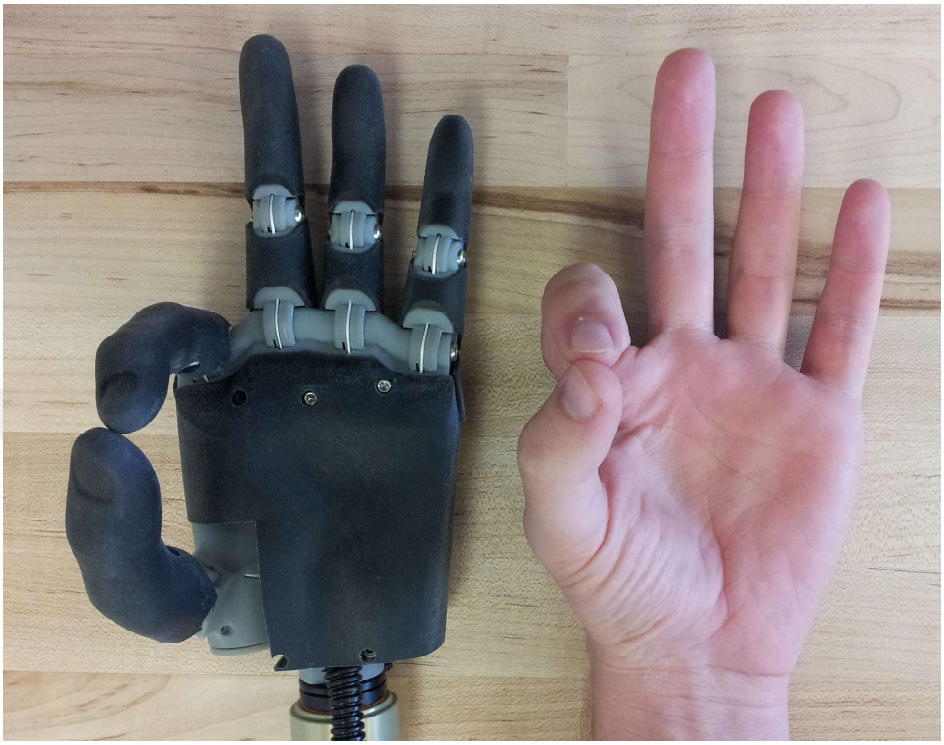

Figure 2.6: Third generation Venderbilt hand by Center for Intelligent Mechatronics, Vanderbilt University, USA [Dalley et al., 2009]

2.2.3 TBM Hand - University of Toronto - Canada

Toronto Bloorview Mcmillan or TBM hand developed in University of Toronto, Canada [Dechev et al., 2001]. The TBM is one of the early hand prosthesis developed with an underactuated design. It consists of one four bar and one five bar mechanism combine to perform the rotation of the finger (as shown in Fig. 2.9). The TBM hand uses a single motor with a lead screw mechanism. The lead screw mechanism is attached with a pressure or force plate which is attached to all the fingers (including the thumb) via tension spring. Upon actuation, the lead screw mechanism pulls all the fingers in x-axis direction to perform the flexion, while for extension the motor rotates in the opposite direction. The tension spring helps the fingers to adapt the shape of the object being gripped. The Aluminum is used to manufactured the finger and its mechanism, while the palm and thumb base is manufactured using Delrin.

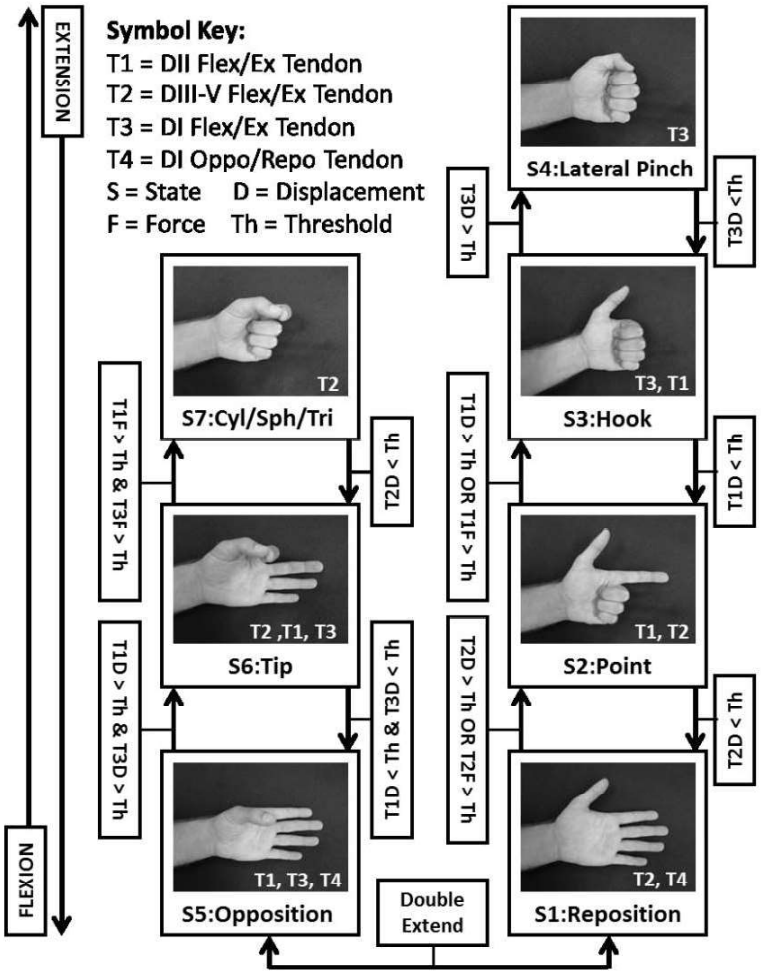

Figure 2.7: The finite state machine of the Vanderbilt hand [Dalley et al., 2009]

2.3 3D Printing Prosthetic Hands

The 3D printed technology allows researchers to developed aesthetic prosthetic hands that reduce the cost of manufacturing, adaptability, and customizability. A number of open-source prosthetic hands are available online which are ready to print according to the requirement, [Raptor hand, Dextrus, Tact, Inmoov] to name a few.

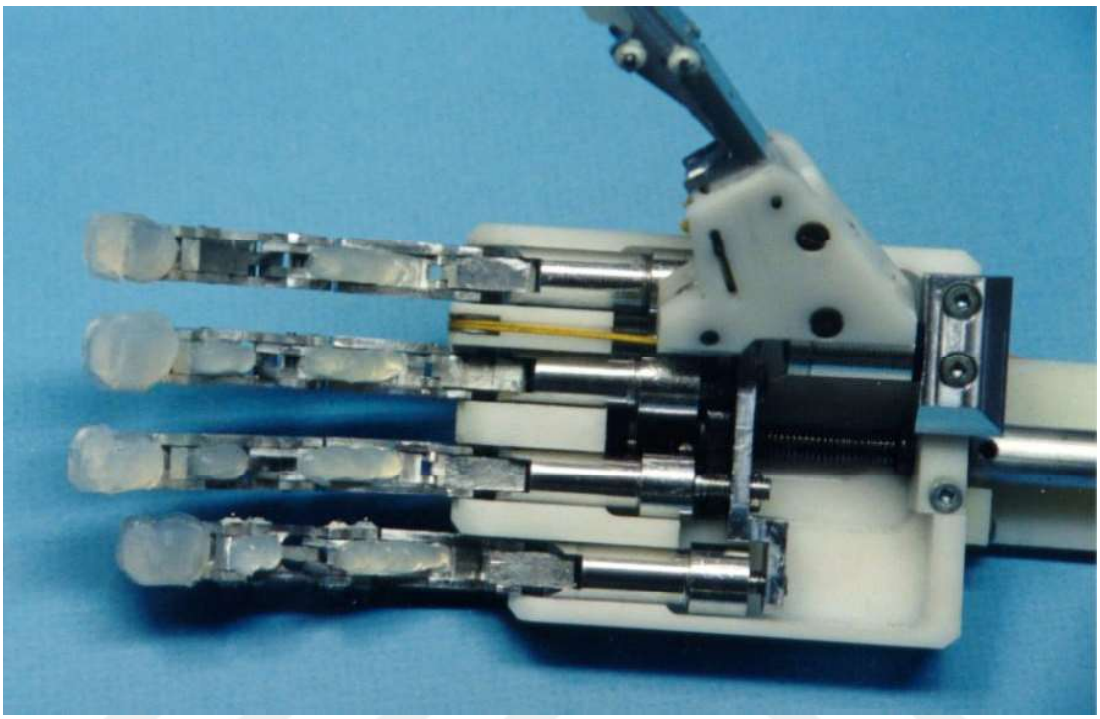

Figure 2.8: Toronto Bloorview Mcmillan (TBM) hand [Dechev et al., 2001]

2.3.1 Raptor Hand - e-NABLE

Raptor hand [e–NABLE Organization, 2017] is a simple, mechanical hand, that can be used by the amputee who has a partial hand or wrist amputation. Due to lack of actuators, sensors, and control, the Raptor hand is a body-powered prosthetic hand that can only perform an open-close operation, executed by the residual limb via a cable or wire.

2.3.2 InMoov - An Open Source Robot

The InMoov [Langevin, 2014] robots hand is another example of the open source 3D printing based artificial hand, that can be slightly modified to be used by the transhumeral amputee. The mechanism of the InMoov hand is based on tendons that wrap on a spool mounted on a servo motor. The clockwise rotation of servo produces flexion while anticlockwise rotation produces an extension of the finger. Since the

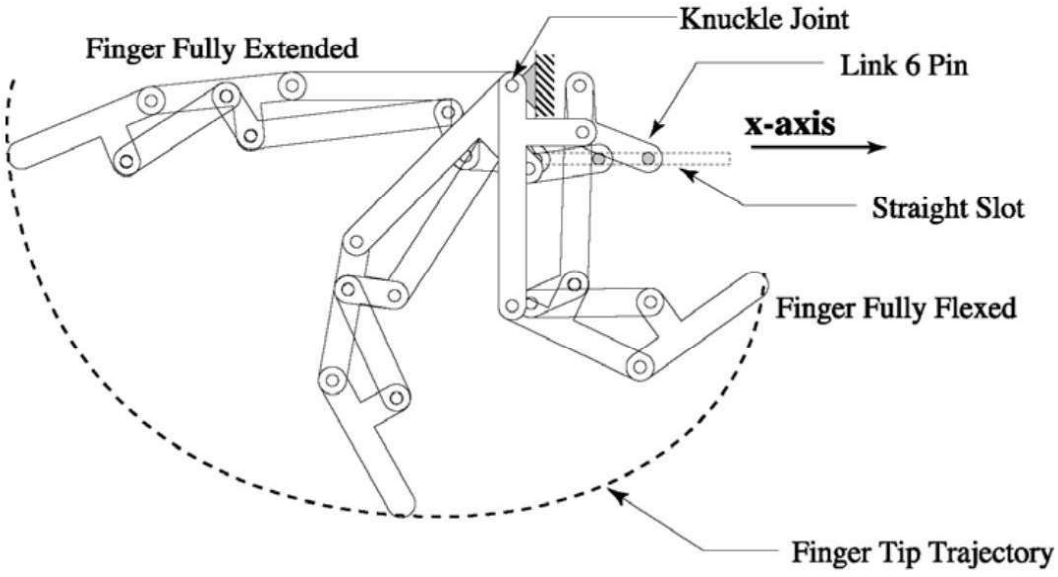

Figure 2.9: TBM hand mechanism, comprises of one five bar and one four bar mechanism, showing complete flexion of the finger upon pulling it in x-axis direction along the straight slot [Dechev et al., 2001]

design is available to be used with the robots, it lacks the control interface with an amputee and can only be used by transhumeral amputee due to the placement of the actuators in the forearm.

2.3.3 Dextrus Hand - Open Hand Project

Dextrus hand [Gibbard, 2013] overcome these issues by replacing the servo motors with DC motors and placed them in the palm area of the hand. Dextrus hand uses similar tendon based mechanism with the integration of spring that enables the hand to adapt the shape of the object being gripped. However, the thumb circumduction servo and the thick palm reduce the aesthetic look of the hand (shown in Fig. 2.12). Dextrus uses 2-channel EMG signal to control the FSM designed for Dextrus hand. The FSM control scheme comprises of 6 different grips requires for Activities of Daily Life (ADL). The wrist flexion-extension is used to control the opening and closing of

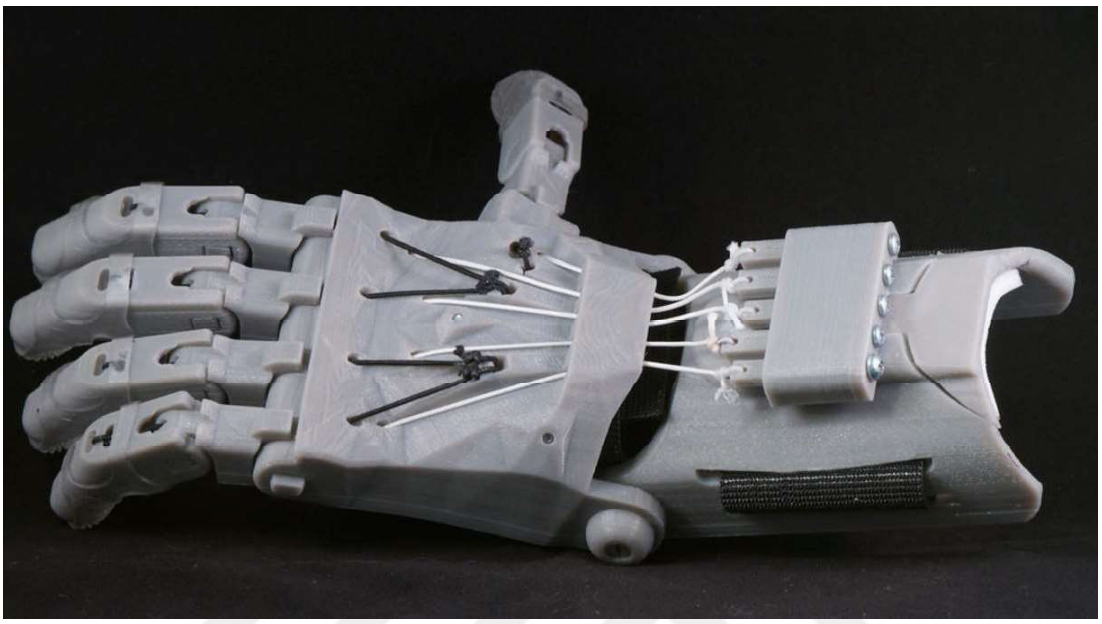

Figure 2.10: The Raptor hand by e-NABLE [e–NABLE Organization, 2017]

the hand while prolong extension can switch the state only when the hand is in open state.

2.3.4 Ada Hand - Open Bionics

The successors Ada hand [Bionics, 2016] use a single cable driven mechanism and uses a flexible material for 3D printing of flexure based finger joints. The linear actuators produce flexion of the finger while the extension is produced by the flexure joints while releasing the cable from the linear actuator. Ada hands reduce the thumbs actuators by using a single linear actuator to produce a combination of abduction-flexion and adduction-extension, as a result, the hand is unable to achieve grips required non-oppose thumb position i.e. adduction-flexion (Fig. 2.13). The control scheme of the Ada hand is analogous to its predecessor Dextrus hand.

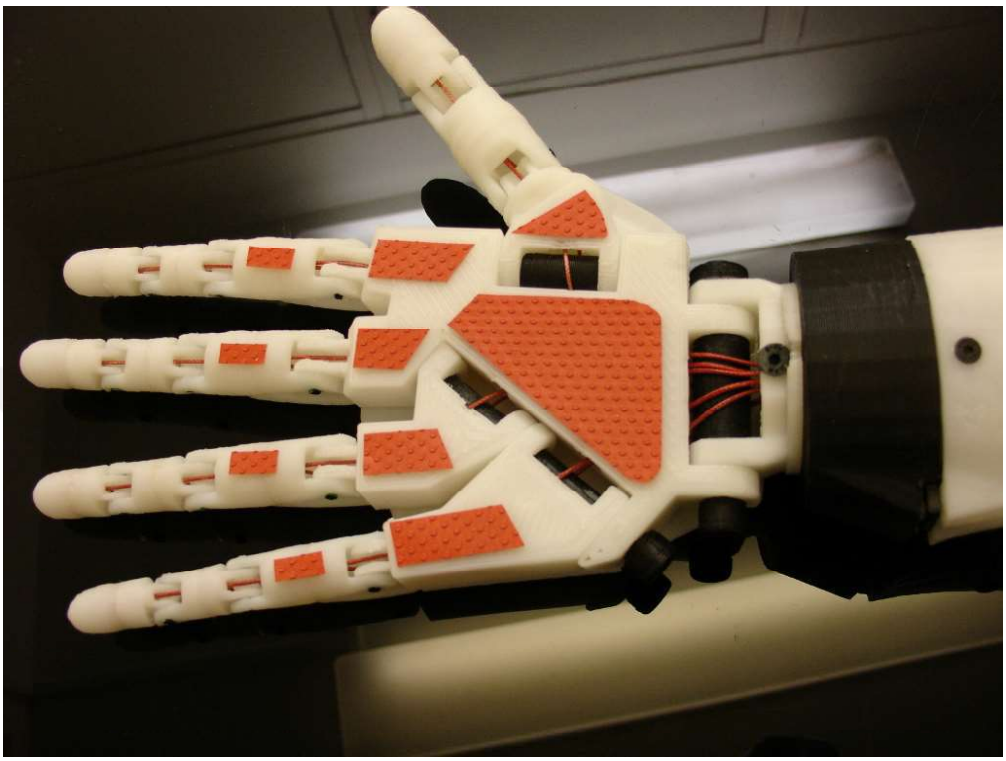

Figure 2.11: The InMoov hand [Langevin, 2014]

2.3.5 Tact hand - University of Illinois

The Tact hand [Slade et al., 2015] subdue the problem of adduction-flexion of thumb by using two separate actuators, one servo motor for the abduction and adduction and one DC motor for the flexion-extension as in Dextrus hand, in the meantime, reduces the palm thickness approximately to the half of the Dextrus hand. The Tact hand uses four bar mechanism driven by a DC motor through a cable, whose one end is attached to the anterior side of the proximal-distal phalange portion while the other end winds on a spool mounted on the motor shaft. The inclusion of the cable simplifies the driving mechanism of the Tact hand, which also results in the requirement of rubber bands as an elastic material at the back of Meta Carpo Phalangeal (MCP) joint for the extension of the fingers. The placement of rubber bands for extension and servo motors for the circumduction gives the hand unnatural look that cannot be gone

Figure 2.12: The open source Dextrus hand by Open Hand project [Gibbard, 2013]

unnoticed when using the hand in public (Fig. 2.14).

Figure 2.13: Ada hand, the successor of the Dextrus hand by Open Bionics (former Open Hand Project) [Bionics, 2016]

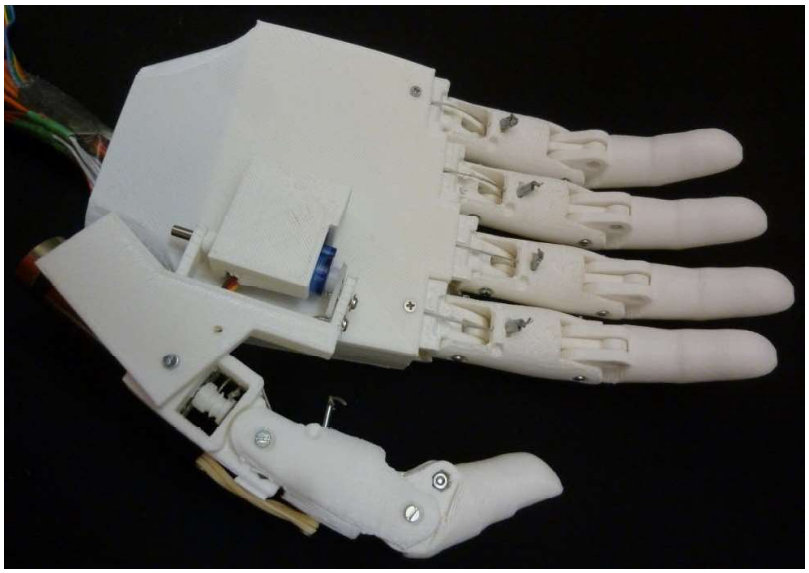

Figure 2.14: Tact: An open source hand prosthesis [Slade et al., 2015]

Chapter 3

THE MARCAPH: MECHANISM

The human hand is a complex system, comprises of several subsystems to accomplish the most complicated tasks, and it is nearly impossible to accomplish and accommodate all the systems into the artificial hand with the same scale as of human hand even in this era of technological advancements [Roche et al., 2014]. To simplify the system, MARCAPH is divided into number of sub-systems; Actuation unit, Mechanism Design, EMG signal acquisition, and Control.

In order to reduce the time and cost for the development and research of the MARCAPH; off-the-shelf components are selected for the actuation. The selecting parameters for the actuators are the dimensions, velocity, driving force and non-back driving force. After careful consideration a micro linear actuator (Actuonix PQ-12 [Actuonix, 2017]) is selected for its compact size, light weight, non-back driveability (up to 25 N) with maximum lifted force of 45 N and peak power output of 30 N at 8 mm/sec. Not only the actuator plays an important role in defining the artificial hand's gripping forces and velocity, but also, it has a significant influence on the artificial hand's dimensions and appearance. By considering the dimensions of the commercial state of the art prosthetic hand [Bionics, 2017] [Medynski and Rattray, 2011], palm area is selected to place the acquired actuators. This placement leads to a joint coupling mechanism, a four-bar mechanism is opted for the Meta Carpo Phalange (MCP) joint to Proximal Inter Phalange (PIP) joint instead of using a tendon based mechanism to flex the finger.

3.1 Finger Mechanism

Four bar mechanism is being the most common choice among the prostheses community, due to its ability to produce uniform motion and a significant amount of force as compared to tendon-based mechanisms and designs. MARCAPH uses four bar mechanism in inverse form when the driving and follower link is crossing each other. The four-bar mechanism is driven by a linear actuator via the slider-crank mechanism. The crank of the slider-crank mechanism is fixed with the driver link of the four bar mechanism. Moreover, the slider of the slider-crank mechanism is attached to the shaft of the linear actuator that translates to perform the flexion-extension of the finger. The objective of the entire finger mechanism is to have a minimal translation motion of the actuator for the maximum rotation of the finger. For this purpose, two mechanisms were optimized and linked together to form a single mechanism comprises of a slider-crank-four-bar mechanism.

3.1.1 Four Bar Mechanism

The lengths of the four bar mechanism's links are first selected by considering the dimensions of the state of the art prostheses [Bionics, 2017] and the rotation angles required for the human finger to flex [Jones, 1990]. Since, the four bar mechanism only constitutes the proximal phalange portion with MCP and PIP joints, a portion comprises of middle and distal phalanx with a fixed Distal Inter Phalangeal (DIP) joint is added to the coupler link CB of the four bar mechanism as CE and BE (as shown in Fig. 3.1). Then, the dimensions of the four bar mechanism's links were optimized by considering the trajectory required to follow by the fingertip Fig. 3.1. The kinematics analysis of the mechanism is performed using MATLAB [The MathWorks, 2017]. The link AD is fixed, AB is driver link, CB is coupler link and CD is follower link. For trajectory of the tip, the mechanism is solved by finding points B and C at every instant of ϕ. The point B can be found with reference to point A using Eq. 3.1 and

Eq. 3.2.

$$xB = AB\cos(\theta + \phi) + xA \tag{3.1}$$

$$yB = AB\sin(\theta + \phi) + yA \tag{3.2}$$

where:

θ is the angle between the crank RA and driver AB links

ϕ is the angle of the crank RA from the *x-axis* and it depends on the linear actuator displacement

The point C cannot be determined by only using the fix point D, instead, it also needs a reference from the link AB. To determine the point C Eq. 3.3 and Eq. 3.4 are solved simultaneously to find the exact position of point C (Fig. 3.1).

$$(xC - xD)^2 + (yC - yD)^2 = CD^2 \tag{3.3}$$

$$(xC - xB)^2 + (yC - yB)^2 = BC^2 \tag{3.4}$$

The positions of point C and point B give us the slope and length of the link CB. As discussed earlier the link CB define the base of the middle phalange. The middle phalange also contains the distal phalange with a fix 20° of DIP joint. To avoid the complexity in calculation a point E is selected as the fingertip (Fig. 3.1). To find the point E, Eq. 3.5 and Eq. 3.5 are solved simultaneously using MATLAB.

$$(xE - xC)^2 + (yE - yC)^2 = CE^2 \tag{3.5}$$

$$(xE - xB)^2 + (yE - yB)^2 = BE^2 \tag{3.6}$$

For the complete analysis of the trajectory, a value of ϕ should be increased in an iterative manner. The value of ϕ depends on the position of the slider of the slider-crank mechanism and it is driven by linear actuator Fig. 3.1.

The velocity and acceleration analysis shows smooth movements without any jerk. The graph for the position, velocity and acceleration for the links BE and CD are shown in Fig. 3.2.

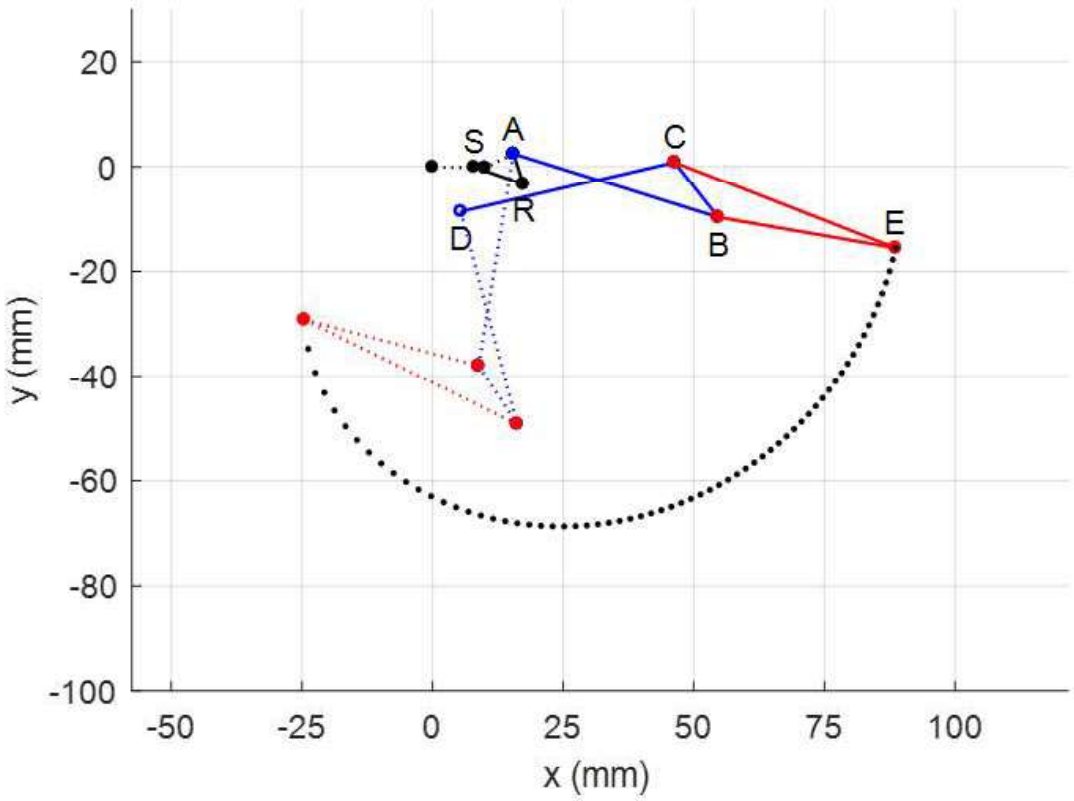

Figure 3.1: Trajectory of fingertip analyzed during optimization process in MATLAB, slider-crank mechanism is shown in black with links SR and RA, four bar mechanism in blue with links AB, BC, and CD, and fingertip in red with links CE and BE

3.1.2 Slider Crank Mechanism

The slider-crank mechanism is responsible for transmitting the actuator translation to the driver link AB of four bar mechanism. The slider S is attached to the shaft of the linear actuator and the crank AR is attached to the driver link AB at pin joint A with an angle θ. In order to find the point R of the coupler and crank attachment, Eq. 3.7 and Eq. 3.8 are solved simultaneously using MATLAB.

$$(xR - xS)^2 + (yR - yS)^2 = SR^2 \tag{3.7}$$

$$(xR - xA)^2 + (yR - yA)^2 = AR^2 \tag{3.8}$$

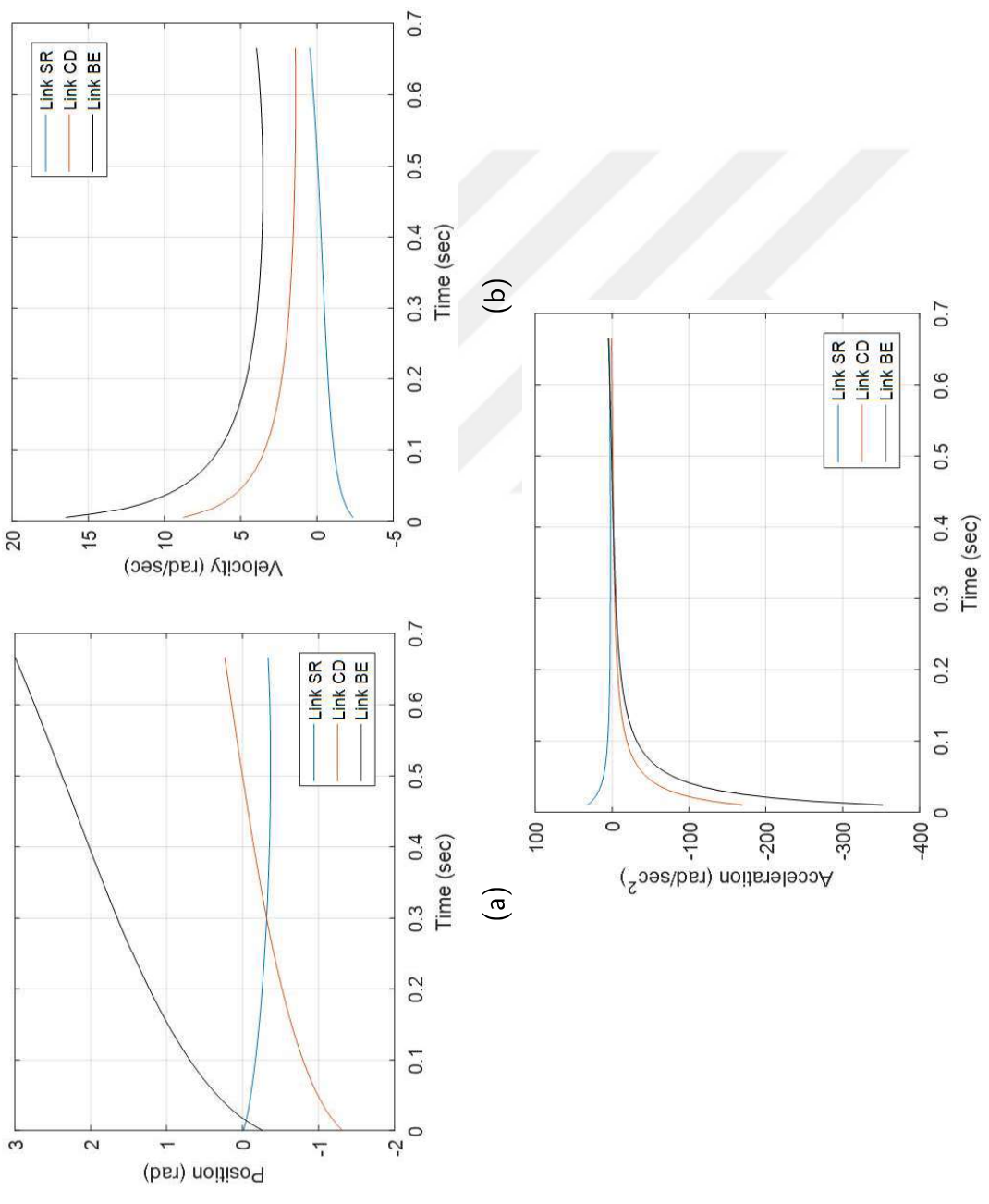

Figure 3.2: Analysis of the four bar mechanism of point C (a) Position (b) Velocity (c) Acceleration

The links for slider-crank mechanism are optimized by considering the angular displacement ϕ required for the driver link of four bar mechanism for a complete flexion of the finger with the available actuation of the linear actuator. Initially, a displacement of 10 mm is considered for the finger to flex completely and later it is optimized to 8 mm. This leads the finger to complete a flex operation in 1 sec under maximum load and 0.5 sec on no load conditions. The optimized lengths of the coupler SR and crank AR results in a constant value of 55° for the θ.

The position, velocity and acceleration graphs for the link SR is shown in Fig. 3.2. The point R is the critical point in transferring the motion of the slider S, as the point A is fixed pin joint (as shown in the Fig. 3.1).

3.2 Thumb Mechanism

Thumb is the complex finger of a human hand, which is controlled by 9 individual muscles having 3 major hand nerves and can perform 6 different movements [Jones, 1990]. Commercial prosthetic such as Bebionics [Medynski and Rattray, 2011] did not automate the control of circumduction movements, instead, the two positions can be stationed manually with external help. On the contrary, few researchers used a single actuator to perform circumduction and flexion-extension concurrently [Bionics, 2016] while the other used two actuators, one for abduction-adduction and another for flexion-extension [Liu et al., 2014] [Dalley et al., 2009] [Slade et al., 2015]. After careful examination of thumb movements two actuators based design is selected to control the circumduction and flexion-extension individually. For both movement sets, the slider-crank mechanism is optimized with the slider as the driving link attached to the shaft of the linear actuator. The linear actuator shaft displaced 16 mm to rotate the thumb from 0 ° to 115 °. Figure 4.5a shows a hand of normal adult and the proposed slider-crank mechanism is analyzed by drawing the links on the thumb. Moreover, the analyzed mechanism is then simulated and optimized for the complete circumduction of 115 ° using MATLAB (Fig. 4.5b). The Fig. 3.3b shows the trajectory of the thumb base during circumduction process. The slider-crank mechanism is

shown in black while the triangle in red color shows the thumb base (view from the bottom). The dotted lines show the initial position of the thumb and solid lines shows the final position. The trajectory is plotted with black dots as the thumb rotates. The center of the rotation is the attachment of the thumb base with the palm and the rotating point is the MCP joint of the thumb as shown in Fig. 3.3.

The trajectory of the thumb's tip is analyzed from the palm side of the hand. The proposed slider-crank mechanism is first analyzed by drawing the links on top of the thumb from the palmer view of the hand, as shown in the Fig. 3.4a. Moreover, the links' lengths are analyzed and then optimized for the complete flexion-extension movements of 95 ° for the slider displacement of the 16 mm.

The dotted line shows the starting position of the thumb and solid lines shows the final position of the thumb after a full extension (Fig. 3.4). For the simplicity of the analysis, the slider axis is aligned with the *y-axis* in MATLAB simulations. In Fig. 3.4b, the slider crank mechanism is shown in black while the thumb (comprises of middle and distal phalanx) is shown by the red lines. The dashed line shows the path of the linear actuator and the dotted line shows the trajectory of the thumb's tip for 16 mm displacement of the linear actuator shaft.

The velocity and acceleration of the slider-crank mechanism for the thumb circumduction and flexion are also analyzed in MATLAB. The Fig. 3.5 and Fig. 3.6 shows the position, velocity and acceleration graphs for the links SR and RE for the circumduction and flexion of the thumb respectively.

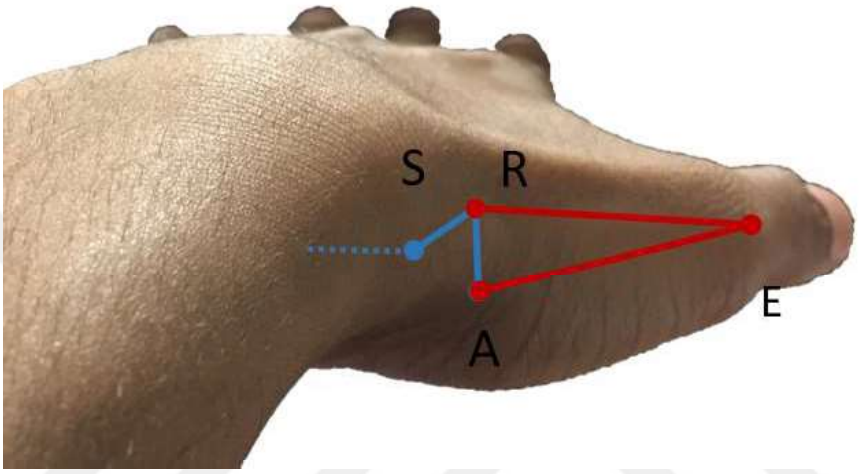

(a)

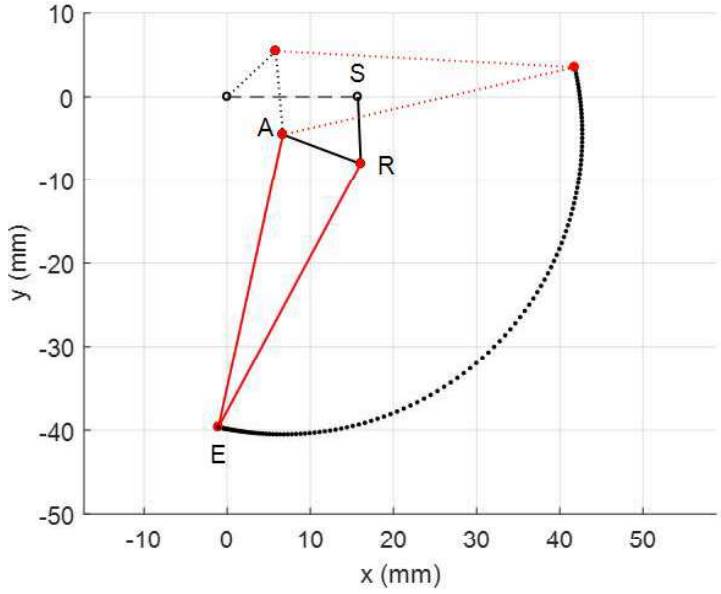

(b)

Figure 3.3: Analysis of the designed thumb circumduction trajectory during optimization process in MATLAB, slider-crank mechanism is shown in black and thumb base in red.

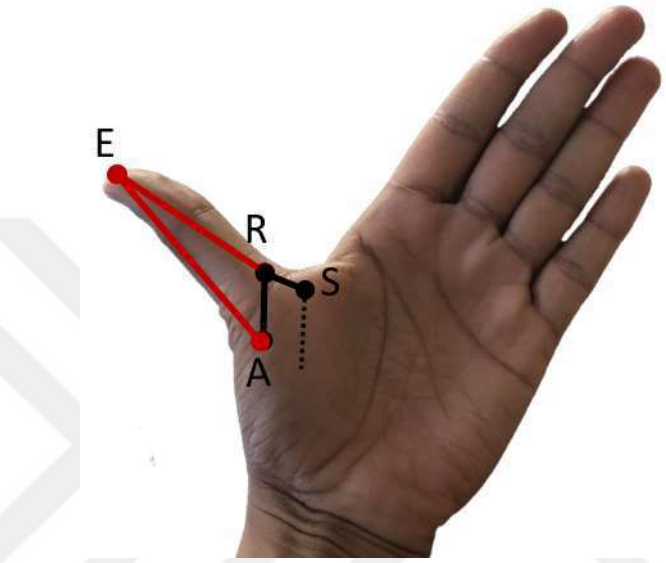

(a)

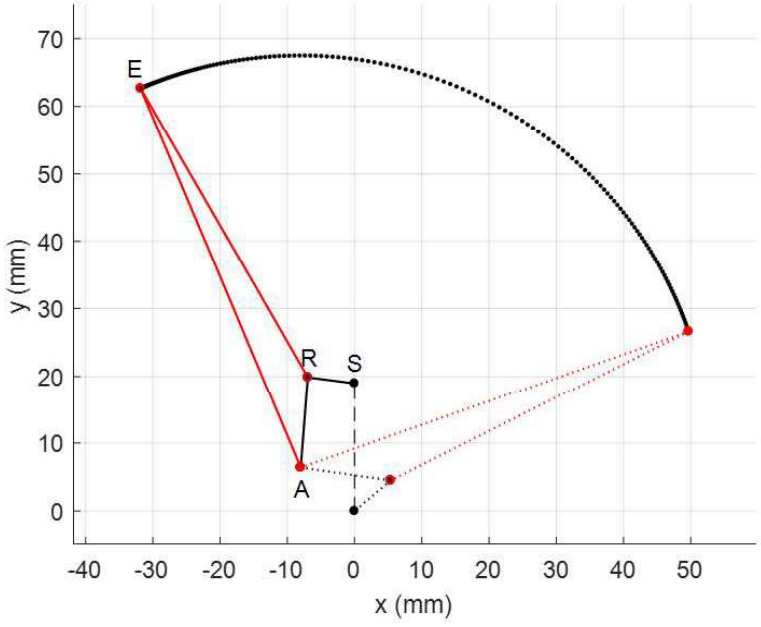

(b)

Figure 3.4: Analysis of the designed thumb flexion during optimization process in MATLAB, slider-crank mechanism is shown in black and thumb base in red.

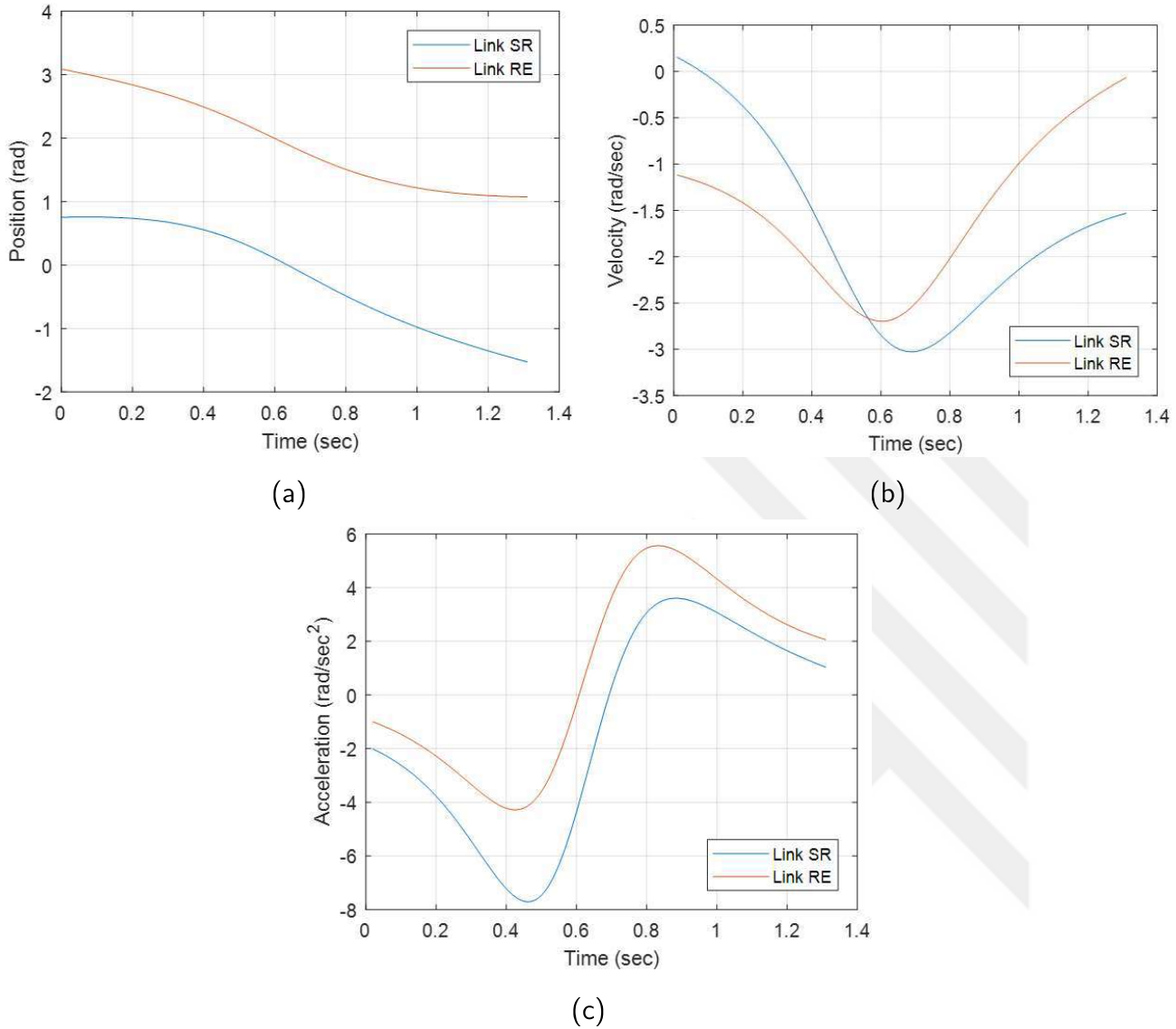

Figure 3.5: Analysis of the slider-crank mechanism of Thumb circumduction for point R (a) Position (b) Velocity (c) Acceleration

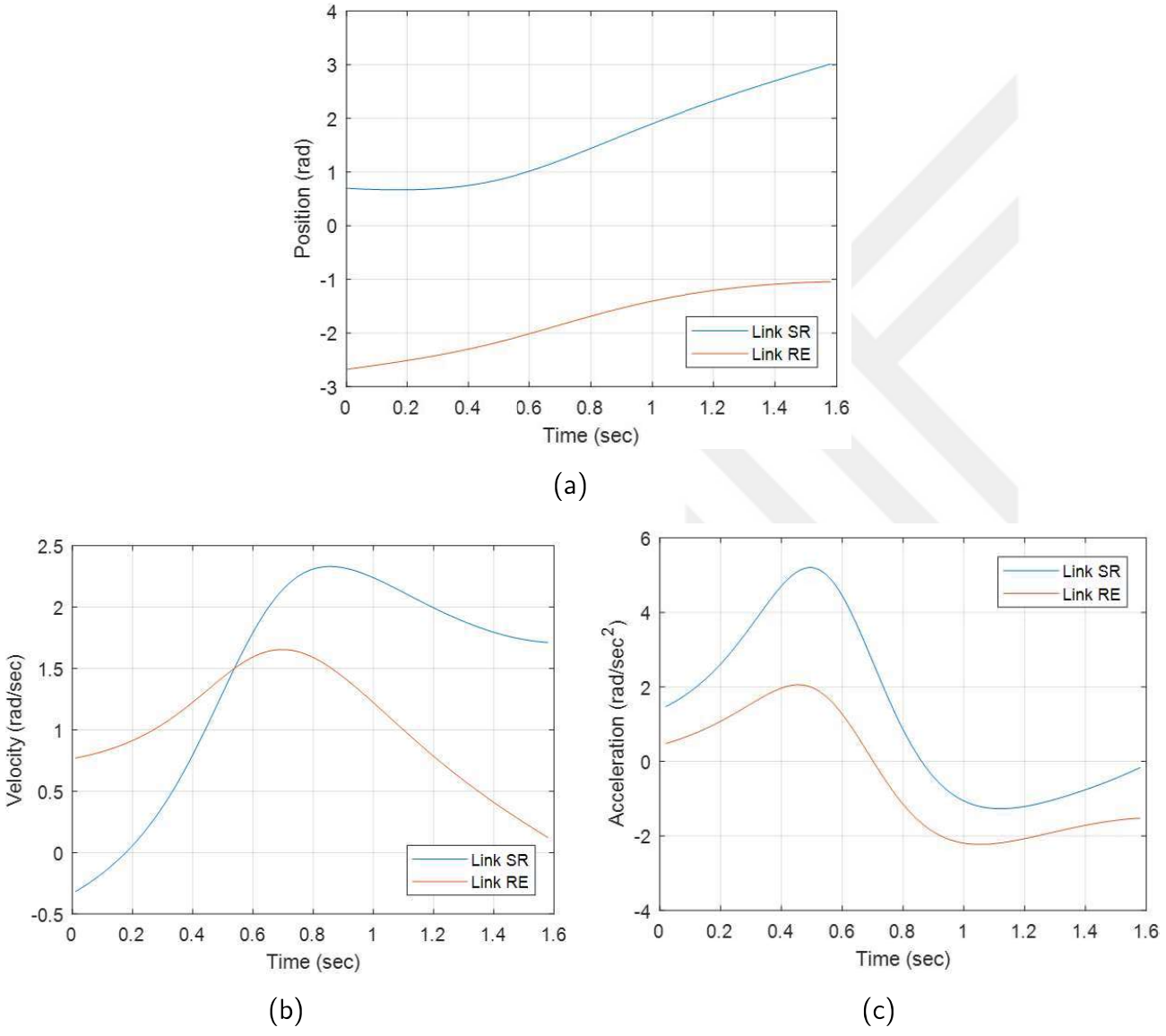

Figure 3.6: Analysis of the slider-crank mechanism of thumb flexion for the point R (a) Position (b) Velocity (c) Acceleration

Chapter 4

THE MARCAPH: DESIGN

After successfully analyzing the mechanism for the fingers and thumb the real challenge is to design the fingers with the same link's length and at the same time retain the dimension of a human hand without losing the aesthetic appearance. This chapter focuses on the designing of the parts of fingers, thumb, actuator housing, palm, and socket.

4.1 Finger Design

Since the four bar mechanism is already optimized for the flexion-extension of the finger and length of all the links is available. The only challenge is to give them shape that is strong enough to withstand the minimum load of 10 N with the 3D printing material i.e. ABS. The simulation is discussed in detail in the chapter 5. The Finger is divided into two parts: 1) The first part consists of the Inter Phalange (IP) and Distal Inter Phalange (DIP) portion and the joint in between them. An angle of 20° is fixed between IP and DIP (Fig. 4.1a). The shape of the nail and the tip of the finger is designed on the distal side of the DIP, while the proximal side of the IP is designed to attach to the distal side of the Proximal Phalange (PP) (Fig. 4.1b) and Link2 (Fig. 4.1c). The link2 is the crank or driving link of the four bar mechanism as the actuator is attached with the link2 via slider crank mechanism. The PP is the follower link of the four bar mechanism and the portion between these two links attachment forms the coupler link.

The PP made hollow from the inside to accommodate the link2 and allow it to drive the mechanism. The proximal side of the PP and link2 is attached to the actuator housing (Fig. 4.1d and Fig. 4.1e). The actuator housing serves as the fixed

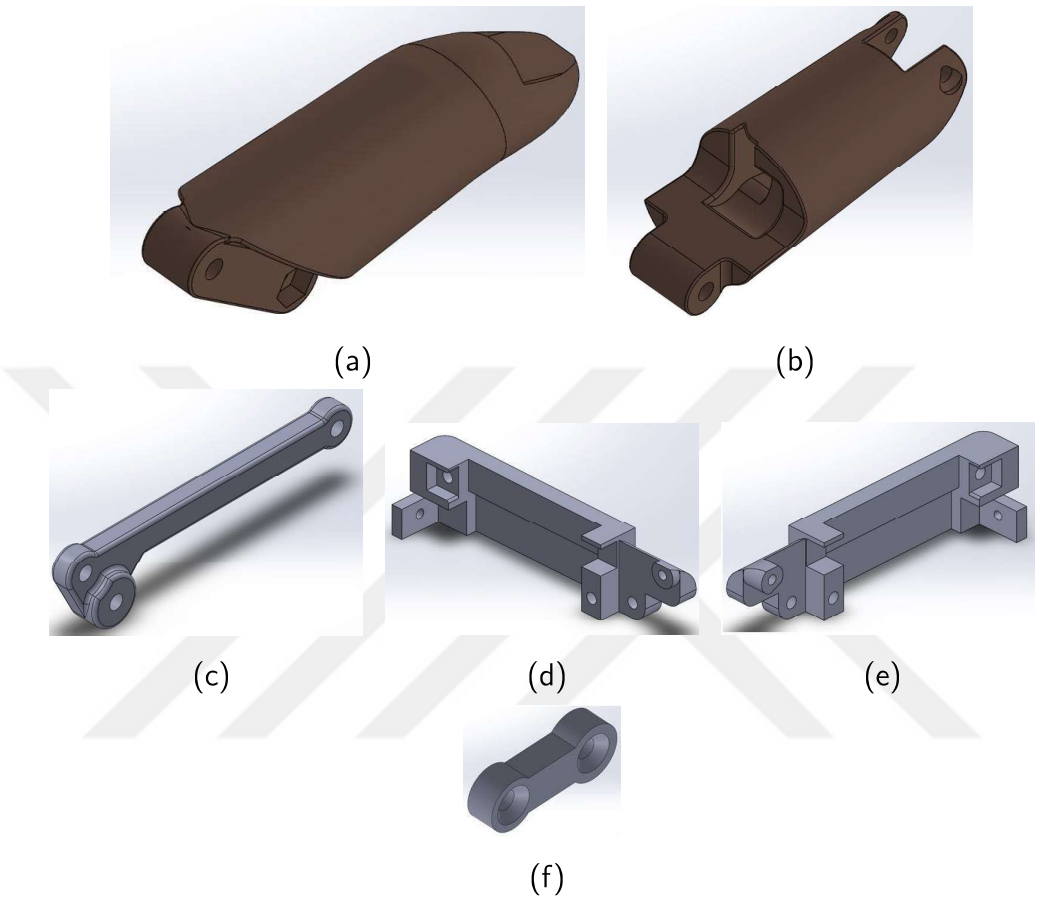

Figure 4.1: The parts of the final designed finger (a) Finger PIP and DIP (b) Finger MCP (c) Finger Link 2 for four bar mechanism (d) The auxiliary link to connect the four bar mechanism to linear actuator and form slider crank mechanism (e) The housing for actuator left side (f) The housing of actuator right side

link of the four bar mechanism. The Link2 (Fig. 4.1c) contains two holes at the distal side. One for the ground or fix link of the four bar mechanism (i.e. Actuator housing) and the second hole is for the attachment of the coupler link (Fig. 4.1f) of the slider crank mechanism (Fig. 4.2a). The portion of the link2 between these two attachment holes forms the crank of the slider crank mechanism. The other end of the coupler link is attached to the shaft of the linear actuator. The Fig. 4.2a shows the assembled finger with transparent PP and actuator housing. The slider-crank mechanism and four bar mechanism is shown on the top of the finger to understand the mechanism

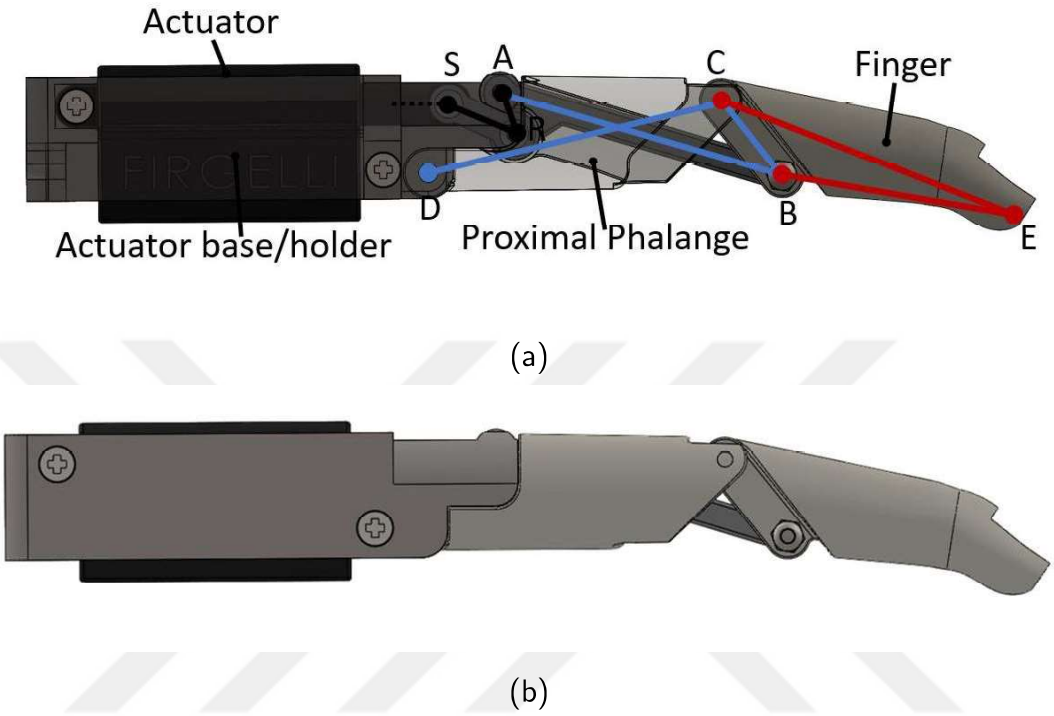

Figure 4.2: The finger assembly, (a) The four bar and slider crank mechanism is shown on the top of the finger assembly. (b) The complete finger assembly.

of the complete finger. The Fig. 4.2b contain the complete CAD assembly of the designed finger.

4.2 Thumb Design

The thumb is consists of two slider-crank mechanisms, one for the circumduction and another for the flexion-extension of the thumb. The Fig. 4.3 shows the parts of the thumb. The thumb DIP and IP portion are fixed at an angle of 20°. A nail like feature is designed on the distal portion of the thumb, to give an aesthetic look to the tip of the thumb. The proximal portion of the thumb is designed to attach to the thumb's base (Fig. 4.3b) and with the connecting link (Fig. 4.3d). The segment between the attachment holes of the thumb base and connecting link forms the crank of the slider crank mechanism. The connecting link is attached to the linear actuator

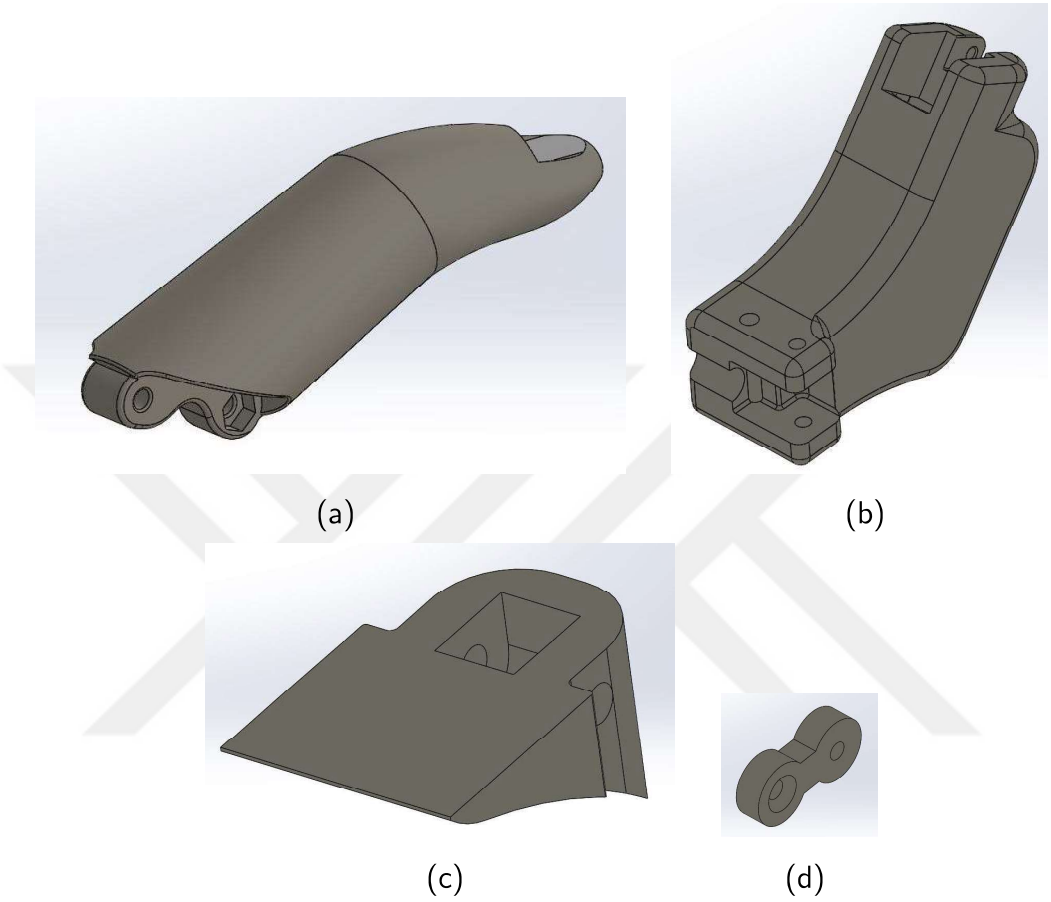

Figure 4.3: The part of the thumb (a) DIP and IP forming the thumb (b) Thumb base holding the actuator for thumb flexion-extension. (c) The thumb base cover to hold the linear actuator inside the thumb base. (d) The connecting link for the thumb flexion-extension slider crank mechanism.

at the other end. The Fig. 4.4a shows the complete assembly of the thumb, with the slider-crank mechanism shown in black and the tip of the thumb shown by the red lines from the crank end points. The ready to print assembly is shown in the Fig. 4.4b. The thumbs axis for the flexion-extension is shown with a black dotted line on the shaft of the linear actuator and the circumduction axis is shown by the dark blue dotted lines (Fig. 4.4a).

The circumduction of the thumb is also achieved by the slider-crank mechanism (Fig. 4.5). The base of the thumb has two holes at the bottom side, one is for the

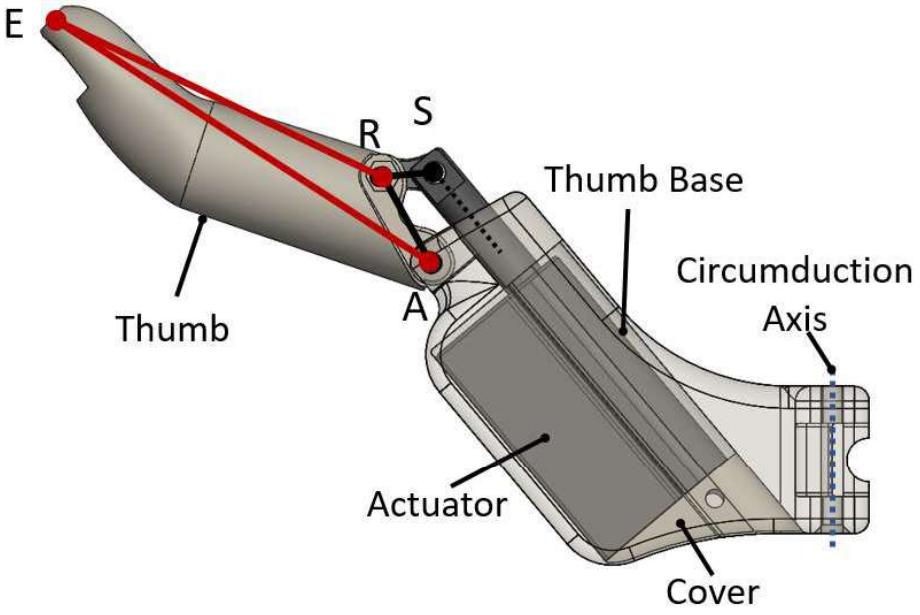

(a)

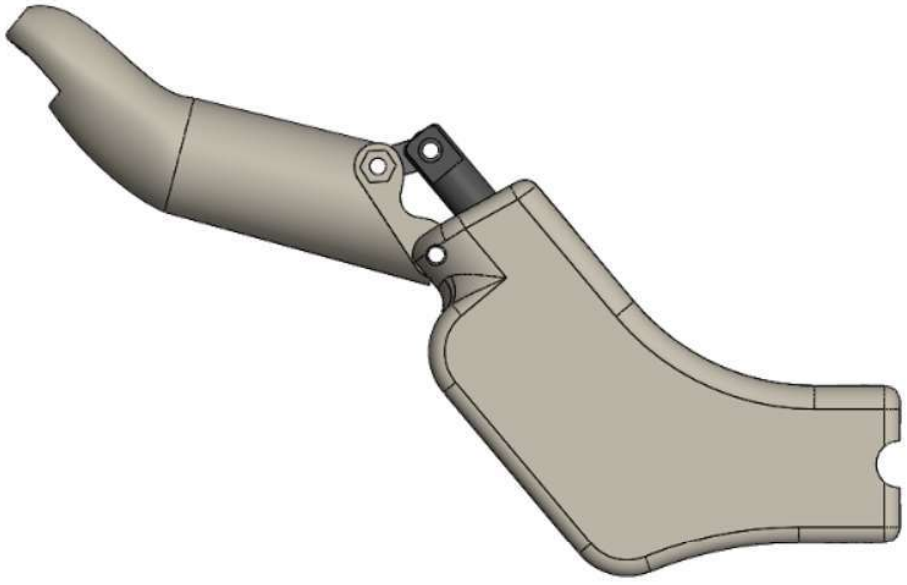

(b)

Figure 4.4: Thumb CAD

attachment of the palm with the thumb base, hence, forming the thumb circumduction axis and another one is for the attachment of connecting link. The segment

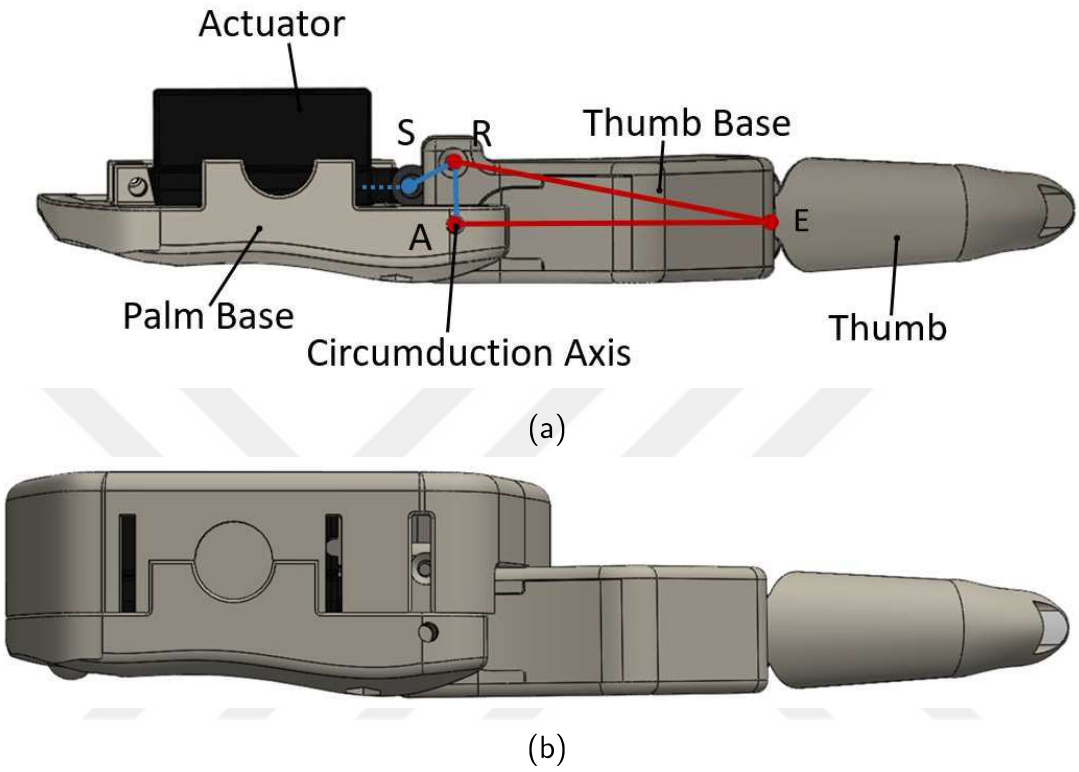

Figure 4.5: Thumb Circumduction (a) The thumb is shown from the bottom side of the hand without the palm cover. The slider crank mechanism is shown in blue and the base is shown in red. (b) the thumb assembly with the palm cover and palm base

between these two attachment forms the crank link of the slider-crank mechanism. The connecting link is also attached to the shaft of the linear actuator which in turn transmits the translation of the actuator to the base of the thumb. The two positions, opposed and non-opposed) of the thumb can be seen in the Fig. 4.6.

4.3 Palm Design

The palm is the most influential part of the hand as it accommodates the fingers and thumb with their actuators and mechanism to give them the shape of a hand. In conformity with the human palm, following characteristic has been adapted to mimic the human hand appearance. 1) An angle of 3° is introduced between the

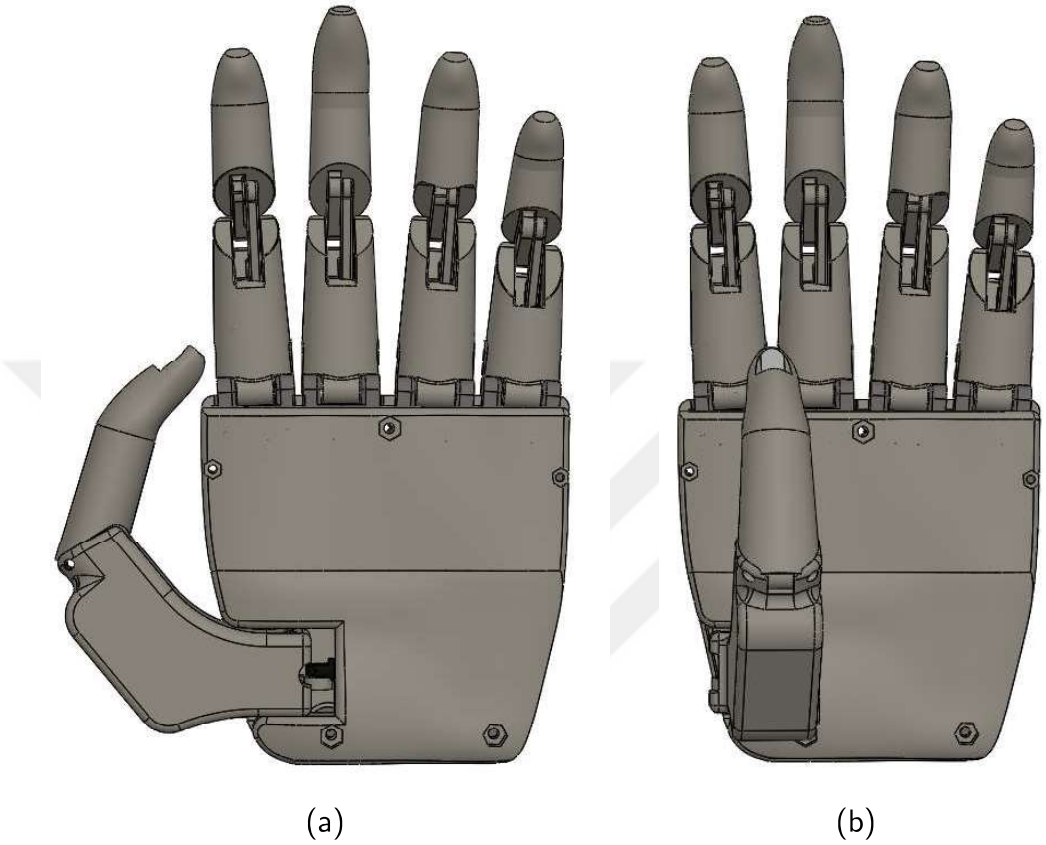

Figure 4.6: 3D CAD model of MARCAPH. Thumb in (a) Non-oppose position (b) Opposed position.

index, middle, ring and little finger, by considering the middle finger as a reference point. 2) Instead of varying the position of the finger base, all the fingers are designed separately with different length. 3) The actuator for circumduction is placed at the bottom portion of the palm and the rotation axis is placed beneath the middle finger actuator. 4) The fingers and thumb are in the same plane when the thumb is fully adducted. 5) The thumb plane is in between the index and middle finger when the thumb is fully abducted. Furthermore, the palm thickness near the thumb attachment and the lower side is slightly increased, as compared with the rest of the palm, to mimic the shape of the human palm (as shown in Fig. 4.7a and Fig. 4.7b). The proximal portion of the palm cover contains a half portion of the bolt housing use

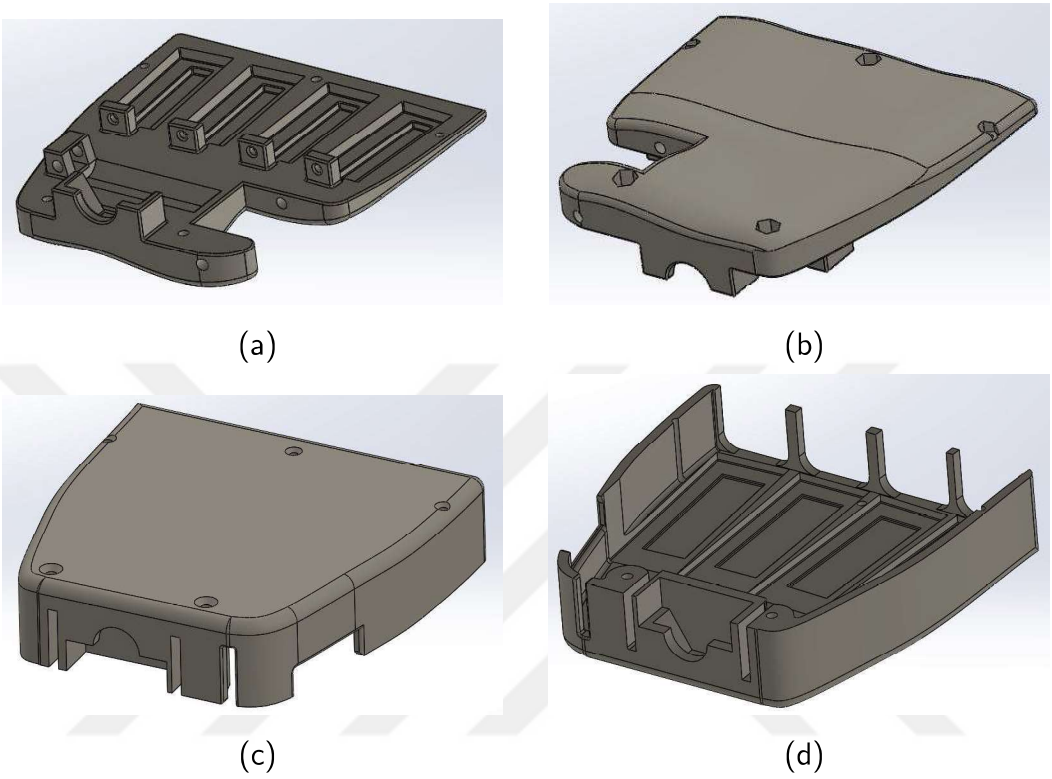

Figure 4.7: The Palm and Cover (a) Isometric top view of the palm shows the groves for the actuator and its housing (b) Isometric bottom view of the palm shows the free form surface has been designed to give palm aesthetic appearance (c) Isometric top view of the palm cover and (d) Isometric bottom view of the palm cover shows the groves design for the actuator and its housing, also the spacer between the finger can be seen in this view.

to attach the socket to the hand. The cover of the palm is designed to support the actuator housing and it also holds the remaining half portion of the housing of bolt required to attach the socket to the hand (Fig. 4.7c and Fig. 4.7d). Two screws are placed on either side of the housing to ensure the firm grip of the bolt by the palm and its cover. The slits on either side of the bolt housing are specifically designed to pass the cables and wires required to control the actuator and sensors. To ensure the 3° angle between the fingers, the spacers are designed at the distal side of the palm cover that separates the fingers at required angle. Also, the grooves at the palm cover ensure the holding of the actuators and their housing during the actuation process.

4.4 Socket Design

Socket design is critical, as it is the main interface between the amputee and the prosthetic hand, that also encases all the electronics, battery and the residual limb. The comfort and effectiveness of the prosthetic hand depend on how snugly it fits on the amputee residual limb. The placement of the battery and circuitry adds weight to the center of the socket mimics the forearm and ease the wearer due to uniformly distributed weight, instead of a having heavy prosthetic hand. To place the battery and control circuitry inside the socket. The socket is divided into two chambers; one for holding the battery and second to hold the control circuitry Fig. 4.8. In order to place the indicator LEDs and a mode control switch in an accessible location to the other limb, the control circuitry is placed on the inner side of the socket and another chamber is used to hold the battery.

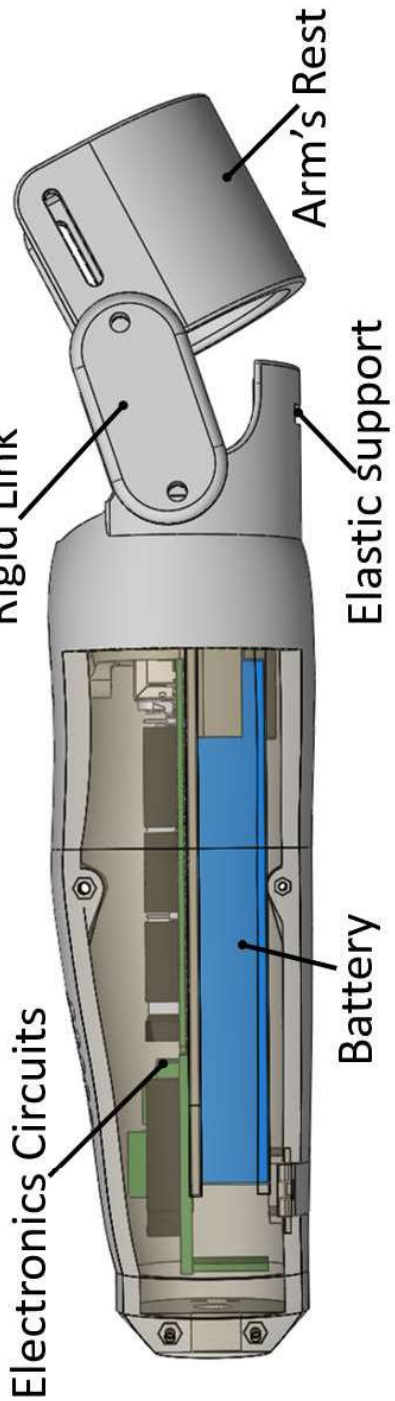

Figure 4.8: Complete assembly of socket with electronic circuits and battery.

Chapter 5

THE MARCAPH: SIMULATIONS

Finite Element Analysis (FEA) is an essential technique to optimize the parts during the design process and to ensure the stress and strain capabilities of the design prior to manufacturing. For this purpose, the fingers and thumb of the MARCAPH are analyzed using an FEA software. The fingers and thumb are analyzed in two positions; One when the finger is fully opened and second in which the finger is fully closed. If the designed finger and thumb or any part of the finger and thumb has higher stress values on the applied forces, then the design of that specific part or assembly is modified or redesigned, until unless it satisfies the required conditions of the MARCAPH. ABS material is an obvious choice for the simulation and analysis since the target of the research is to produce a high-quality prosthetic hand with low cost and manufacturing time that is access-able to a wide range of audience. For connecting pins and screws, stainless steel is selected during simulations as they are off the shelf components. The mesh size of the simulated part starts from 1 mm and reduce by 0.1 mm in each step until unless the stress values of the part is no longer change. On average, the stress values stabilized between the 0.5 mm and 0.3 mm mesh size.

5.1 The Finger

The finger of the MARCAPH is consists of two different mechanisms (four bar and slider crank mechanisms) working together to achieve the desired motion of the finger. In order to simulate the finger using FEA software, two positions of the fingers are used in which both mechanisms are locked. The Fig. 5.1a shows the finger in the full extension state. A 10 N force is applied at the tip of the finger in the *y-axis* direction,

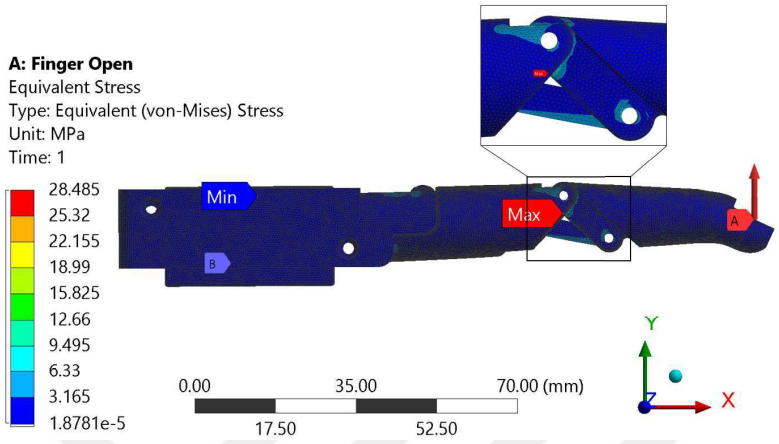

(a)

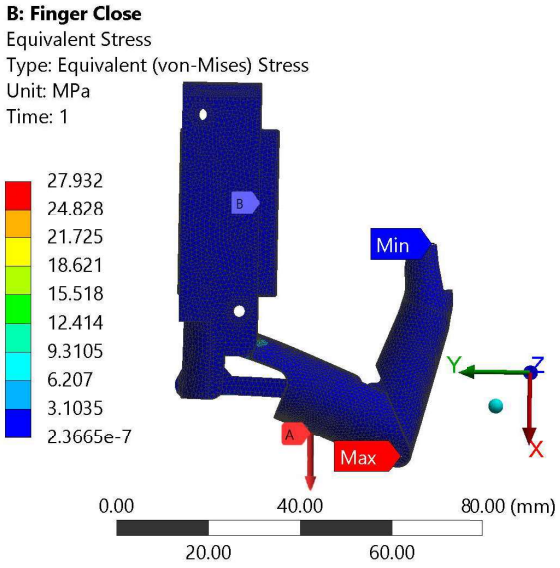

(b)

Figure 5.1: Finger stress distribution for (a) Fully opened finger at 10 N load (b) Fully closed finger at 20 N load

meantime defined the actuator and its base as a fix support. Since the finger length is 90 mm (± 10 *mm* due to the fact that each finger is designed separately to mimic the human hand appearance) it creates a torque of 900 Nmm. Despite the usage of ABS material, the finger stress value is 30% less than the yield stress of the material.

The Fig. 5.1b shows the finger in fully flexed position. A 20 N force is applied at

the proximal phalange (PP) portion of the finger due to the reason that the fingers are used in the hook grip to carry a briefcase or other shopping bags. In this simulation, the actuator and its base are used as fixed support, identical to the earlier simulation. The finger stress value is almost same as the previous simulation despite the fact that the applied force in this simulation is twice as compared to the previous simulation.

5.2 The Thumb

The thumb of the designed hand MARCAPH is consists of a thumb base and thumb tip. The actuator is connected to the thumb tip via a link forming a slider-crank mechanism. The FEA simulations are performed in fully flex and fully extend states. The simulation in fully extend state is important as it will help the user to slide the object close to the palm during a grasp. The Fig. 5.2a shows the fully extend version of the thumb simulations. The force is applied at the tip of the thumb and the circumduction axis of the thumb used as a fix support during the simulations. The maximum stress is found at the joining point of the thumb tip and thumb base. At this joint a dowel pin of stainless steel is used to increase the life of the component. The maximum stress at 10 N applied force in fully extend mode is 37% less than the yield stress of the ABS material. The Fig. 5.2b shows the thumb in fully flexed position. This position of the thumb plays an important role by putting force on the gripped object and did not let the object to slip. Therefore, in this simulation we increase the applied force on the thumbs tip up to 4 times i.e. 40 N. The maximum stress is found at the joining point of the link and thumbs tip. This joint of the thumb's tip and thumb's link is attached by the stainless screw. The maximum stress found at 40 N applied load at the tip of the thumb in fully flexed position is 35% less than the yield strength of the simulated material.

5.3 Conclusion

The Table 5.1 shows the results of the FEA simulations on the final optimized design of the finger and thumb. The finger and thumb are loaded with 10 N force in the open

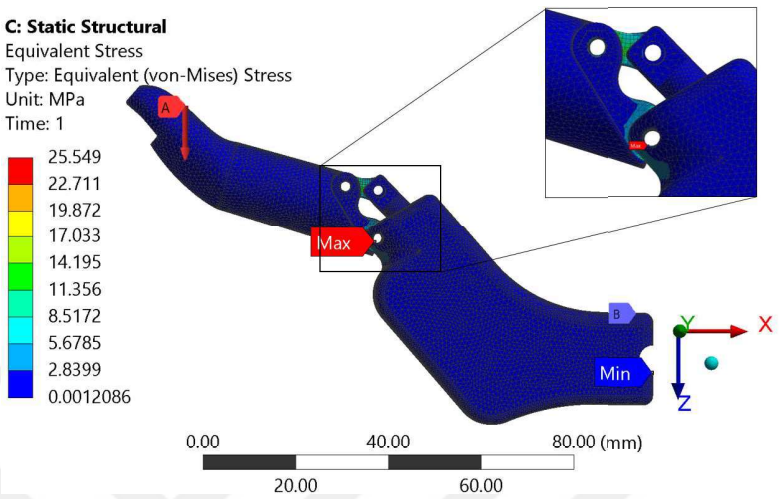

(a)

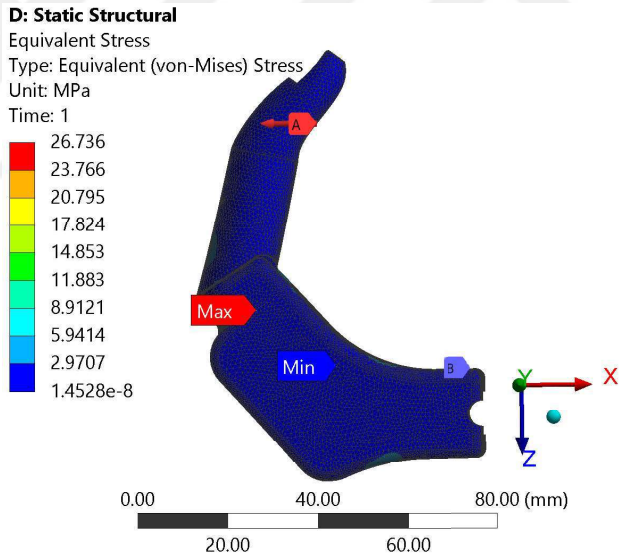

(b)

Figure 5.2: Thumb stress distribution for (a) Fully opened thumb at 10 N load (b) Fully closed thumb at 40 N load.

state. The finger is loaded with 20 N in the close state while the thumb is analyzed with a load of 40 N (twice as of a finger), due to the reason that the thumb has to bear all the forces alone in comparison to four fingers. The 10 N load at the fingertip along *y-axis* produces 28.485 MPa stress (as shown in Fig. 5.1a) and a load of 20 N at the proximal phalange portion of the finger along *x-axis* produces 27.932 MPa (as

Table 5.1: FEA Simulations Results

State	Applied Force (N)	Max. Stress (MPa)
Finger Open	10	28.485
Finger Close	20	27.932
Thumb Open	10	25.549
Thumb Close	40	26.736

Table 5.2: ABS Plastic Properties [Test Standard Labs, 2017]

Properties	Value	Unit
Density	1.04	g/cc
Tensile Strength, Yield	42.5 - 44.8	MPa
Flexural Yield Strength	60.6 - 73.1	MPa
Flexural Modulus	2.25 - 2.28	GPa
Elongation at Break	23 - 25	%

shown in Fig. 5.1b). The 10 N load at the tip of the thumb along *z-axis* produces 26.54 MPa (as shown in Fig. 5.2a) and a load of 40 N at the tip of the thumb along negative *x-axis* produces 26.736 MPa (as shown in Fig. 5.2b)

Chapter 6

THE MARCAPH: EMG SIGNAL ACQUISITION

The main focus of the research is to develop a prosthetic system for transhumeral or near elbow amputees, thus, the option for acquiring sEMG signal is limited to triceps and biceps muscles. This also limits the no. of electrodes to 2, one for each muscle, as compared to the freedom of placing several electrodes on the forearm in the case of transradial or near wrist amputation [Tenore et al., 2007]. This section discusses in detail the acquisition of sEMG signal from triceps and biceps muscles and control scheme of the MARCAPH.

6.1 EMG Signal

Electromyogram (EMG) is the electrical activity produced by a contracting muscle. EMG signal is extensively used in the field of rehabilitation, biomechanics, orthopedics, ergonomic product design and prostheses. Due to the fact that EMG allows to directly look into the muscle and measure the muscular performance. It also helps in decision making both before and after surgery. The basic functional element that is responsible for producing the EMG signal is called the motor unit (MU). The MU consists of an $\alpha - motorneuron$ that has cell body in the spinal cord and extends its axon from the spinal cord to the skeletal muscle fiber (as shown in the Fig. 6.1), where it innervates and forms a junction, usually called motor end-plates.

The signal from the α-motorneuron causes depolarization in the muscle fiber that travels in either direction from the junction and creates a potential difference. This difference is measured by the electrodes. The muscle fibers connected to a single neuron react together and hence termed as Motor Unit. The signal generates by the MU is called motor unit action potential (MUP). The resulting EMG signal is the

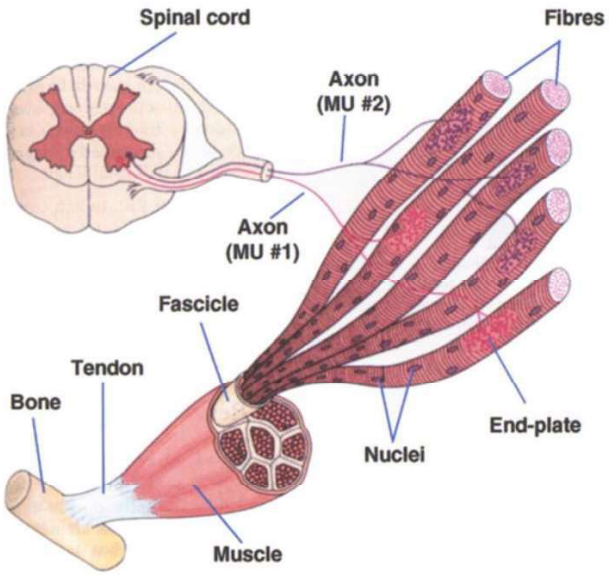

Figure 6.1: A typical $\alpha - motorneuron$ extend from the spinal cords and ends at the motor end-plates in the skeleton muscle fiber [Muzumdar, 2004]

sum of all activated MUs during the contraction of that muscle. When the signal is acquired using surface electrodes the signal has to travel through the remaining tissues before reaching the electrodes. This traveling of the signal results in the decaying of the signal amplitude.

6.2 EMG Signal Acquisition

The signal generates due to the contraction of the muscle can be detected by placing the electrode on the surface of the muscle. The electrode placement is the main challenge in the acquisition of the surface EMG (sEMG), as the strength of EMG signal varies significantly if the electrodes are slightly displaced from the previous position [Hermens et al., 2000]. In this research, the electrodes have been placed on the triceps and biceps muscles. The placement on the triceps muscle is quite a challenge due to its small size. We searched the spot on the subject for the best EMG signal acquisition. The signal detects by the surface electrodes can be seen in the

Fig. 6.2a and termed as a raw EMG signal.

The raw EMG signal is then passed through an instrumentation amplifier with high common mode rejection ratio (CMMR). The instrumentation amplifier is configured in differential amplification mode to eliminate the noises using the CMMR feature. The gain of the instrumentation amplifier is set as high as 1000 to amplify the minute EMG signal, as the typical EMG signal amplitude measures around 100 μV. After successfully eliminating the common noises and amplification, the amplified EMG signal is passed through a bandpass filter of a low cutoff frequency of 450 Hz and a high cutoff filter of 10 Hz for further filtration. This filtered EMG signal is then passed through a notch filter to eliminate the 50 Hz line frequency. The final filtered EMG signal is then rectified and passes through a smoothing filter to obtain the processed EMG signal. This signal is then used by the controller to execute the control algorithm. The Fig 6.3 shows the flow of the EMG signal acquisition and process while Fig. 6.2 shows the EMG signal obtained at each step of the EMG signal acquisition i.e. after the acquisition, then filtration, then rectification and then smoothing process (moving average filter and RMS).

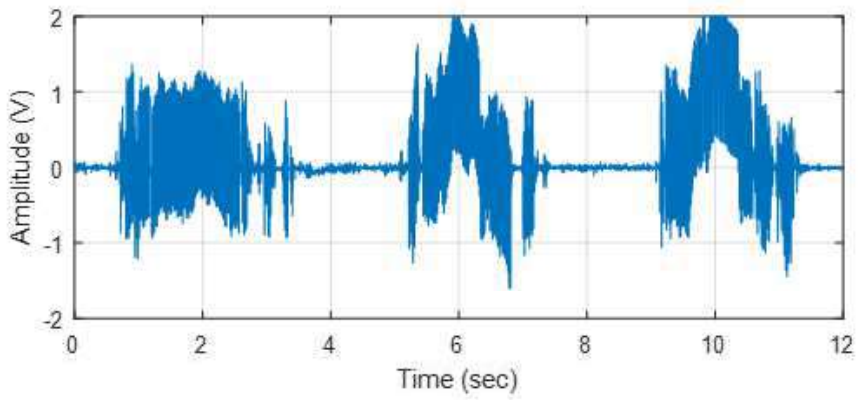

(a)

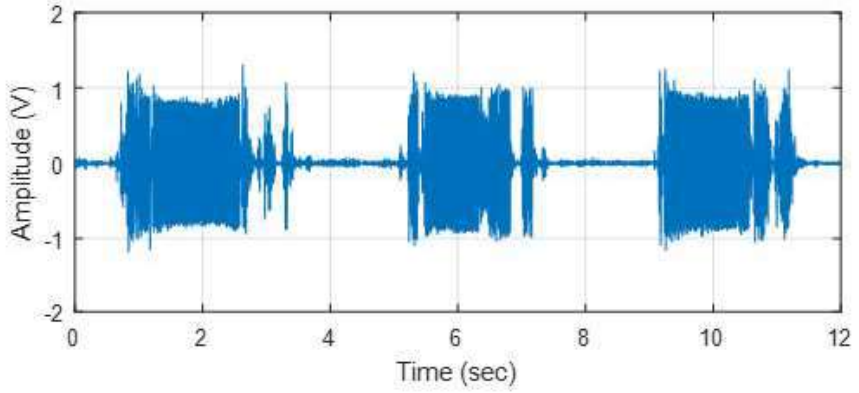

(b)

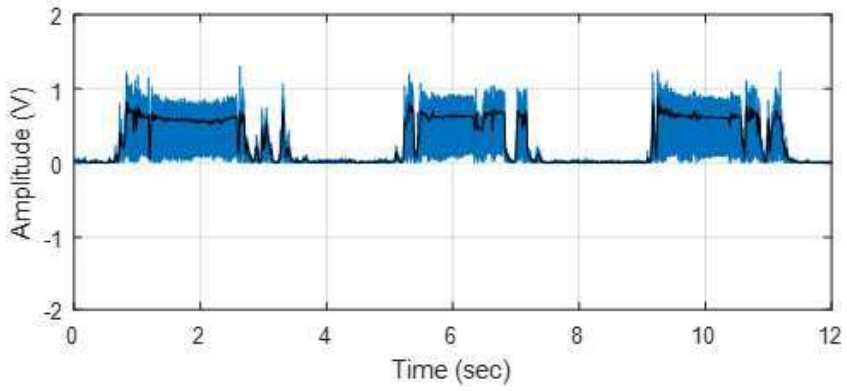

(c)

Figure 6.2: The EMG signal at every step of the EMG signal acquisition (a) Raw EMG of three biceps contraction (b) EMG signal after filtration process (c) Rectified EMG signal in blue and EMG signal after smoothing filter in black

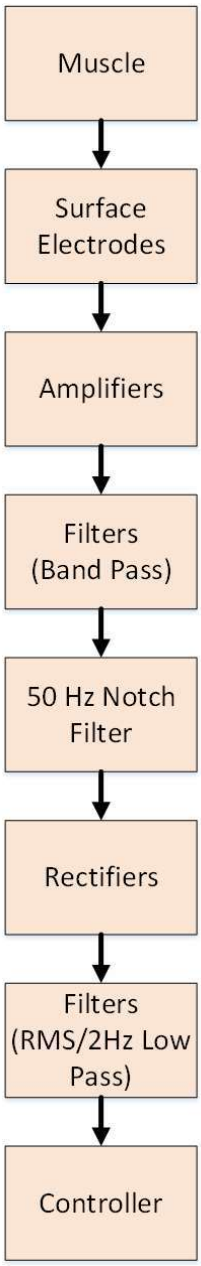

Figure 6.3: sEMG signal acquisition flow chart.

Chapter 7

THE MARCAPH: CONTROL SCHEME

The controlling of the prosthesis is quite difficult due to the fact that each amputee has different sets of muscles in the residual limb, that can be used to drive the prosthesis. The most common technique used in state of the art research and commercial prostheses is a Finite State Machine (FSM) based control scheme. A typical FSM control scheme uses EMG signals from two distinct muscles, usually, wrist flexion-extension, to open and close the hand. The user can switch between the states of the FSM by co-contracting the muscles which normally used as the trigger for switching states [Bionics, 2017] [Medynski and Rattray, 2011] [Controzzi et al., 2016]. Segil et al. [Segil et al., 2014] developed a technique called Postural controller in which they use EMG signal from ulnar deviation with the existing EMG signals of wrist flexion and extension to control the states of the prosthesis. In this technique, the amputee can select six grips instantaneously, three grips by contraction of the individual muscle and three grips by the co-contraction of any two muscles. Since our targeted amputees are near-elbow or transhumeral amputees, thus, acquiring EMG signal from three distinct muscles is impossible. In This chapter discuss a typical FSM followed by the modified FSM to reduce the training time and at the same time reduce the stress on the transhumeral amputee by avoiding the co-contraction of the biceps and triceps muscles. Then the chapter focuses on the control flow of the algorithm.

7.1 Finite State Machine

The typical control scheme of a prosthetic hand consists of a finite state machine with a trigger to switch the state. Normally, the trigger consists of the co-contraction of the two muscles (extensor and flexor muscles of the wrist). The contraction of

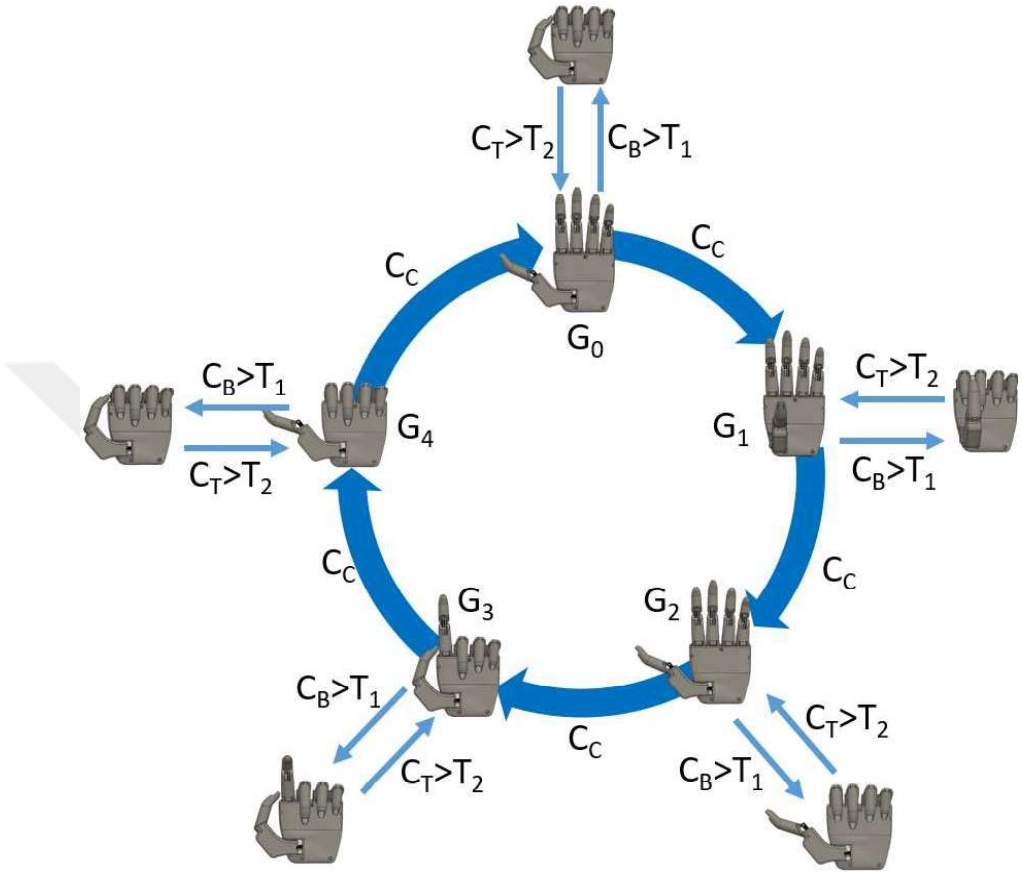

Figure 7.1: Finite State Machine (FSM) with 5 essential grips for ADL. The trigger C_C is used to switch the states, biceps signal C_B to close the hand and triceps signal C_T to open the hand.

one muscle is used to control the opening and contraction of other muscle is used to control the closing of the hand in that particular state. The opening and closing action will be executed only when the processed sEMG signal passes the set threshold level. The threshold level is set according to the strength of the sEMG signals of the user [Segil et al., 2014].

Initially, a finite state machine common among most of the prosthetic hand has opted. Later, a unique finite state machine is programmed according to the need of the subject (Fig. 7.1). The MARCAPH finite state machine consists of five different grips, the grips can be switched with a trigger signal C_C. Upon switching a grip,

the MARCAPH positions the fingers (including the thumb) according to the grip and hold the position until the next trigger occurs. The biceps contraction C_B above the threshold T_1 closes the hand while triceps contraction C_T above threshold T_2 opens the hand. A brief description of the fingers and thumb positions in each grip is as follows;

7.1.1 Non-Opposed Grip G_0

The thumb is in the same plane as the fingers and makes a flat hand when in open state. Upon close signal, all fingers and thumb close simultaneously. This grip is the combination of lateral and hook grip and can be used for both purposes.

7.1.2 Power Grip G_1

In this grip, the thumb moves and become opposite to the index and middle finger. This grip is the most commonly used grip for ADL. Upon close signal, all fingers and thumb close together and remain close until the open signal is received.

7.1.3 Hook Grip G_2

In hook grip, the thumb moves back to non-oppose position and remains open. All the fingers will close and open upon the close and open signal from the controller.

7.1.4 Index Pointing G_3

In this grip, all fingers and thumb except index finger close. Upon close signal, index finger closes partially and can be used for typing purposes. Upon open signal, the index finger will open completely and can be used for pointing purposes.

7.1.5 Lateral Grip G_4

The lateral grip is used to hold the card or paper with the help of thumb. In this grip, all the fingers close and only thumb remain open in non-oppose position. The open and close signal is used to open and close the thumb to hold the object.

The subject, near elbow amputee, found the triggering mechanism quite difficult, due to the fact that the co-contraction of the biceps and triceps muscles is difficult as compared to the co-contraction of the wrist flexor and extensor. In order to comfort the subject, a triggering button is added in parallel with the existing triggering mechanism. This allows the subject to switch finite state machine manually and avoid any damage to the subjects muscles due to excessive contraction and fatigue.

7.2 The MARCAPH FSM

The initial FSM developed in the MARC is discussed in the previous section. It uses EMG signals of two muscles, one for opening and another for closing the hand and co-contraction to change the grip mode. Since the EMG signal acquisition site, in our case, are the biceps and triceps, thus achieving co-contraction was not an easy task. To cope with this issue, we used the technique of multiple threshold level detection [Roche et al., 2014]. Therefore, in the updated version of MARCAPH FSM, the triggering mechanism is modified and replaced by a single activation of the triceps muscle and the double threshold levels is introduced for biceps contraction while keeping the FSM states and their sequence intact. The MARCAPH FSM can be seen in the Fig. 7.2. The threshold level T_1 is set at 50% of the full biceps muscle activity and T_2 is set at 75% of the full biceps muscle activity. Also, a threshold level T_G for triceps is set at 50% of full triceps activity. The trigger level T_1 is used for the closing of the hand and trigger level T_2 is used for the opening of the hand. The reason behind setting the low threshold for closing and high threshold for opening is that during holding an object if there is mild muscle activity, the control algorithm will do nothing, contrary, if lower threshold is for opening, the residual hand's mild muscle contraction during holding activity may release the object as control algorithm read this mild contraction as an open signal. This may lead to falls and losing of the gripped object. In our case, the user has to perform an intentionally stiff contraction than normal to release the object by performing the opening of the hand. The final version of the MARCAPH FSM contains five states similar to the first version. Since

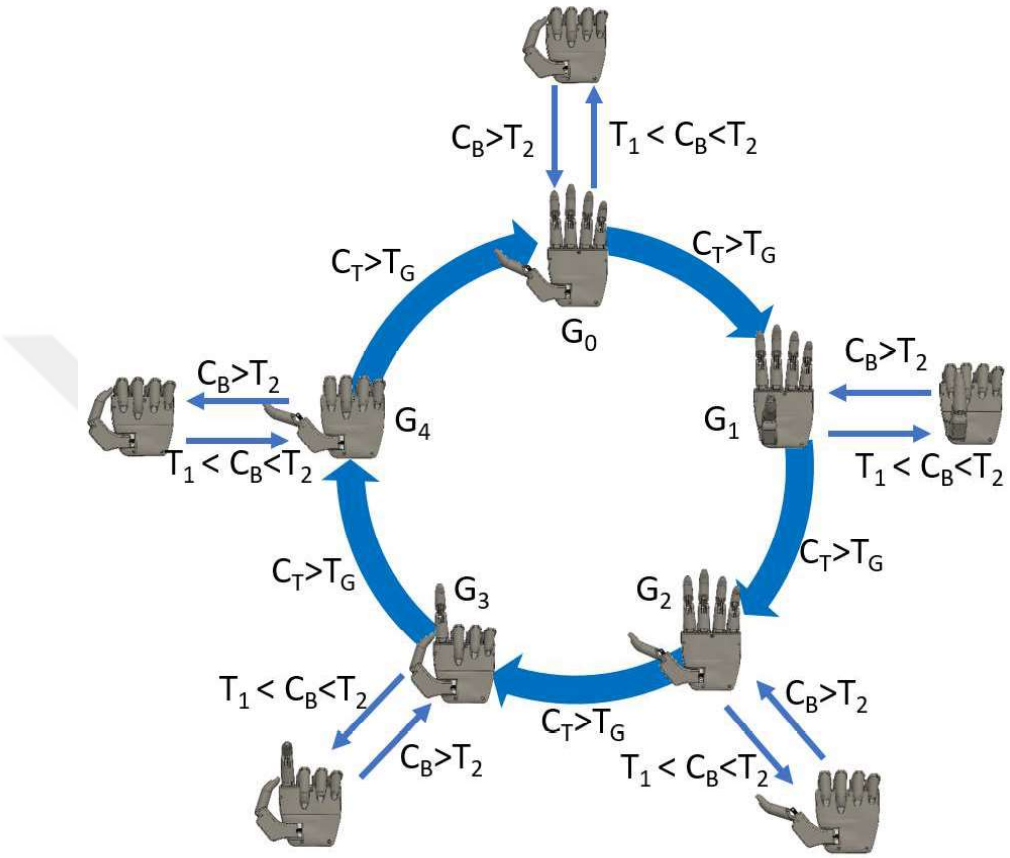

Figure 7.2: MARCAPH FSM: The trigger T_G is achieved by the contraction of triceps C_T. The double level threshold technique is implemented on the biceps C_B. A close operation will be performed when the biceps contraction level is in between the trigger T_1 and T_2. An opening of the hand will be achieved when the biceps contraction level is higher than the T_2 trigger.

the control algorithm has the ability to adapt and customize according to the need of the user and MARCAPH has the ability to perform most of the ADL, more states can be added or remove from the FSM.

7.3 The Control Algorithm

In order to control the prosthetic hand in real-time, the sEMG signals from the triceps and biceps muscles are used as input to the control algorithm (shown in Fig. 7.3). The

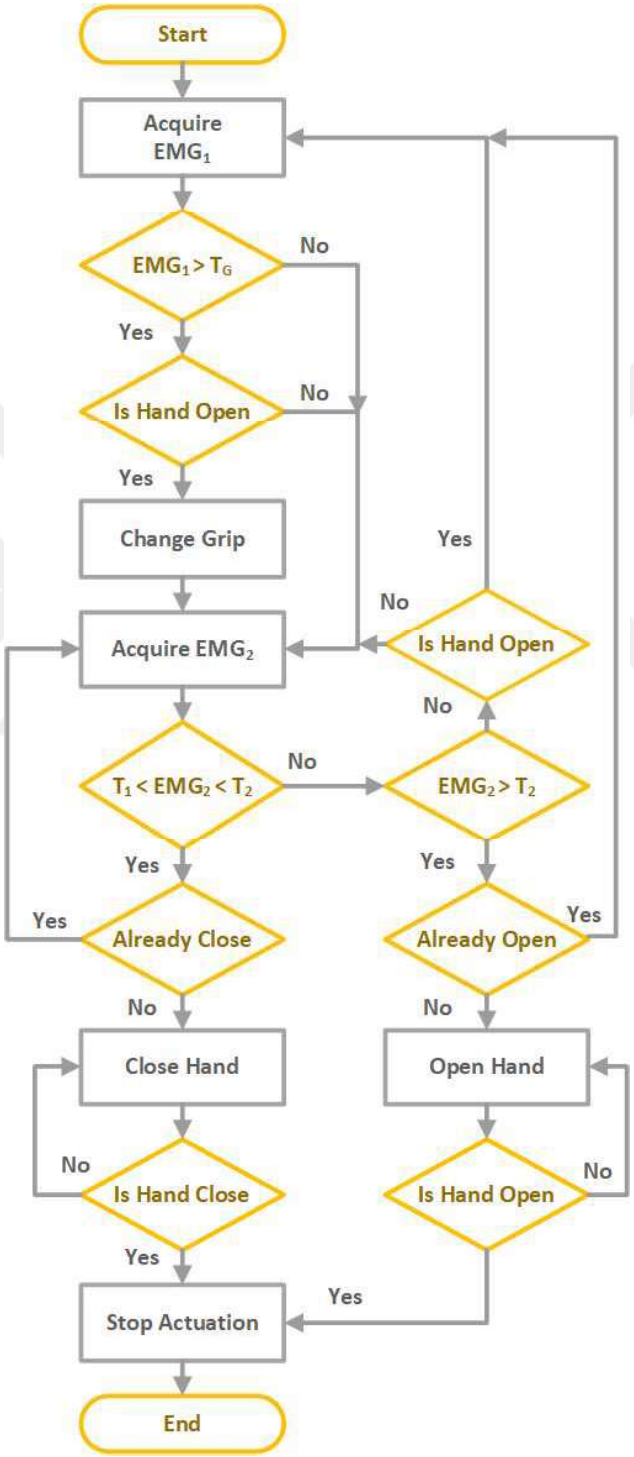

Figure 7.3: Control Flow chart

triceps signal is labelled as EMG_1 and biceps signal is labelled as EMG_2. Since the co-contraction of the triceps and biceps muscle is quite difficult, and subjects having a weak triceps muscle, the control algorithm is designed to switch grips with the triceps muscle actuation. A double threshold level detection is applied to the biceps muscle for opening and closing of the hand. The threshold level to change the grip is T_G, while threshold level requires to close the hand is T_1 and threshold level requires to open the hand is T_2. The T_2 is less than T_1 while the T_G value is in between the T_1 and T_2. The control algorithm first checks the input EMG_1 signal with T_G. If the T_G is smaller than the EMG_1, the algorithm changes the grip mode from 1 to 2, if the T_G is greater than the EMG_1 the algorithm will remain in the current grip mode. After evaluating the EMG_1 for the grip mode, algorithm will check whether the EMG_2 value lies in between the threshold levels T_1 and T_2, if yes then the algorithm will check whether the hand is already in close state or not. If the hand is in the close state, the algorithm will not perform any operation and refer back to the acquisition of EMG_1 signal and if the hand is not already in the close state the algorithm will perform the close operation until the hand is completely closed. And if EMG_2 signal has higher value than the threshold T_2, the algorithm will check whether the hand is in open state or not. If the hand is open state no operation will be performed and the algorithm will refer back to the acquisition of EMG_1 signal. If the hand is not in open state, an open operation will be performed on the hand until the hand is completely opened.

Chapter 8

THE FEEDBACK SENSOR

This chapter presents a fingertip force transducer for the detection of contact forces using the optical technique in a prosthetic hand. Prosthetic hand, requires continuous interaction with its surroundings, is suitably in need of a sensor to monitor the contact forces. For a human hand, during a grasp, the tip of the finger is in contact with the object and the feedback force is transmitted to the finger base via Distal Inter-Phalangeal (DIP) Joint. Therefore, a monolithic flexure based semi-rigid joint is introduced in place of the DIP Joint. The deflection of semi-rigid joint, upon force exertion, can be detected using the optical technique. The optical technique is immune to electromagnetic interference, lightweight and requires simple electronics. Simulation conducted using Finite Element Analysis (FEA) software leads to the manufacturing of designed sensor. The Manufactured sensor is calibrated using a multipoint calibration and curve fitting technique. The analysis and results ensure the robustness and capability of the designed sensor to be used as the feedback contact force sensor for the prosthetic hand.

8.1 Introduction

The human hand can adopt different grasps and movements naturally to achieve complex and sophisticated daily life tasks. In order to achieve these tasks, human brain monitors and regulates the force exerted by the finger on the object. Although the artificial hand has evolved a long way in mimicking the mechanism of the human hand, nevertheless, it continues to lack an intelligent and robust feedback mechanism to accomplish fundamental daily life tasks. Researchers have acknowledged this gap by building feedback sensors [Sani and Meek, 2011][Shams et al., 2011]

[Palli and Pirozzi, 2011] [Stachowsky et al., 2016] to detect force, pressure, slipping and position sensors.

Sani et al. [Sani and Meek, 2011] used the Avago optical sensor to detect the slipping of the object which is in contact with the finger. The performance of the proposed technique varies with the properties of the surface in contact. Moreover, they tested the sensor for flat surfaces and there is no data for the irregular shaped surfaces. Sarmad et al. [Shams et al., 2011] used a similar sensor to detect the force by mounting the sensor on a cantilever that is connected with the flat surfaces in a box via spring. The displacement detects by the sensor can be translated into 3 DOF force using the stiffness of the spring. The modular approach adopted in the designing of the sensor introduce interference error, hence, a monolithic approach is proposed for sensor design.

Palli et al.[Palli and Pirozzi, 2011] uses the angle-varying radiation pattern of LEDs and responsivity pattern of photodetectors to detect the feedback force. The designed sensor detects tension in the tendon to control the position and gripping force of UBH-IV hand. However, the designed sensor is limited to tendon based systems only. Stefan et al.[Schulz et al., 2011] compared the Force Sensor Resistor (FSR) with the bend-sensor and the Vincent bend sensor. The Vincent sensor, a modified version of flex sensor, shows promising results for partial hand prosthesis control. However, the comparison is limited to two-mode control of the partial prosthetic hand.

Paul et al. [Chappell and Elliott, 2003] developed a capacitance based contact force sensor. The sensor comprises of two capacitance discs with an elastic dielectric material between them. The bottom disc is fixed to the anterior side of distal phalanx while the top disc is designed to move back and forth. The relative motion between the discs allows detection of the contact force. The sensor performed well for up to 20 N, though, it can only detect the forces applied to the center of the anterior side of the fingertip (i.e. the location of the sensor itself). The contact forces which are not in that particular position cannot be estimated, hence, the forces outside the contact area of the sensor went unnoticed.

In this paper, a transducer design is presented for the detection of feedback contact forces in general. A monolithic finger is designed which comprises of the distal phalanx, intermediate or middle phalanx, and distal inter-phalangeal (DIP) joint. The design integrates a flexure or semi-rigid link as the DIP joint between the distal phalanx, and middle phalanx, such that any contact force on the fingertip may result in the flexure deflection and is measured accurately without the fear of having the sensing area being different from the contact area on the fingertip. The paper begins with the description of the overall transducer design; this section contains the description of the optical technique used for sensing the flexure's deflection, the flexure design process, and technique used to communicate with the transducer. Section 3 discusses the FEA simulation results of the designed flexure. The following section explains the calibration and integration process of the photocoupler and design flexure, followed by the discussion of the experimental results. Finally, the advantages and outcomes of the designed transducer are discussed and future work is proposed.

8.2 The Transducer

The transducer consists of a sensing element, interface electronics, and flexure hinge. The sensing element is further divided into photocoupler, which consists of a light source and light detector, and a light interrupter or beam blocker. The photointerrupter and photocoupler are placed opposite to each other in a way that the slightest deflection of the flexure can cause the blockage of the light falling on the light detector (as shown in Fig. 8.1).

8.2.1 The Photointerrupter

There are many techniques to detect the force by detecting the deflection of the beam. The strain gauge [Liang et al., 2009] is the most common type, it is usually used in the Wheatstone bridge configuration. Due to its susceptibility to humidity and temperature, a compensation strain gauge is also used, that might increase the electronics and required area to glue the strain gauge. Other alternatives in-

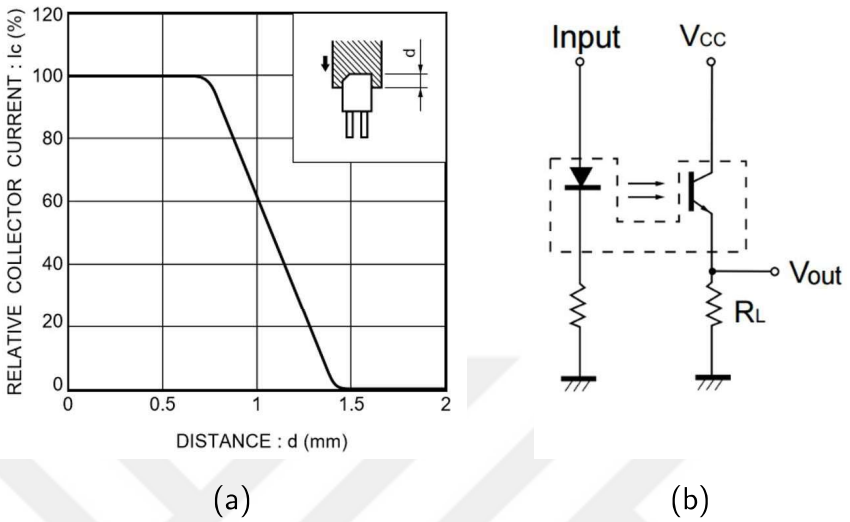

Figure 8.1: Concept Flexure design (a) Front View (b) Top View

clude piezoresistive [Estevez et al., 2012], piezoelectric [Rakotondrabe et al., 2015], capacitive [Chappell and Elliott, 2003] and inductive techniques [Takenawa, 2009]. Conversely, the optoelectronics technique among them has simpler electronics, light weight, compact and immune to electromagnetic interference with high spatial resolution [Tiwana et al., 2012]. Due to these reasons, researchers are focusing on the optical technique as an alternative to developed sensors that can detect force & displacement [Shams et al., 2011], torque [Shams et al., 2012], and tension in the string [Palli and Pirozzi, 2011]. These points make the optical technique ideal to employ for the contact force detection. The photocoupler selected for this purpose, is compact (4.2 x 4.2 x 5.2 mm), light (0.05 gm) [ROHM Semiconductor, 2017] and can be easily install in the distal phalanx area of the finger (Fig. 8.2).

Photocoupler contains an infrared Light Emitting Diode (LED) and a phototransistor. The voltages are applied to the input, controls the illumination of the LED, this illumination causes the transistor to conduct current resulting in the output voltage across the load resistor R_L (Fig. 8.1(b)). The voltage across the load resistor can vary by varying the voltages of the LED or by placing a beam blocker between the LED and phototransistor. In this case, a beam blocker, i.e. Photointerrupter, is used

to block the light from reaching the base of the phototransistor, while keeping the input voltage fixed at 5 V with R_L of 10 kΩ. The photointerrupter is placed between the LED and phototransistor in a way that half of the light falls on the base and half of the light is blocked by the interrupter. Therefore, the deflection and force can be measured in either way, by pulling or by pushing the tip of the finger.

The Photocoupler can detect the maximum deflection of 0.7 mm between the range of 0.7 mm to 1.4 mm. In this region, the collector current of the phototransistor falls from 100 % (at 0.7 mm interrupter position) to 0 % (at 1.4 mm interrupter position in Fig. 8.1(a)). This region is used to detect the relative displacement of the interrupter to detect the exerted force.

8.2.2 Flexure Design

Flexure design is the critical part of the transducer, as the flexure should be flexible enough to sense the minute deflection causing by the sub-newton force and at the same time, it should be rigid enough to withstand the axial and shear forces. Another critical point in the designing of the transducer is the placement of flexure, as the contact area during grasp is not the center of the anterior side of the distal phalanx [Mirkovic and Popovic, 2014][Bianchi et al., 2013][Vecchi et al., 2001]. Mirkovic et al. addressed this issue by determining optimized number of preferred positions of sensors on the prosthetic hand. The experiment was conducted on 12 healthy individuals of age 22 – 25 years. During the experiment subject has to grip different objects, namely, coffee cup, glass, solder reel, a sponge and a plastic cup, and at the same time, the subject has to mark the points for the contact region and temperature sensation on the computer screen. The optimized number of force sensor position is found at the anterior side of the distal phalanx, however, the portion of the distal phalanx is different on each finger [Mirkovic and Popovic, 2014]. Therefore, the position of the flexure is locked between the distal and middle phalanx to detect the forces at anterior and posterior sides of the distal phalanx. The flexure is designed as a bridge between the distal phalanx and middle phalanx such that slightest force

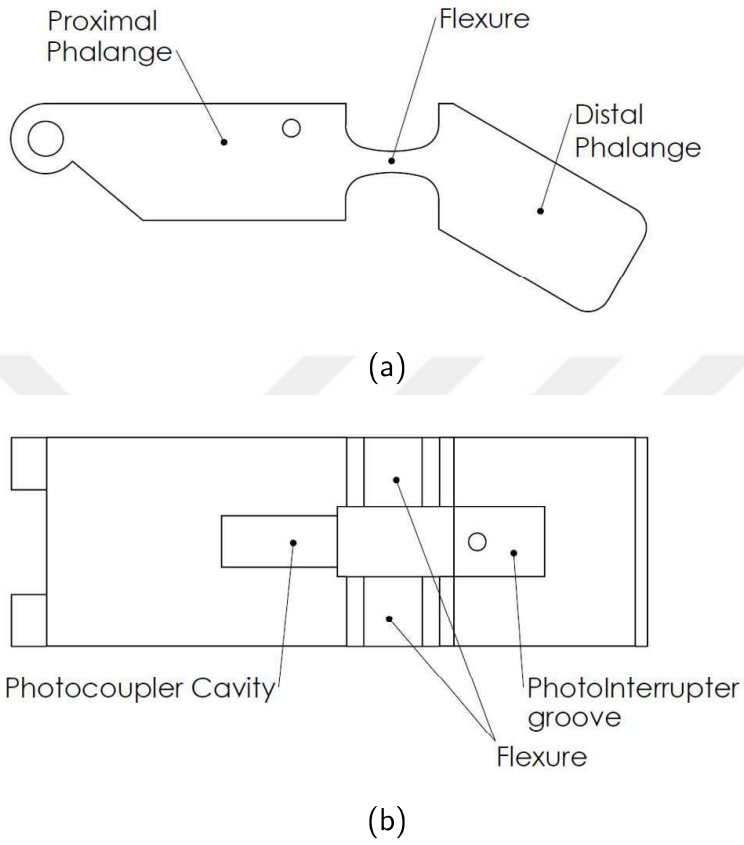

Figure 8.2: Concept Flexure design (a) Front View (b) Top View

exerted at the distal portion results in the deflection of the flexure. A photocoupler is placed at the middle phalanx while a photointerrupter is placed at the distal portion as discussed in the previous section.

The main constraint of the flexure design is the maximum deflection that photocoupler [ROHM Semiconductor, 2017] can detect linearly. The second constraint is the maximum force required to detect by the transducer (i.e. 50 N) with a safety factor of 2. Initially rectangular and circular beam flexures were considered for the finite element analysis (FEA). The analysis ruled out the rectangular beam due to its higher stiffness and lower deflection for the same dimensions and loads. The circular beam parameters were later optimized for the deflection of ± 0.35 mm (Fig. 8.2) at the applied load of ± 100 N [Dirksen and Lammering, 2011].

Table 8.1 shows the flexure design specification. The optimized design consists of

Table 8.1: Transducer Design Specification

	Thickness/ Depth (mm)	Width (mm)	Length (mm)
Flexure	2	6	8
Distal Phalanx	10	18	25
Middle Phalanx	10	18	30
Photocoupler Cavity	4.5	4.5	10
Photointerrupter Grove	4.5	6	7.5

two circular beams or flexures of radius 10 mm. The flexures emerge from middle phalanx portion and diffuse into the distal phalanx portion of the finger making it one monolithic structure. The uniformity is important to maintain and detect the deflection in micrometer scale. The flexures are 8 mm long, 6 mm wide and 2 mm thick at the center. The cavity between the flexures serve two purposes; first, it decreases the hardness of the flexure making it more sensitive to respond to the minute change of load, second, it creates a space for the mounting of photointerrupter and photocoupler. The dimensions of distal and middle phalanx portions are considered by keeping in mind that the resultant structure should look like an actual finger.

8.2.3 DAQ and Software

Since Arduino board is convenient, mobile and capable of handling multiple sensors at a time, as in the case of a prosthetic hand, Arduino is used to communicate with the designed transducer. An LED display is placed on the top of the Arduino board to instantly read the force value using the Hookes law, where x is the displacement caused by the load at the fingertip. Since Arduino is not capable of logging data for later analysis, Graphical User Interface (GUI) has been created and data is acquired into

the computer using NI DAQ card (NI PCI 6259 & NI SCC-68). The GUI contains three waveform graphs, first is used to track the applied force on the transducer, second for the commercial dynamometer output and third for the comparison of both. The data acquire during experiments is also logged into files for further analysis with MATLAB [The MathWorks, 2017].

8.3 Simulations

Before manufacturing the designed flexure, the CAD model is tested for the linear deflection and stress at maximum load with the FEA software. Three materials i.e. stainless steel, aluminum, and titanium are considered for the simulations. Among these, the aluminum is selected due to light weight, low cost, and easy machining. The flexure is simulated for a load capacity of 5 kg with a safety factor of 2, hence the total simulation force is ±100 N. For linearity test, force is applied from 0 N to 100 N with an interval of 10 N as shown in Table 8.2. The Table shows the deflection at the place of the photocoupler and photointerrupter area since the photointerrupter is placed at the medial phalanx while the photocoupler is placed at distal phalanx (Fig. 8.2), hence the difference between the deflection of both the places will be the net deflection of the flexure. Moreover, the graph (Fig. 8.5) between the net deflection and applied force shows that the flexure design retains a linear behavior and is appropriate for manufacturing. The last column in Table 8.2 shows the maximum stress the flexure will undergo during the application of the force. The maximum stress at the force twice as greater than the actual force is found to be 244.27 MPa which is less than the half of yield strength of aluminum.

8.4 Manufacturing and Experiments

The 3 axis machine (Mazak FJV-200 UHS) is used to machine the designed flexure from a single workpiece of aluminum Al-7050 to keep the part monolithic. Keeping the structure monolithic adds strength and ensure linear behavior of the flexure. In order to mount the photocoupler on the middle phalanx, a cavity of the same size

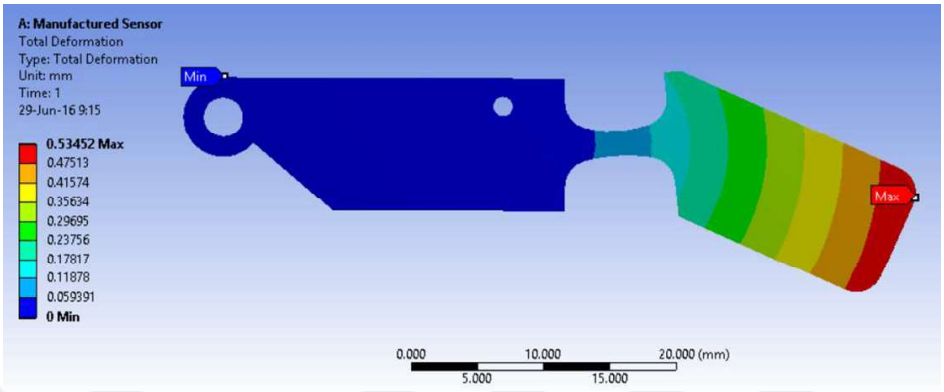

Figure 8.3: Deflection results of the simulation at 100 N

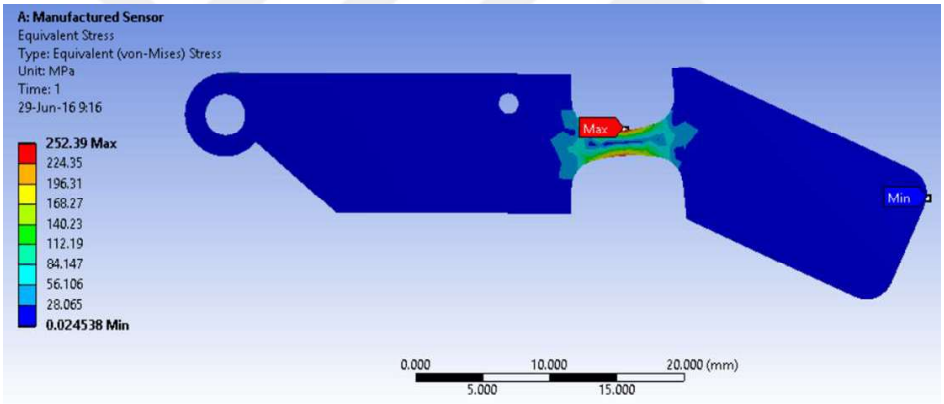

Figure 8.4: Stress results of the simulation at 100 N

as photocoupler is machined (Fig. 8.6) with the screw hole to keep the photocoupler fixed on the phalanx portion during the application of the force. A groove is machined on the distal phalanx portion of the designed transducer to accommodate the photointerrupter. Next section discusses in detail about the possibilities and combination in which photointerrupter and photocoupler can be placed in the manufactured transducer.

8.4.1 Placement of Photointerrupter and Photocoupler

The photointerrupter is designed in such a way that after mounting on the transducer the photointerrupter may slide to and fro to adjust the amount of light blocked by it

Table 8.2: Simulation results

Applied Force (N)	Max. Deflection (mm)	Optocoupler Area (mm)	Blocker Area (mm)	Net Deflection (mm)	Max. Stress (MPa)
0	0	0	0	0	0
10	0.053	0.003	0.029	0.025	24.43
20	0.107	0.007	0.058	0.050	48.85
30	0.161	0.011	0.087	0.075	73.28
40	0.214	0.014	0.115	0.101	97.71
50	0.268	0.018	0.144	0.126	122.13
60	0.322	0.022	0.173	0.151	146.56
70	0.375	0.025	0.202	0.177	170.99
80	0.429	0.029	0.231	0.202	195.41
90	0.483	0.033	0.260	0.227	219.84
100	0.534	0.037	0.289	0.252	244.27

(Fig. 8.6). This adjustment allows the user to customize the transducer in following three modes.

Mode 1 - Half Block and Half Allow

Since the total active region of the photocoupler is 0.7 mm in which it detects the deflection linearly, beyond this limit the transducer is either saturated (100 % output) or in cutoff (0 % output) state. The photointerrupter is placed in a manner that it will

block half of LEDs light and permit half of it, this position provides photointerrupter to move 0.35 mm in both directions. Therefore, the transducer will detect 100 N of force in either direction. Thus, this mode can be used to detect the force in either direction i.e. pushing and pulling of a fingertip.

Mode 2 - Full Block

In this position, the photointerrupter is adjusted such that the light from the LED is completely blocked and the phototransistor will not sense any light, hence, the output voltage of the optocoupler will be 0 V. In this mode, the transducer can detect the force in only one direction (i.e. pushing of the fingertip) but the magnitude of the detection force can be increased as much as twice as compared to the previous mode.

Mode 3: Full Allow

This mode can detect the same amount of force as in full block mode but in opposite direction. The photointerrupter is placed such that it will not block the light instead allow all of the LED light to fall on the phototransistors base, results in the 100 % of the output voltages.

8.4.2 Calibration Process

The multipoint calibration method is used to ensure that the manufactured transducer possesses linear behavior. For this purpose, five weights of known values 0, 1, 2, 3, 4 and 5 kg were loaded on the string (Fig. 8.6). The photointerrupter and photocoupler are placed at the distal and middle phalanx respectively as described in the previous section. A test bench is set up for the calibration of the transducer as shown in the (Fig. 8.6). To calibrate the transducer, known value load is applied and recorded the transducer outputs multiple times to eliminate any error due to loading and unloading of the weights. A resultant straight line, from the curve fitting procedure, using MATLAB shows that the transducer is capable of producing linear output (Fig. 8.7). Furthermore, (8.1) shows that the slope of the line or sensitivity of the manufactured

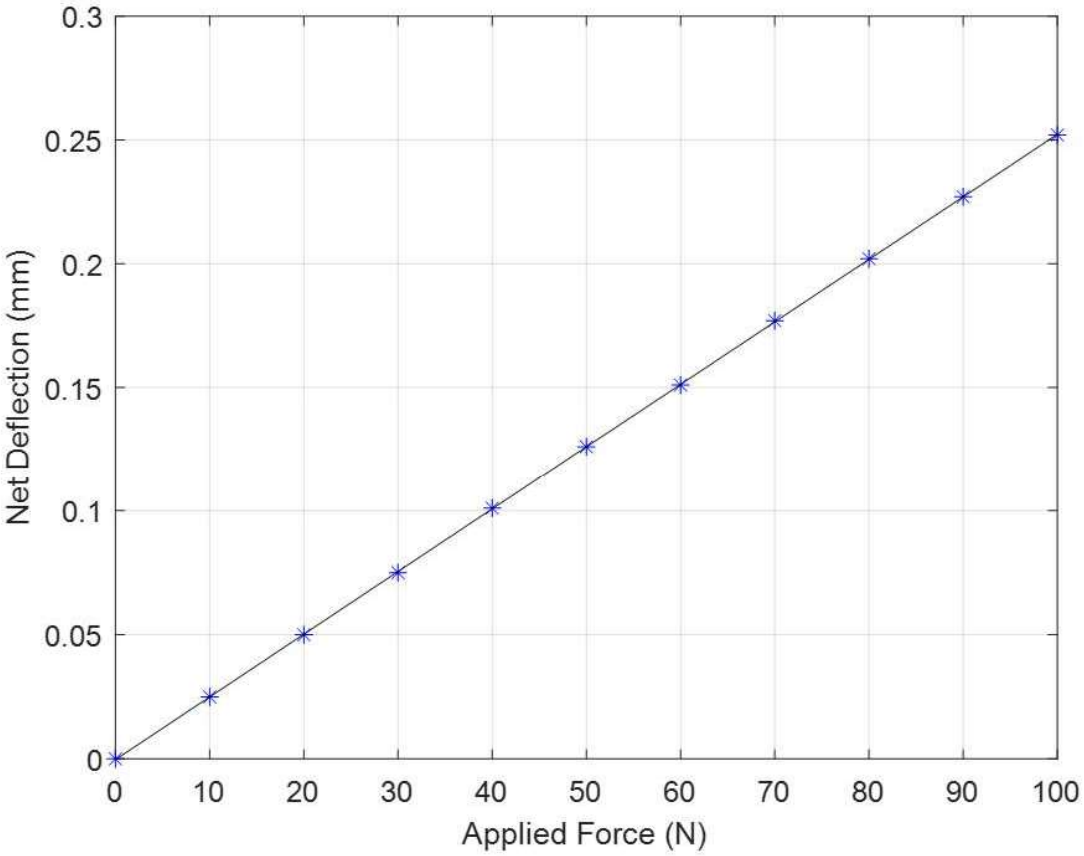

Figure 8.5: Deflection results of FEA analysis

transducer is 0.0137 V/N, where x is the applied force, y is the transducer output in volts and C is the offset voltages at no load condition.

$$y = 0.0137x + C \tag{8.1}$$

8.4.3 Linearity Test

After the calibrating, the transducer is tested for the linearity test by applying known value force and reading the force value at the output of the transducer using (8.1). The experiment is repeated several times to ensure the accuracy of the transducer output. The mean value, the maximum and minimum limits of the transducer found during

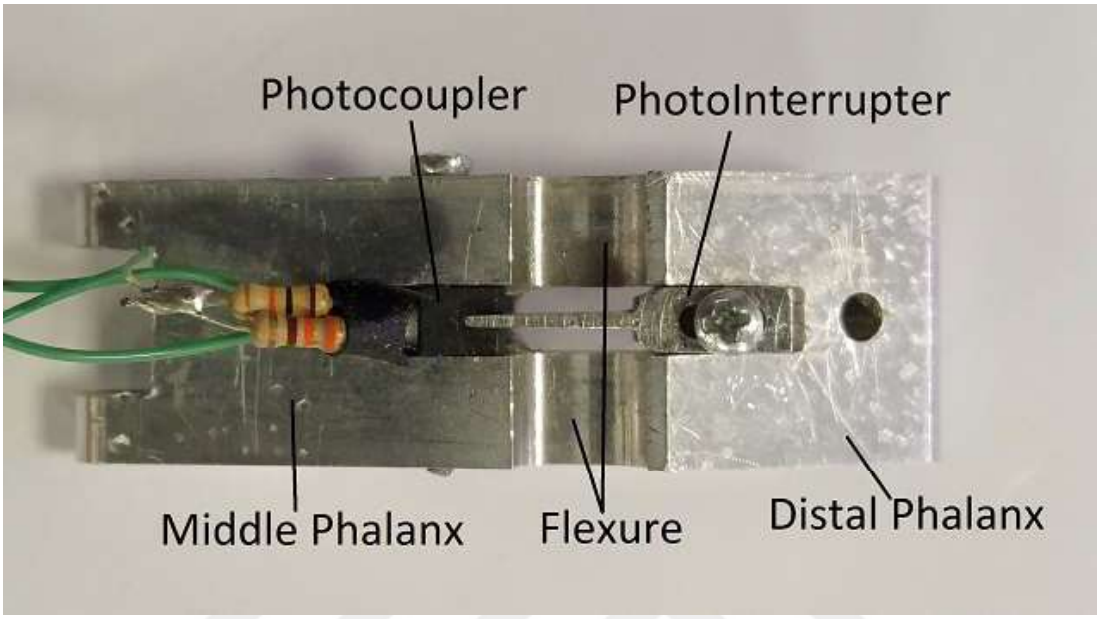

(a)

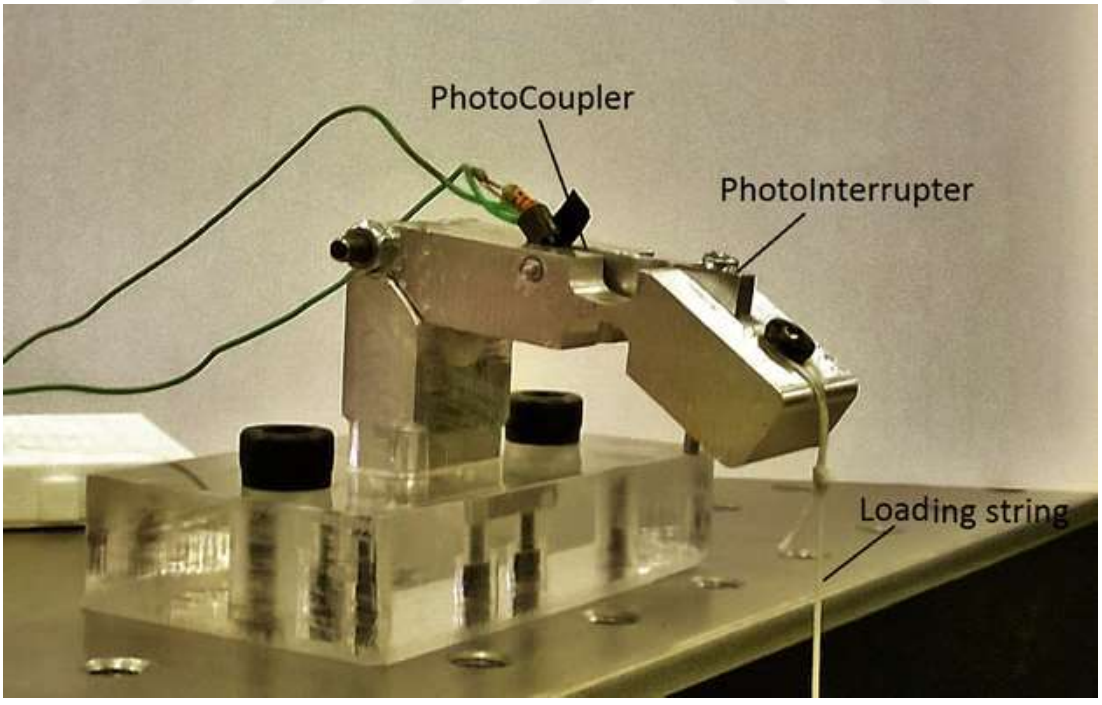

(b)

Figure 8.6: (a) Top view of the transducer with photocoupler and photointerrupter. (b) Transducer test bench for the calibration process and experiments.

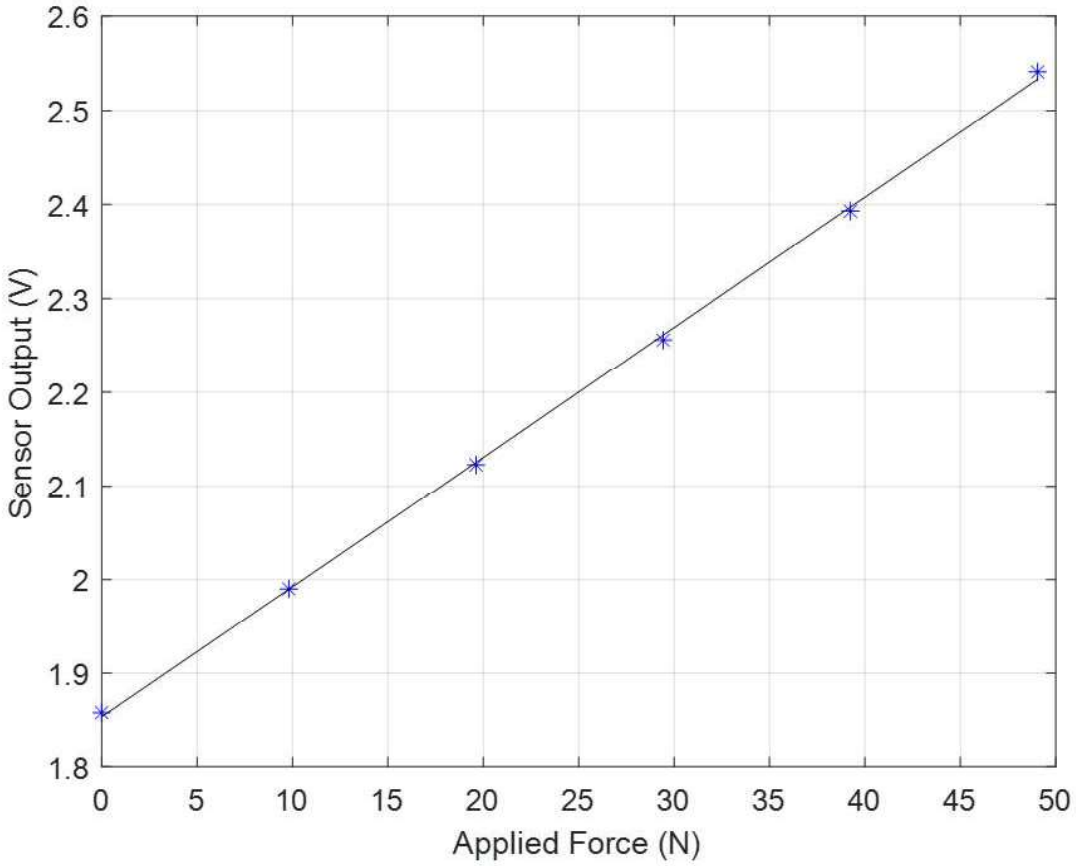

Figure 8.7: Multipoint calibration curve of the manufactured transducer.

experiments can be seen in Table 8.3. The maximum error between the average and calculated values found is 1.3 % or a voltage error of 0.006 V, which is significantly low as compare to the step size of the transducer.

8.4.4 Hysteresis

Hysteresis is an important factor to control the gripping force of a prosthetic hand, because during gripping and releasing of an object the transducer should be able to produce the same measurement precisely in order to complete the entire task smoothly. For this purpose, the transducer is tested for the hysteresis by loading and unloading of weights and recording the calibrated force outputs. To ensure that the forces are recorded accurately, hysteresis experiment is repeated six times. Table 8.4

Table 8.3: Experiment results of linearity experiments and calculated values with error

Force (N)	Min. Value (V)	Max. Value (V)	Mean Value (V)	Calculated Value (V)	Error (V)	%
0	0.000	0.003	0.001	0.000	-0.001	-0.094
9.81	0.131	0.138	0.134	0.135	0.001	1.018
19.62	0.263	0.273	0.268	0.271	0.003	1.087
29.43	0.395	0.406	0.401	0.406	0.006	1.372
39.24	0.532	0.544	0.539	0.542	0.003	0.533

shows the average data of loading and unloading experiments done for the hysteresis. Since the error is in order of milli-newtons, three significant digits are used to highlight the hysteresis in the transducers output. It is difficult to visualize the hysteresis error on the graph (Fig. 8.8a), due to the overlap of the loading and unloading data points, so the error graph is shown separately in Fig. 8.8b.

8.4.5 Repeatability

Besides linearity and hysteresis, repeatability is an important parameter to estimate the performance and characteristics of the transducer. Therefore, rigorous repeatability tests are conducted on the transducer by applying the force load of 9.81 N, 19.62 N, 29.43 N and 39.24 N numerous times. The graph in Fig. 8.9 shows that the transducer can produce the same output accurately and repeatedly with a deviation of 0.1860 N for 9.81 N, 0.2459 N for 19.62 N, 0.3017 N for 29.43 N and 0.4125 N for 39.24 N. Table 8.5 shows the standard deviation, which is significantly low as compared with the step size of the transducer, shows the tendency of the transducer to

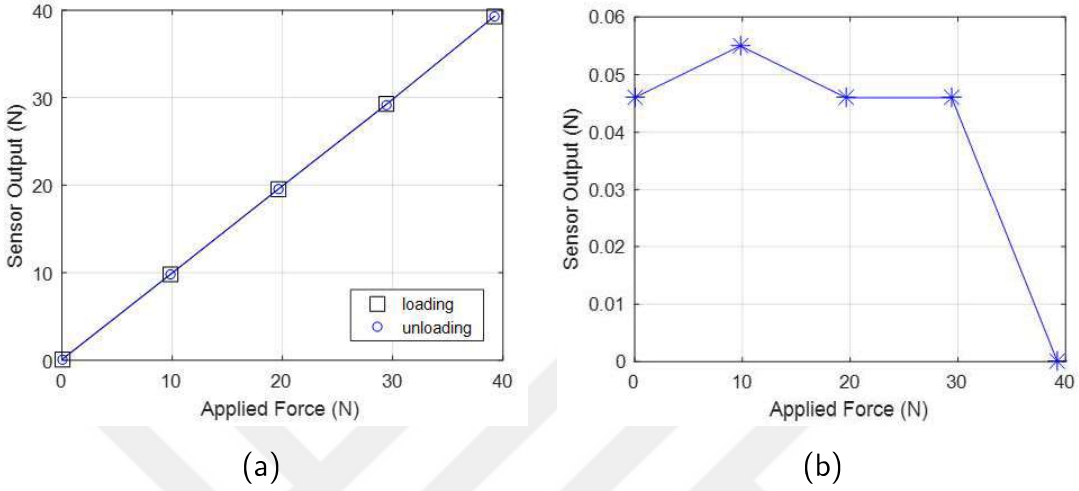

Figure 8.8: Results of the experiments conduct for (a) Hysteresis, and (b) Loading and unloading difference

Table 8.4: Hysteresis and loading unloading difference

Applied Force (N)	Loading O/p (N)	Unloading O/p (N)	Difference (N)
0	0.091	0.046	0.046
9.81	9.808	9.754	0.055
19.62	19.571	19.526	0.046
29.43	29.261	29.215	0.046
39.24	39.316	39.316	0.000

produce the same output for a given load.

8.4.6 Step Response

In the end, the transducer is compared with the commercially available dynamometer for dynamics loading and unloading of the load, as the transducer is designed to

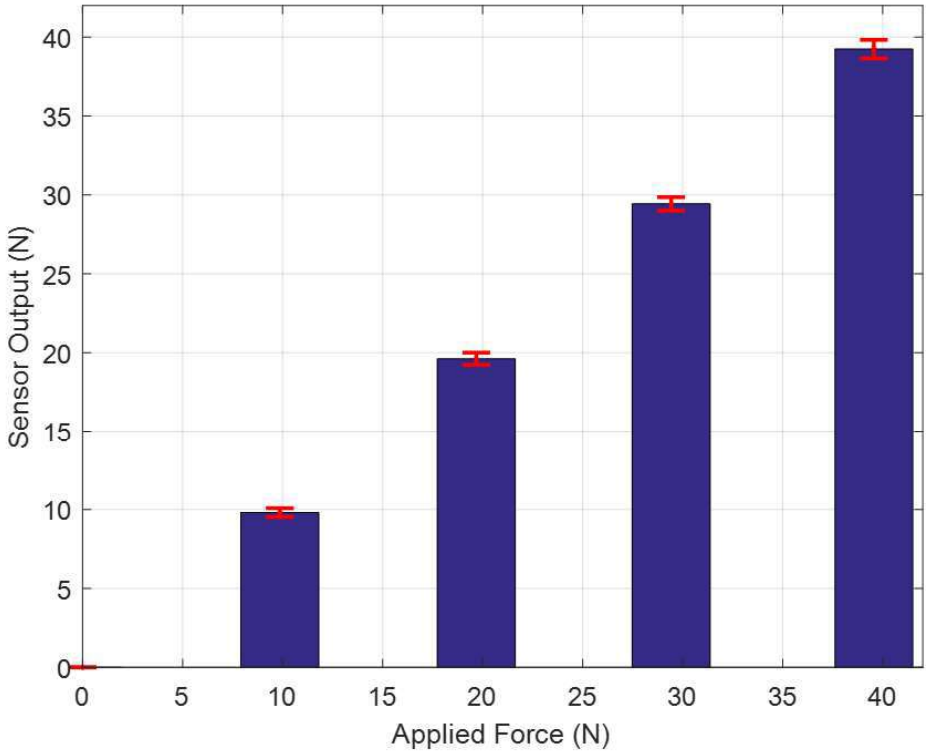

Figure 8.9: Repeatability graph of the manufactured transducer

Table 8.5: Repeatability

Applied Force (N)	Mean O/p Force (N)	Standard Deviation (σ)
0	0	0
9.81	9.8603	0.186
19.62	19.683	0.2459
29.43	29.4223	0.3017
39.24	39.5579	0.4125

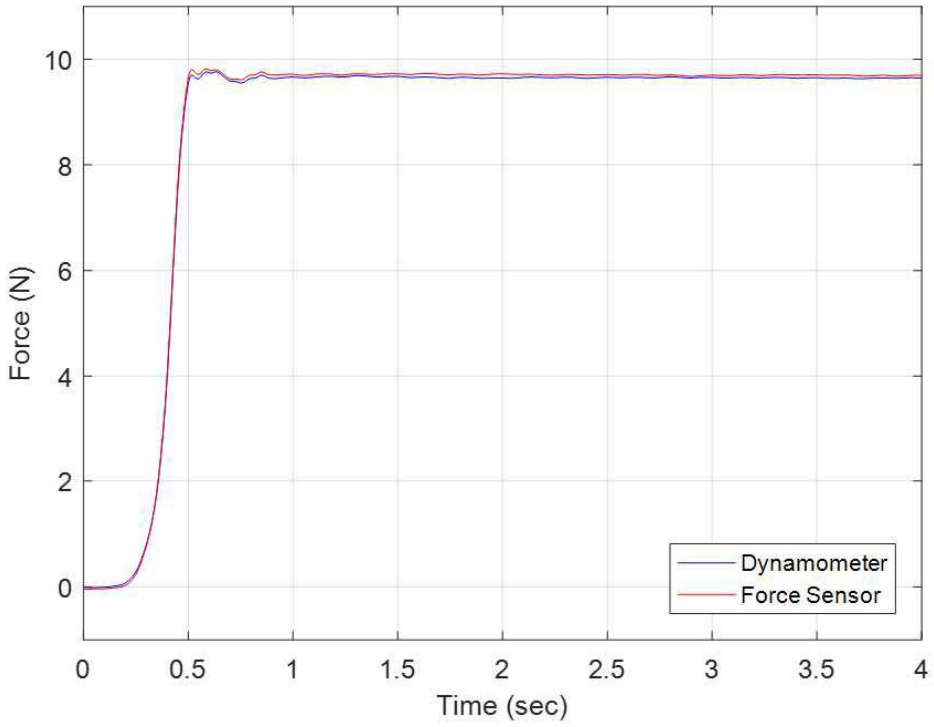

Figure 8.10: Step Response of force transducer and dynamometer output

place on the fingertip and the user interact with the environment through it, so it is necessary to test the transducer under dynamic conditions. For this purpose, the transducer is placed on the top of a commercially available table top dynamometer, such that the force transducer axis is aligned with the z-axis of the dynamometer. The CutPro [MAL Manufacturing Automation Laboratories, 2017] software is used to acquire the data from the dynamometer and the designed force transducer after converting the voltage output of the transducer into the forces using calibration curve obtained during calibration experiments. The experiment is conducted by applying a step input of load 9.8 N (as shown in Fig. 8.10). The time response of the force transducer is found slightly prevailing as compared to the commercially available dynamometer, it is due to the factor that dynamometer uses charge amplifier to produce the output as compare to the simple photocoupler with a 5 V DC supply.

Beside the step response comparison, the manufactured transducer is further com-

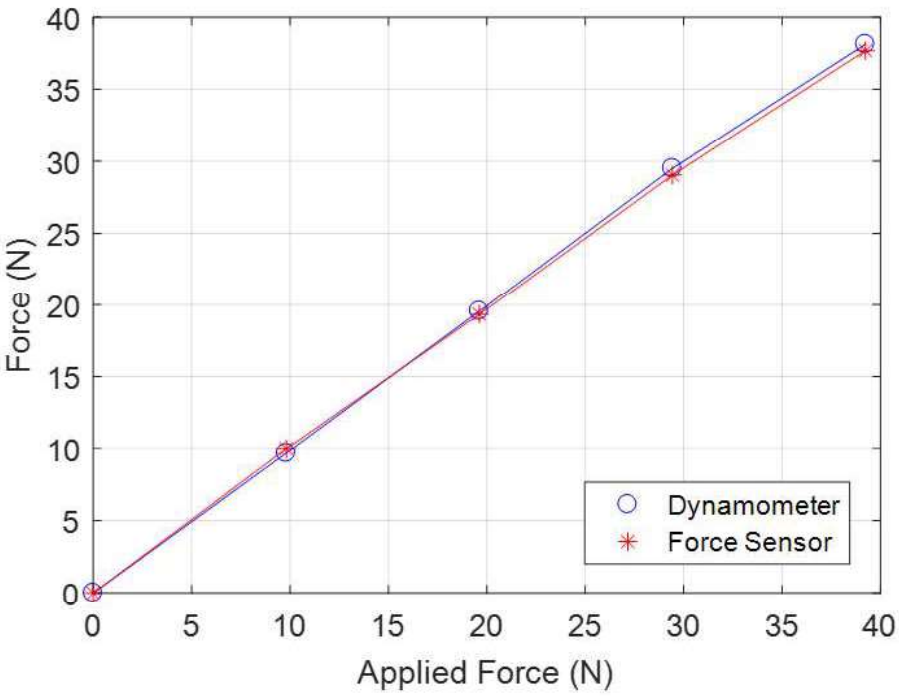

Figure 8.11: Comparison of force transducer with dynamometer

Table 8.6: Parameters Obtained from FRF Analysis

Mode No.	Frequency (Hz)	Damping Ratio (%)	Modal Stiffness (N/m)	Mass (kg)
1	821.62	0.20	9.015 e05	0.034

pared with the commercial dynamometer by applying load of 1 kg to 4 kg with a step of 1 kg. The experiment is repeated several times and the mean values obtained from the experiments are plotted in the Fig. 8.11. The graph in Fig. 8.11 shows the mean output of the dynamometer and force transducer. The transducer outputs the same value as of dynamometer with a range of ±1.5 %.

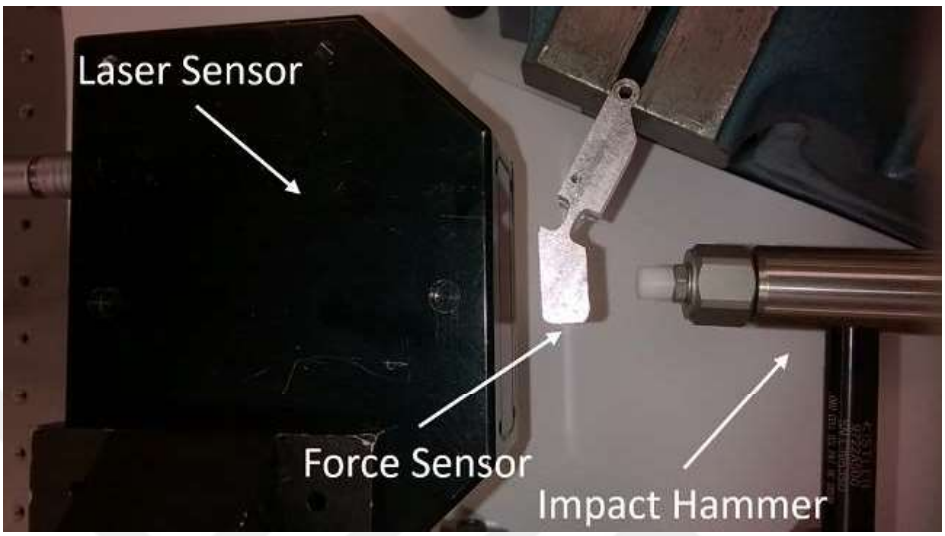

Figure 8.12: Setup for Frequency Response Function analysis

8.4.7 Frequency Response Function Analysis

Frequency Response Function (FRF) Analysis of the force transducer is investigated using Impact hammer test. The transducer's structure is excited by a random force using an impact hammer (Kistler 9722A500) while the response of the structure is measured by a laser sensor (LMI LTS 15/2.5) as shown in Fig. 8.12. The input force of impact hammer and output of the laser sensor is logged in the computer for analysis via NI-9259 DAQ. CutPro software is used to examine the natural frequency, modal stiffness and damping ratio as shown in Table 8.6. The real and imaginary plots obtained from the FRF analysis is shown in Fig. 8.13.

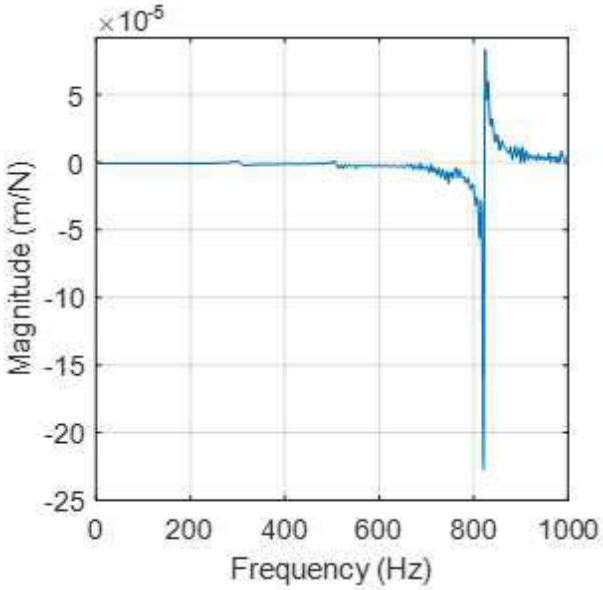

(a)

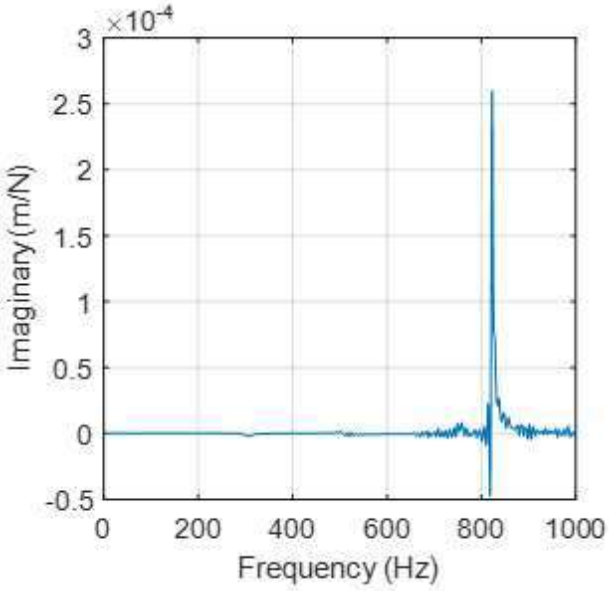

(b)

Figure 8.13: (a) Real and (b) Imaginary plot of the Frequency Response Function

Chapter 9

EXPERIMENTS AND RESULTS

MARCAPH is manufactured using the μPrint 3D printer. Total time to print the parts of MARCAPH is around 22 hours which allow to prepare a complete hand in a couple of days and ready it for use. The parts required for a finger, consists of a linear actuator, three screws and three pins, with 3D printed parts, fingertip, finger PP, actuator housing, link2 for four bar mechanism, and auxiliary link for slider crank mechanism (as shown in Fig. 9.1). The finger can be assembled with one hand by attaching one part at a time starting from the fingertip. Fig. 9.2 shows the step by step process to assemble a finger. Initially, attach the fingertip with the finger PP using an M2 pin of 12 mm long (Fig. 9.2a), then assemble the link2 with the fingertip. After assembling the link2 with the fingertip (as shown in Fig. 9.2b) attach the auxiliary

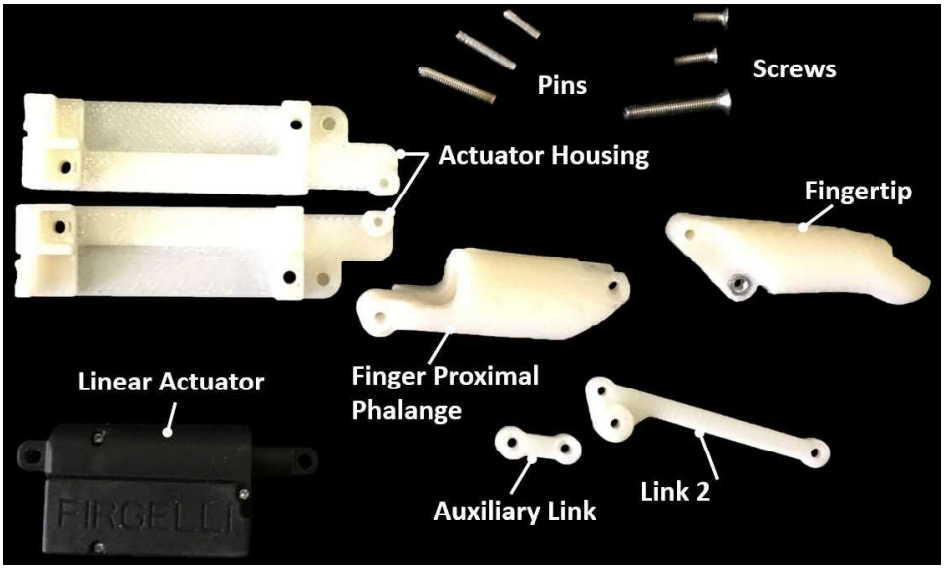

Figure 9.1: Parts for one finger assembly

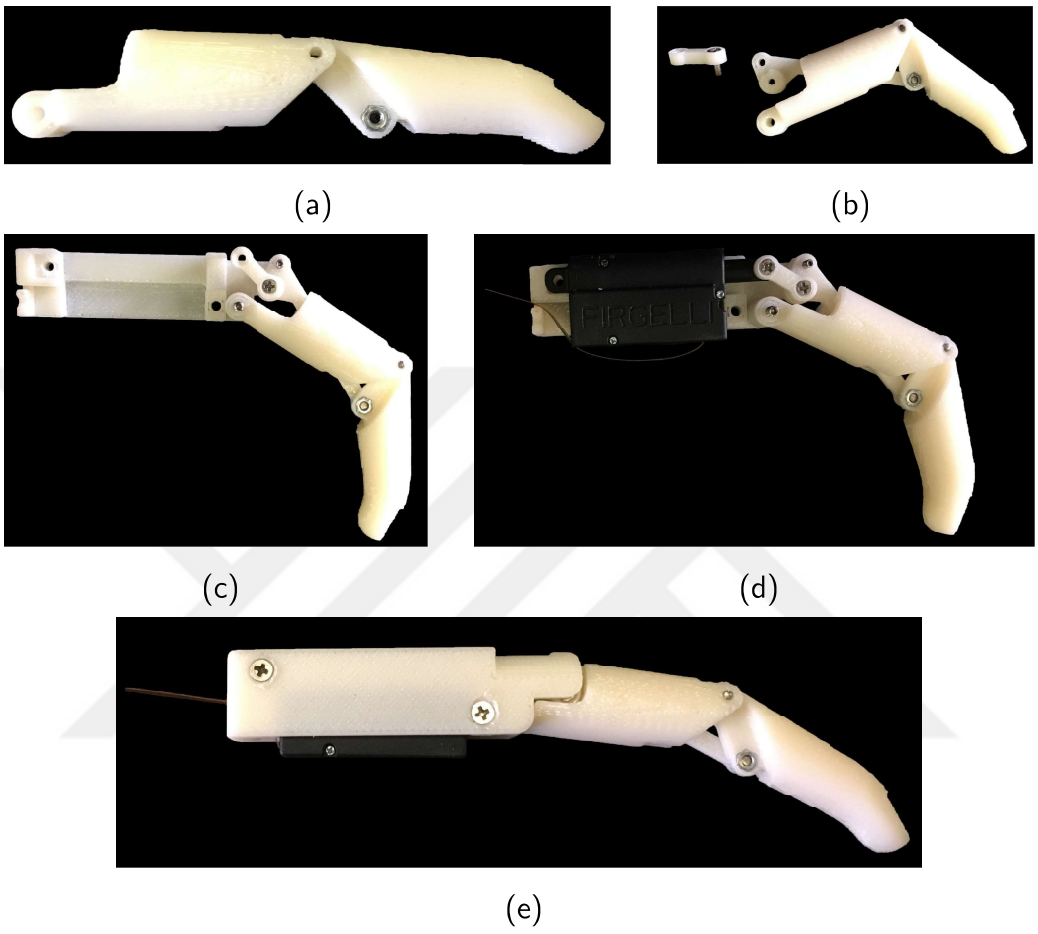

Figure 9.2: Step by step process for the finger assembly

link with the link2 using an M2 screw 6 mm long. Now attach the assembly to the actuator housing using an M2 pin (8 mm long) at the link2 and an M2.5 pin (14 mm long) at the finger PP (Fig. 9.2c). Next step is to place the actuator in the actuator housing and attach the auxiliary link with the actuator using an M2 screw 6mm long (Fig. 9.2d). The last step is to put the other side of the actuator housing on the top and use two M2.5 screws of length 19 mm, to attach the both sides of the actuator housing. The complete assembled finger can be seen in the Fig. 9.2e. These simple steps allow the amputee to assemble the MARCAPH by himself in a few simple steps.

After assembling the finger, finger is experimented to check the strength and loading capabilities, as designed initially to withstand a load of about 10 N. The

experiment setup is built by placing the finger on the test bench and hold it from actuator base. After holding the finger load is applied at the fingertip when the finger is in the open state. Initially, a load of 100 gm is applied and gradually increase the loaded mass by 50 to 100 gm at a time. The finger broke at the load of 20 N which is twice the simulated load. After the assembling and testing of fingers (including the thumb) separately, all the fingers are placed in the palm and covered by the palm cover as seen in the Fig. 9.3a. After completing the assembly, the MARCAPH is compared with a normal adult hand for referencing the size of the manufactured hand (Fig. 9.3b). Afterward, MARCAPH is tested for the fingers and thumb motions to verify the initially designed range of motion. Since MARCAPH uses 6 actuators in total, in which 5 actuators used for the flexion-extension of the fingers and one actuator is used for the circumduction of the thumb. This allows the MARCAPH to adopt almost all of the essential grips required to perform ADLs. Most common ADL grips are shown in Fig. 9.4. Figure 9.4a shows a spherical object being held by the fingers with the palm as opposition in palmar prehension grip mode. Fig. 9.4b shows the MARCAPH holding a screwdriver in power grip mode. Fig. 9.4c shows the index pointer grip mode and Fig. 9.4d shows MARCAPH in lateral prehension grip mode. Fig. 9.4e shows the pinch mode of the MARCAPH holding a credit card and Fig. 9.4f shows that the MARCAPH is also capable of tip prehension or key grip. The Fig. 9.4g shows a mobile phone is being grasped by the MARCAPH. The experiments are also performed on a near-elbow amputee. The control parameters for the amputee subject is modified due to the fact that the muscles of the amputee have low power EMG signal as compared to the normal subjects. The amputee subject successfully controlled MARCAPH without assistance after a short training and capable of performing the desired operation.

9.1 Tests on an Amputee Subject

The MARCAPH shows compelling results during the laboratory experiments on normal subjects. Therefore, to validate the performance of MARCAPH we recruit a

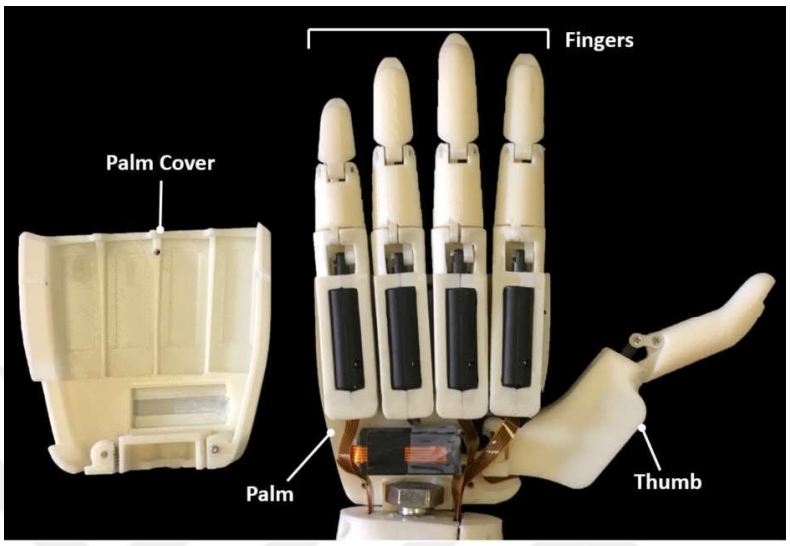

(a)

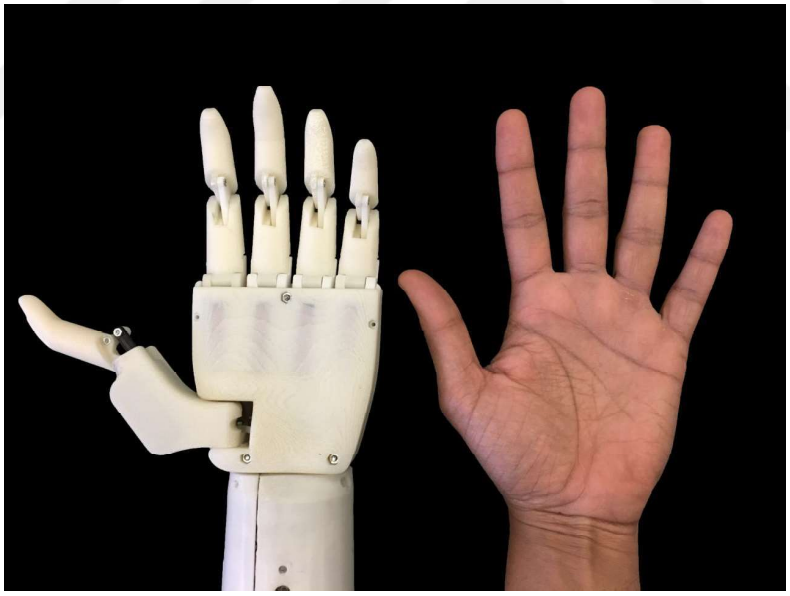

(b)

Figure 9.3: Manufactured hand MARCAPH (a) Hand assembly with open palm cover (b) The MARCAPH compared with an adult hand

near elbow amputee after ethics committee approval. Since the amputee did not have muscles of the forearms, the EMG signals acquired from the biceps and triceps. In order to understand the control flow of the MARCAPH, a LabVIEW ([NI, 2017])

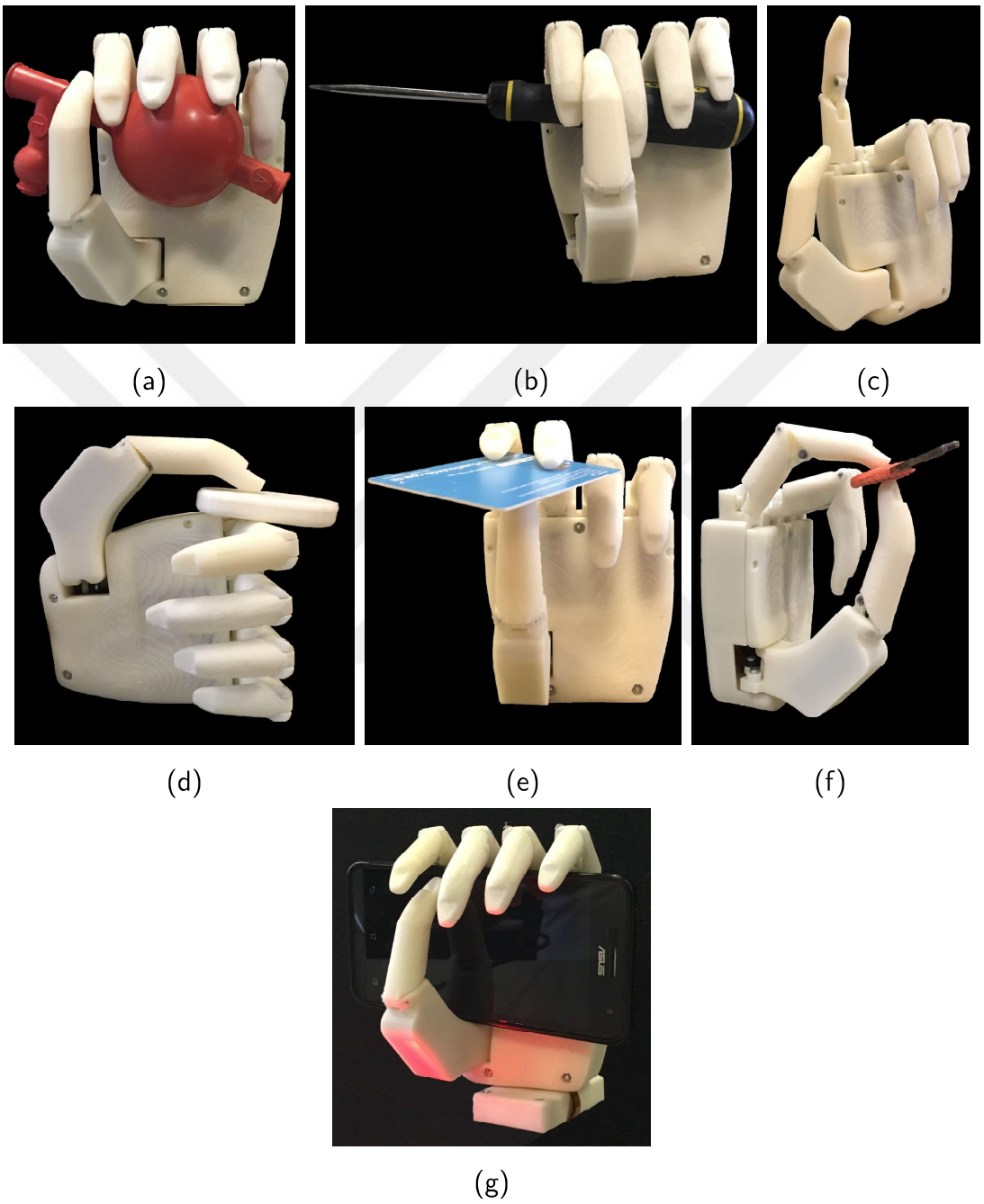

Figure 9.4: Grips MARCAPH can achieve (a) Non-oppose (b) Power (c) Index (d) lateral (e) Pinch (f) Precision (g) Mobile grip.

based Graphical User Interface (GUI) is built (shown in Fig. 9.5). This GUI contains an active display of the MARCAPH FSM states, EMG signals graph, EMG signals RMS values, thresholds level selection and grip mode display. The EMG acquisition

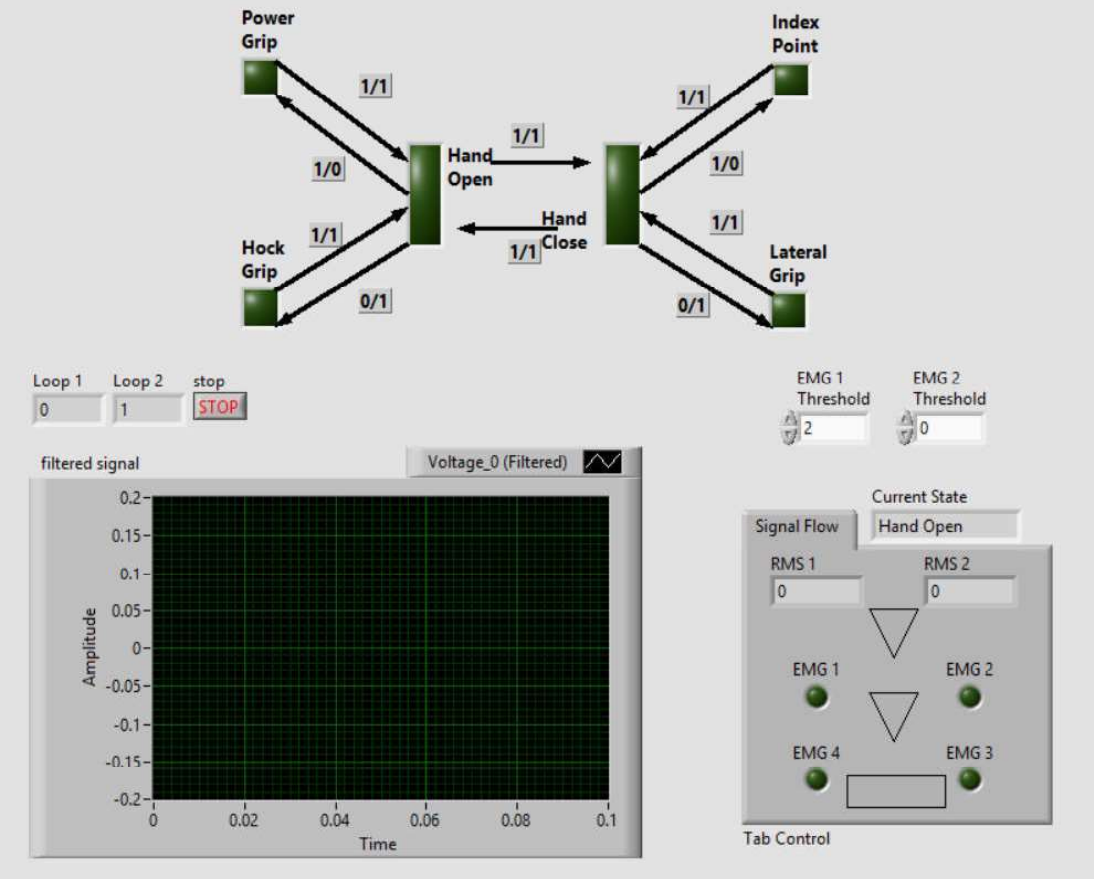

Figure 9.5: LabVIEW GUI for the Amputee subject to understand the flow of the MARCAPH control scheme. The LEDs are used to indicates the state of the hand. Also, the RMS values of the EMG signals are shown with the LEDs on the right side, the LED will glow when the EMG signal passes the threshold levels

circuit along with the NI instruments DAQ is used to acquire the filtered and amplified EMG signal, without rectification. The LabVIEW is used to rectify the EMG signal and then it calculates the RMS value of the signal to compare it with the user defined threshold level. The threshold level can be adjusted during the experiments after observing the subject's EMG of strong and weak contractions. After the setup, the user required to do contraction of the biceps and triceps individually and observe the EMG signal graph. It helps the user to learn how to contract an individual muscle without activating the other. This software also aided the amputee subjects to

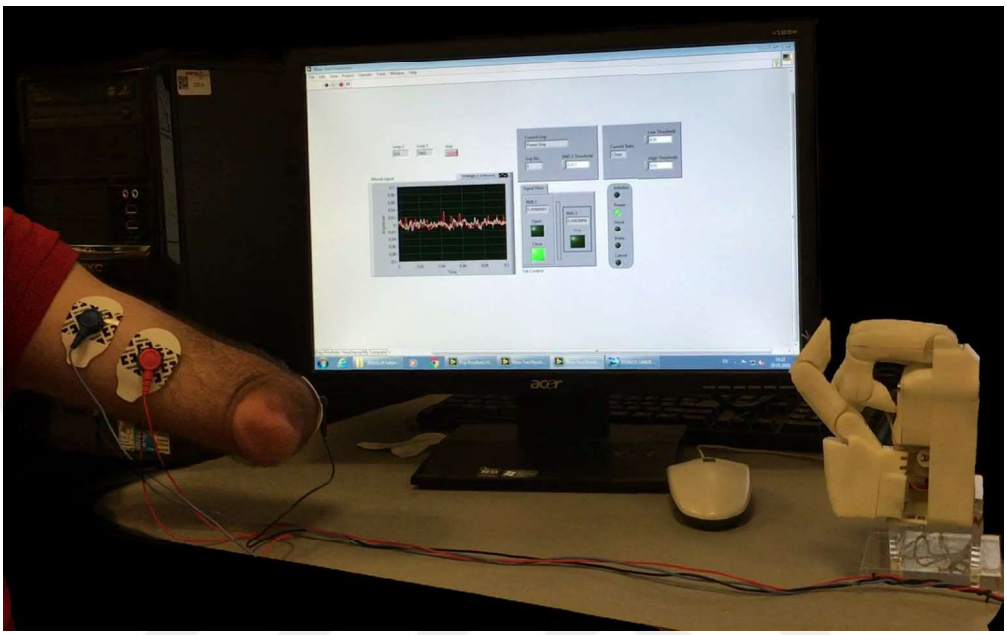

Figure 9.6: Amputee is using the Prosthetic Hand with the training software built in LabVIEW

observe their contraction level and practice to contract the muscle with high, medium and low intensity.

After the training of the amputee on the training LabVIEW program for few days, we figured it out that the co-contraction of the biceps and triceps muscle with the same level of intensity is quite difficult for the subject. To cope with this issue, MARCAPH FSM is programmed to use triceps muscle to switch the grip mode and biceps muscle to control the opening and closing of the hand in double threshold level detection mode (for detail Section 7.2). After the modification, the amputee took significantly less time to understand and control the FSM states in an improved manner.

Then a prosthetic hand is connected with the LabVIEW via NI DAQ card and a subVI is programmed to use the states generated by the LabVIEW GUI to control the actuators of the prosthetic hand using motor driver circuits (shown in Fig. 9.6). The amputee, then trained to focus on the prosthetic hand instead of the GUI on the

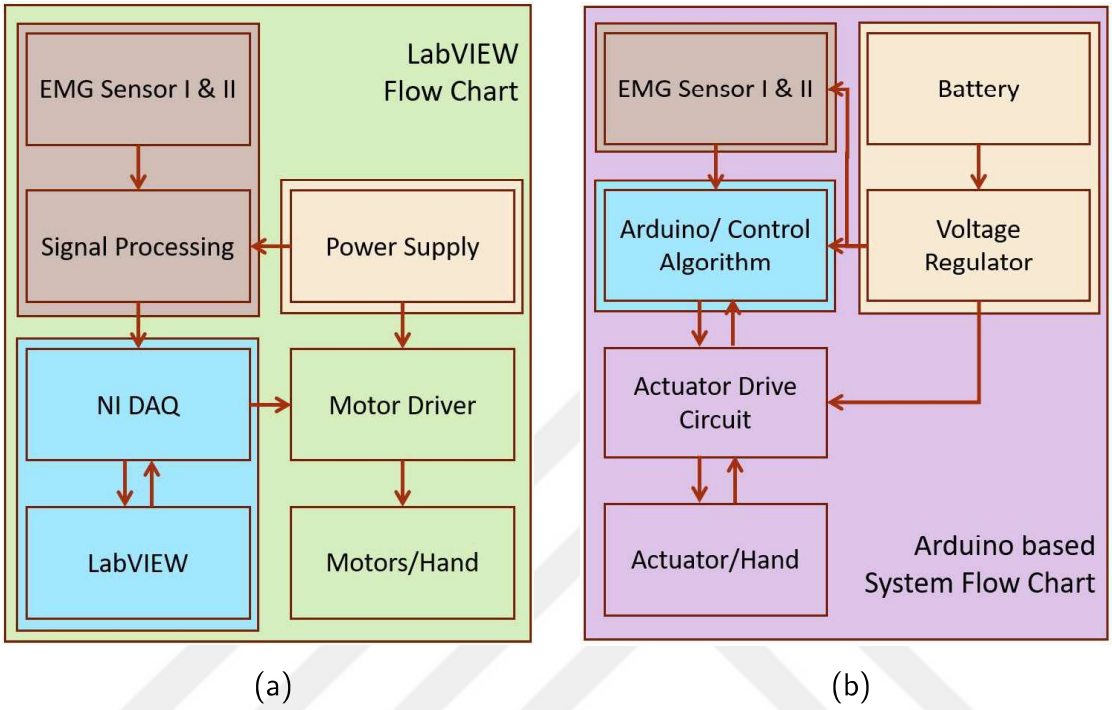

Figure 9.7: A comparison of the system flow of the LabVIEW and Arduino based systems

monitor and performed the same pattern of contraction in order to accomplish the opening and closing of the desired grip.

After the successful training on the LabVIEW based GUI program and hardware in the loop, we developed a mobile system that has all the capabilities of the previous system and it can be fit into the socket of the amputee's artificial limb. This system allows the amputee to move around and perform the ADL without anyone's assistance. Fig. 9.7 shows a brief comparison between the LabVIEW based and mobile system. In the mobile version of the system, we used battery (7.4 V 4000 mAh Lipo) to provide power to the system through a 5 V voltage regulator, that also has temperature and high current protection, in order to prevent any short circuit and damage to the amputee and electronic circuit.

The final assembled MARCAPH can be seen in the Fig. 9.8. The MARCAPH contains the electronic circuit and battery in the socket. The LED are used to indicate

Figure 9.8: The final version of the MARCAPH

the states of the grip and opening & closing of the MARCAPH. A push button is also placed in order to switch the mode of the MARCAPH. The EMG electrodes can be attached to the amputee via the black cables emerging from the socket. An on/off switch is also integrated into the system in order to control the operation of the MARCAPH and it can be used to turn off the MARCAPH when it is not in use. The MARCAPH is given to the amputee subject multiple times, to use it in his office. The Fig. 9.9 shows MARCAPH in different states to accomplish ADL by an amputee. Fig. 9.9a shows that the amputee is using the MARCAPH in hook grip mode to open a drawer. The Fig. 9.9b shows that the amputee subjects is holding a shopping bag, the MARCAPH is in the hook grip mode. The Fig. 9.9c shows the amputee is holding a bottle placed on the table using the power grip mode of the MARCAPH. The Fig. 9.9d is showing the same amputee subjects holding a mobile phone in the power grip mode of the MARCAPH during a walk.

The test results show that the MARCAPH control scheme and design are robust. The experiments also indicate that the developed prototype is feasible and can be used by an amputee to accomplish ADL. The customizability of the control scheme allows the amputee to feel comfortable during the operation of the MARCAPH. Also, the non-back-drivability of the designed mechanism allows the amputee to hold an object and walk around without the fear of losing, this feature also enhances the battery life of the MARCAPH.

Figure 9.9: MARCAPH used to accomplish ADL by an amputee subject in his office (a) MARCAPH in Hook grip mode used to open the drawer (b) While holding a shopping bag (c) Power grip mode of MARCAPH used to hold a water bottle (d) Holding a mobile phone in power grip mode

Chapter 10

COMPARISON WITH THE STATE OF THE ART PROSTHESES

Alongside the experimental analysis, MARCAPH is also compared with other anthropomorphic hands, Tact, Ada, i-Limb, and Bebionic [Belter et al., 2013]. Besides state of the art commercial prosthetic hands, i-Limb [Bionics, 2017], and Bebionic [Medynski and Rattray, 2011], Tact [Slade et al., 2015], and Ada hands [Bionics, 2016] are added to the list due to the fact that MARCAPH is 3D printed low-cost prosthetic hand. The average human hand weight about 400 gm [Rf et al., 1975], which makes MARCAPH 25% lighter than the average human hand and lightest among the state of the art prosthetic hands (Table 10.1). The dimensions of the MARCAPH is roughly analogous to 45^{th} percentile male according to the hand anthropometry by Greiner [Greiner, 1991]. The thickness of the MARCAPH is reduced to as low as 26 mm. Which is marginally lower than the tact hand thickness. However, the thickness near the thumb joint is intentionally increased by 3-4 mm to mimic the shape of the human palm. The number of joints in all given hands are 11 except the MARCAPH and Ada. Both MARCAPH and Ada has a thumb with the fix DIP joint. All hands use an actuator for a single degree of freedom (DOF), usually 5 actuators for each finger flexion-extension and 1 actuator for thumb circumduction. Only the Bebionic and Ada uses 5 actuators, excluding a separate actuator for thumb circumduction. Bebionic fills this gap by allowing the user to manually rotate the thumb while Ada uses a single actuator to abduct-flex at the same time. DC motor is the obvious choice for the actuation with the worm gear, lead screw, or spool and tendon, to translate the motor rotation into finger flexion, with the exception of MARCAPH and Ada, they use off the shelf linear actuator (Actuonix PQ12-P [Actuonix, 2017]).

Table 10.1: Characteristic Comparison

Hand/ Developer	Mass (gm)	Size (L x W x H) (mm)	Joints/ DOF	No. of Actuators	Actuation Method	Joint Coupling	Material
MARCAPH/ Koc University	300	185 x 90 x 26-30	10/6	6	Linear Actuator-linkage	Linkage Spanning MCP to PIP	ABS
Tact/ University of Illinois	350	200 x 98 x 27	11/6	6	DC Motor-Tendons	Linkage Spanning MCP to PIP	ABS
Ada V1.1/ Open Bionics	380	215 x 178 x 58	10/5	5	Linear Actuator-Tendons	Tendon Linking to MCP to the Fingertip	Ninjaflex & ABS
i-Limb/ Touch Bionics	450-615	180-182 x 75-80 x 35-41	11/6	6	DC Motor-Worm gear	Tendon linking to MCP to PIP	Aluminum alloy/ Titanium
Bebionic V2/ RSL Steeper	495-539	190-200 x 84-92 x 50	11/6	5	DC Motor Lead Screw	Linkage spanning MCP to PIP	Aluminum alloy
Vincent Hand/ Vincent System	-	-	11/6	6	DC Motor Worm Gear	Linkage spanning MCP to PIP	Aluminum alloy

Table 10.2: Kinematic Comparison

Hand	MCP Joint (°)	PIP Joint (°)	DIP Joint (°)	Thumb Flexion Joint (°)	Thumb Circum-duction Joint (°)	Avg. Finger Speed (°/s)
MARCAPH	0-85	10-85	20	0-95	0-115	230
Tact	0-90	23-90	20	0-90	0-105	249.8
Ada V1.1	0-90	0-90	20	0-60	0-110	300
i-Limb	0-90	0-90	20	0-60	0-95	60.5
Bebionic V2	0-90	0-90	20	-	0-68	96.4
Vincent Hand	0-90	0-100	NA	-	-	103.3

The MARCAPH uses four-bar linkage mechanism spanning from MCP to PIP, similar to Tact and Bebionics.

Table 10.2 contains a comparison of the kinematics of the MARCAPH with given anthropomorphic hands. The range of motion of MARCAPH is analogous to Tact and Ada with a slightly higher circumduction range as compared to commercial prosthetic hands. The circumduction axis parallel to the wrist axis is standard for all prosthetic hands. Parallel placement of the circumduction axis of thumb streamlines prosthetic hands to achieve complex grips. The speed of gripping an object is also a critical performance measure for the prosthetic hand. Speed requirement for most of the pick and place tasks is in the range of 170 to 229 °/sec [Weir and Ph, 2004], that allows the human hand to grip an object within a fraction of a second. The MARCAPH used a linear actuator with a speed of 15 mm/sec (no load) to 8 mm/sec (30 N load).

Linear actuator displacement of 8 mm causes a fully open finger to fully close, thus producing an average speed of fingertip around 230 °/sec.

Chapter 11

CONCLUSION

The aim of the research is to develop a low cost and light weight anthropomorphic prosthetic hand with aesthetic appearance and customization ability, in order to address the vast majority of upper limb amputees. The commercial prosthetic hand exceeds the average weight of human hand, which is about 400 gm, MARCAPH overcome this without compromising the strength of the hand. The finger of MARCAPH is designed by combining a four-bar mechanism with the slider-crank mechanism to perform the complete flexion-extension of the finger. Apart from the finger, MARCAPH contains thumb with the motorized circumduction and flexion-extension based on a slider-crank mechanism each. There are 6 linear actuators to control the individual finger of the hand and one for the circumduction of the thumb. All the fingers have linked based underactuation that eliminate the need of non-backdrivable mechanism resulting not only in simplifying the overall mechanism and control, but also reduce the space required to accommodate the mechanism, actuator, and control circuitry. After the selection of the mechanism, designing of the mechanism is done on CAD software. The CAD models then analyzed for the clearance and interference between the parts during movements. Then, the models are simulated using an FEA software to check the ability of the designed hand model for the reaction forces. The FEA analysis allows us to modify and redesign parts which are unable to pass the FEA test. The final MARCAPH design shows the capability of holding a load of 20 N with a close finger and 40 N with a close thumb during simulation. During the experiments, it is confirmed that the loading strength of the 3D printed fingers is 10 N as it broke at 20 N when fully extended position. Furthermore, the mechanism, design, and individual actuator to control the individual finger of the MARCAPH allow it

to form almost all of the essential grips required for ADL. Among those grips, five essential grips are programmed in transhumeral amputee centered FSM. The MARCAPH FSM allows the subject (near elbow amputee) to adapt the functionality of the hand faster and better as compared to the conventional FSM. Which results in reducing the training time of the subject significantly. Hence the overall performance of the MARCAPH is found adequate as compared with the state of the art prosthetic hands in the field.

11.1 Future Work

While the MARCAPH has demonstrated potential improvements in the current low-cost prosthesis and their control scheme, many opportunities for extending the scope of this research remain. This section presents some of these directions.

11.1.1 Battery

The MARCAPH has reduced the weight of the prosthesis significantly and is the lightest of all the prosthesis hand as compared in chapter 10. Still, the subjects have some reservation for the weight of the prosthesis. In order to improve the user satisfaction, one can reduce the size of the battery. The current battery can power the hand for a period of 2-3 days without charging. This battery (7.4 V 4000 mAh Lipo) weights around 230 gm can be replaced by a smaller (7.4 V 2000 mAh Li-ion) battery of 70-90 gm.

11.1.2 Actuators

The MARCAPH uses 6 linear actuators, each weight around 15-20 gm. In order to reduces the weight in the hand and create room for electronics, a single actuator based mechanism may be adapted to control the middle, ring, and little finger. This helps to create space in the palm portion of the hand and allows the designer to place the electronic circuit in the palm region. This configuration also reduces the electronic circuitry required to control the actuators.

11.1.3 Palm Design

The MARCAPH is designed to mimic the appealing appearance of the human hand. This feature is achieved by introducing angles between the finger and deliberately designing the middle finger longer and little finger shorter as compared with the ring and index fingers. However, the palm portion is still lacking some features of the human hand. In the next version of MARCAPH, it is highly recommended to improve the palm design and make it curve from the sides to form a bowl shape during the power grip. Also, silicon or rubber sole can be used to place on the palm and inner side of the fingers (like Bebionics). This placement of the silicon or rubber also aids the user in gripping different shape objects easily by providing friction between the hand and the object.

11.1.4 Mechanism

The MARCAPH mechanism is based on one of the robust and widely used mechanisms, i.e. four-bar mechanism. And with the 3D printed material, it shows remarkable stability against the load and during experiments, it is proved that each finger can bear a load of 10 N comfortably. However, if the driving link or link2 (as discussed in section 3.1) has been manufactured using a metal it will add a significant amount of ruggedness into the mechanism as compared to the current 3D printed version. Also, it is observed that by introducing a passive elastic element in the mechanism may increase the adaptive grip ability of the system. This feature also prevents the mechanism and hand to break during an impact and shock.

11.1.5 Sensors

The feedback force sensor has been designed during the research of the prosthetic hand. However, in the current design of MARCAPH, only the position feedback sensor is used to control the motion of the fingers. The designed feedback force sensor can be integrated into the next prototype of the MARCAPH. In addition to the force feedback sensor, a temperature sensor can be used to detect the temperature

of the object being grasped. A vibro-motor can be used with the temperature sensor. The intensity of the vibration from the vibro-motor can be used to warn the user about the temperature of the object.

11.1.6 Pattern Recognition based Myoelectric Control

The control of the MARCAPH is based on finite state machine (FSM). That uses the threshold level detection of the EMG signal to control the MARCAPH. Nevertheless, an intelligent deep learning based algorithm may be designed and implemented. In order to accomplish deep learning based control, an EMG data acquisition system should be developed separately. The deep learning based system must have amputee subjects and huge EMG signal data in raw form should be collected and stored first. Later, this data set should be used to train different deep net models.

BIBLIOGRAPHY

[Actuonix, 2017] Actuonix (2017). Pq12-p linear actuator with feedback. *pp. Available: https://s3.amazonaws.com/actuonix/Actuonix+PQ12+Datasheet.pdf.*

[Belter et al., 2013] Belter, J. T., Segil, J. L., Dollar, A. M., and Weir, R. F. (2013). Mechanical design and performance specifications of anthropomorphic prosthetic hands: a review. *Journal of rehabilitation research and development*, 50(5):599–618.

[Bennett et al., 2016] Bennett, D. A., Mitchell, J., Truex, D., and Goldfarb, M. (2016). Design of a Myoelectric Transhumeral Prosthesis. *IEEE/ASME Transactions on Mechatronics*, 4435(c):1–1.

[Bianchi et al., 2013] Bianchi, M., Salaris, P., and Bicchi, A. (2013). Synergy-based hand pose sensing: Optimal glove design. *The International Journal of Robotics Research*, 32(4):407–424.

[Bionics, 2016] Bionics, O. (2016). Ada hand. *pp. Available: https://www.openbionics.com/, License: https://creativecommons.org/licenses/by-sa/4.0/.*

[Bionics, 2017] Bionics, T. (2017). Touch bionics product catalog. *Available: http://www.touchbionics.com/sites/default/files/files/Touch.*

[Chappell and Elliott, 2003] Chappell, P. H. and Elliott, J. a. (2003). Contact force sensor for artificial hands with a digital interface for a controller. *Measurement Science and Technology*, 14(8):1275–1279.

[Cheesborough et al., 2015] Cheesborough, J. E., Dumanian, G. A., Smith, L. H., and

Kuiken, T. A. (2015). Targeted Muscle Reinnervation and Advanced Prosthetic Arms. *Journal of Plastic Surgery*, 29(1):62–72.

[Chorost, 2012] Chorost, M. (2012). A True Bionic Limb Remains Far Out of Reach. *https://www.wired.com/2012/03/ff_prosthetics/all/*.

[Controzzi et al., 2016] Controzzi, M., Clemente, F., Barone, D., Ghionzoli, A., and Cipriani, C. (2016). The SSSA-MyHand: a dexterous lightweight myoelectric hand prosthesis. *IEEE Trans. on Neural Systems and Rehabilitation Engineering*, 4320(c).

[Dalley et al., 2009] Dalley, S. a., Wiste, T. E., Withrow, T. J., and Goldfarb, M. (2009). Design of a multifunctional anthropomorphic prosthetic hand with extrinsic actuation. *IEEE/ASME Transactions on Mechatronics*, 14(6):699–706.

[Dechev et al., 2001] Dechev, N., Cleghorn, W. L., and Naumann, S. (2001). Multiple finger, passive adaptive grasp prosthetic hand. *Mechanism and Machine Theory*, 36(10):1157–1173.

[Dianceht, 2017] Dianceht, S. d. C. (2017). Cosmetic Prosthesis,Centro Mdico Puerta de Hierro Sur . *http://www.manosydedos.com/index_sel_dedos.html*.

[Dirksen and Lammering, 2011] Dirksen, F. and Lammering, R. (2011). On mechanical properties of planar flexure hinges of compliant mechanisms. *Mechanical Sciences*, 25194(10):109–117.

[e–NABLE Organization, 2017] e–NABLE Organization (2017). The raptor hand. *pp. Available: http://enablingthefuture.org/upper-limb-prosthetics/the-raptor-hand/*.

[Estevez et al., 2012] Estevez, P., Bank, J. M., Porta, M., Wei, J., Sarro, P. M., Tichem, M., and Staufer, U. (2012). 6 DOF force and torque sensor for micromanipulation applications. *Sensors and Actuators, A: Physical*, 186:86–93.

[Gibbard, 2013] Gibbard, J. (2013). Dextrus hand. *pp. Available: http://www.openhandproject.org/dextrus.php.*

[Greiner, 1991] Greiner, T. M. (1991). Hand Anthropometry of U.S. Army Personell. *Technical Report Natick*, TR-92/011:434.

[Hermens et al., 2000] Hermens, H. J., Freriks, B., Disselhorst-Klug, C., and Rau, G. (2000). Development of recommendations for SEMG sensors and sensor placement procedures. *Journal of Electromyography and Kinesiology*, 10(5):361–374.

[Johannes et al., 2011] Johannes, M. S., Bigelow, J. D., Burck, J. M., Harshbarger, S. D., Kozlowski, M. V., and Van Doren, T. (2011). An overview of the developmental process for the modular prosthetic limb. *Johns Hopkins APL Technical Digest (Applied Physics Laboratory)*, 30(3):207–216.

[Jones, 1990] Jones, S. F. (1990). The Physiology of the Joints. *Physiotherapy*, 76(1):52.

[Langevin, 2014] Langevin, G. (2014). Inmoov-open source 3d printed life-size robot. *pp. Available: http://inmoov. fr, License: http://creativecommons. org/licenses/by–nc/3.0/legalcode.*

[Liang et al., 2009] Liang, Q., Zhang, D., Ge, Y., and Song, Q. (2009). A Novel Miniature Four-Dimensional Force/Torque Sensor With Overload Protection Mechanism. *IEEE Sensors Journal*, 9(12):1741–1747.

[Liu et al., 2014] Liu, Y. W., Feng, F., and Gao, Y. F. (2014). HIT prosthetic hand based on tendon-driven mechanism. *Journal of Central South University*, 21(5):1778–1791.

[MAL Manufacturing Automation Laboratories, 2017] MAL Manufacturing Automation Laboratories, I. A. r. r. (2017). CutPro Simulation Software MAL Inc. *http://www.malinc.com/products/cutpro/.*

[Medynski and Rattray, 2011] Medynski, C. and Rattray, B. (2011). Bebionic Prosthetic Design. *MEC 2011 Symposium MyoElectric Controls/Powered Prosthetics Symposium*, pages 1–4.

[Mirkovic and Popovic, 2014] Mirkovic, B. and Popovic, D. (2014). Prosthetic hand sensor placement: Analysis of touch perception during the grasp. *Serbian Journal of Electrical Engineering*, 11(1):1–10.

[Muzumdar, 2004] Muzumdar, A. (2004). *Powered Upper Limb Prostheses: Control, Implementation and Clinical Application*. Springer Science & Business Media.

[NI, 2017] NI, N. I. C. (2017). LabVIEW System Design Software - National Instruments. *http://www.ni.com/labview/*.

[Nova Scotia and Wellness, 2017] Nova Scotia, D. o. H. and Wellness (2017). Upper Limb Amputations, Amputee Rehabilitation, Musculoskeletal Program. *http://www.cdha.nshealth.ca/amputee-rehabilitation-musculoskeletal-program/patient-family-information/upper-limb-amputations*.

[OttoBock, 2017] OttoBock (2017). Ottobock Health Care. *http://www.ottobockus.com/prosthetics/upper-limb-prosthetics/solution-overview/body-powered-prosthetics/*.

[Palli and Pirozzi, 2011] Palli, G. and Pirozzi, S. (2011). Force sensor based on discrete optoelectronic components and compliant frames. *Sensors and Actuators, A: Physical*, 165(2):239–249.

[Rakotondrabe et al., 2015] Rakotondrabe, M., Ivan, I. A., Khadraoui, S., Lutz, P., and Chaillet, N. (2015). Simultaneous displacement/force self-sensing in piezoelectric actuators and applications to robust control. *IEEE/ASME Transactions on Mechatronics*, 20(2):519–531.

[Rf et al., 1975] Rf, C., Ce, C., Jt, M., and Hm, R. (1975). Investigation of inertial properties of the human hand. *Defense Technical Information Center, Tech. Rep.*

[Roche et al., 2014] Roche, A. D., Rehbaum, H., Farina, D., and Aszmann, O. C. (2014). Prosthetic Myoelectric Control Strategies: A Clinical Perspective. *Current Surgery Reports*, 2(3):1–11.

[ROHM Semiconductor, 2017] ROHM Semiconductor, Mouser Electronics, A. D. (2017). Photointerrupter RPI-131. *http://www.mouser.com/ds/2/348/rpi-131-210869.pdf*.

[Sani and Meek, 2011] Sani, H. N. and Meek, S. G. (2011). Characterizing the performance of an optical slip sensor for grip control in a prosthesis. *IEEE International Conference on Intelligent Robots and Systems*, pages 1927–1932.

[Schulz et al., 2011] Schulz, S., Eichelbaum, D., Valencia, R., and Stach, B. (2011). Sensor Options For Multi-Articulating Partial Hand Prostheses. In *Proceedings of the 2011 MyoElectric Controls/Powered Prosthetics Symposium*, New Brunswick, Canada.

[Segil et al., 2014] Segil, J. L., Controzzi, M., Weir, R. F. F., and Cipriani, C. (2014). Comparative study of state-of-the-art myoelectric controllers for multigrasp prosthetic hands. *Journal of rehabilitation research and development*, 51(9):1439–54.

[Shams et al., 2011] Shams, S., Kim, D. S., Choi, Y. S., and Han, C. S. (2011). A novel 3-DOF optical force sensor for wearable robotic arm. *International Journal of Precision Engineering and Manufacturing*, 12(4):623–628.

[Shams et al., 2012] Shams, S., Lee, J. Y., and Han, C. (2012). Compact and lightweight optical torque sensor for robots with increased range. *Sensors and Actuators, A: Physical*, 173(1):81–89.

[Slade et al., 2015] Slade, P., Akhtar, A., Nguyen, M., and Bretl, T. (2015). Tact : Design and Performance of an Open-Source , Affordable , Myoelectric Prosthetic Hand. *2015 IEEE International Conference on Robotics and Automation (ICRA)*, pages 6451–6456.

[Stachowsky et al., 2016] Stachowsky, M., Hummel, T., Moussa, M., and Abdullah, H. A. (2016). A Slip Detection and Correction Strategy for Precision Robot Grasping. *IEEE/ASME Transactions on Mechatronics*, 21(5):2214–2226.

[Strait et al., 2006] Strait, E., McGimpsey, G., and Bradford, T. (2006). Limb Prosthetics Services and Devices. *White Paper*, (January):1–35.

[Takenawa, 2009] Takenawa, S. (2009). A soft three-axis tactile sensor based on electromagnetic induction. *IEEE 2009 International Conference on Mechatronics, ICM 2009.*

[Tenore et al., 2007] Tenore, F., Ramos, A., Fahmy, A., Acharya, S., Etienne-Cummings, R., and Thakor, N. V. (2007). Towards the control of individual fingers of a prosthetic hand using surface EMG signals. *Conference proceedings : ... Annual International Conference of the IEEE Engineering in Medicine and Biology Society. IEEE Engineering in Medicine and Biology Society. Conference*, 2007:6146–9.

[Test Standard Labs, 2017] Test Standard Labs, LLC, U. (2017). Abs material data sheet. *Available: http://www.teststandard.com/data_sheets/ABS_Data_sheet.pdf.*

[The MathWorks, 2017] The MathWorks, I. (2017). Matlab - the language of technical computing. *pp. http://www.mathworks.com/products/matlab/.*

[Tiwana et al., 2012] Tiwana, M. I., Redmond, S. J., and Lovell, N. H. (2012). A review of tactile sensing technologies with applications in biomedical engineering. *Sensors and Actuators, A: Physical*, 179:17–31.

[Van Der Riet et al., 2013] Van Der Riet, D., Stopforth, R., Bright, G., and Diegel, O. (2013). An overview and comparison of upper limb prosthetics. *IEEE AFRICON Conference*.

[Vecchi et al., 2001] Vecchi, F., Micera, S., Zaccone, F., Carrozza, M., Sabatini, a. M., and Dario, P. (2001). A sensoried glove for applications in Biomechanics and motor control. *Conference of the International FES Society*, pages 0–2.

[Weir and Ph, 2004] Weir, R. F. and Ph, D. (2004). Design of Artificial Arms and Hands for Prosthetic Applications. *Standard Handbook of Biomedical Engineering and Design*, pages 1–61.